THE ROLE OF VOID

DISTRIBUTIONS ON VOID

FRACTION MEASUREMENTS

THE ROLE OF VOID DISTRIBUTIONS ON VOID FRACTION MEASUREMENTS

By:

HENRI PAUL ARCHER, B.SC.

A Project Report
Submitted to the School of Graduate Studies
in Partial Fulfilment of the Requirements
for the Degree
Master of Engineering
McMaster University
AUGUST 1978

McMASTER UNIVERSITY
HAMILTON, ONTARIO

MASTER OF ENGINEERING (1978)

TITLE:	The Role of Void Distributions on Void Fraction Measurements
AUTHOR:	Henri Paul Archer, B.Sc. (U.N.B.)
SUPERVISOR:	Professor A.A. Harms
NUMBER OF PAGES:	xii, 125

ABSTRACT

The distribution of voids in a nuclear reactor is of great importance due to their effect on the neutron flux and on the reactor dynamic characteristics in addition to the well known thermohydraulic problems they create.

The possibility of using scattered neutrons to measure voids in a liquid flow is investigated experimentally. The appealing property of a scattering technique as compared to the well known transmission method, is that multiple detectors could be used for additional information about the distribution of the voids as well as their void fraction.

For this purpose a beam of neutrons has been extracted from the McMaster University 5MW pool type nuclear reactor. Cylindrical pieces of Lucite have been used to simulate a column of water; this material has neutron transport properties which are very similar to those of liquid water.

The neutron diagnostic method of detection has the advantage of not disturbing the flow of the fluid like devices such as probes and isolating valves would do.

A BF_3 detector mounted on an arm which rotates about the axis of the cylindrical samples was used as the experimental set up. Lucite samples of different void fractions and possessing different void distributions were prepared. Different numbers of circular holes and of different relative sizes were drilled in the samples providing the possibility of simulating many void distributions by simply rotating the samples. Counting times of the order of 100 seconds were used in order to provide sufficient statistical accuracy to observe the differences in counts.

ACKNOWLEDGEMENT

I wish to express my appreciation to Dr. A.A. Harms for his useful advice and his patience throughout the completion of this work. I am also greatly indebted to McMaster University for the financial support which has made the realization of this project possible. I also wish to express my thanks to the McMaster University reactor staff which has tolerated my presence around the reactor at any hour of the night.

Special mention is made to Miss Jacki Sharp who has dedicatedly typed this report.

TABLE OF CONTENTS

LIST OF FIGURES

LIST OF TABLES

LIST OF FIGURES

NOMENCLATURE

α = void fraction, dimensionless

$\emptyset$ = scattering angle; angle between beam axis and detector axis, [deg]

θ = sample orientation angle; angle between neg. beam axis and sample axis, [deg]

N = total count, (0)

t = counting time, (s)

R = count rate, (s^{-1})

$T = \frac{R-Rb}{R_T}$ transmittance; rate measured less background normalized by full unattenuated beam rate; (0)

$RES = \frac{CR_d}{CR_f}$ response function; corrected rate normalized by the corrected rate for a no void sample; (0)

G = geometry number of voids in samples; there are 5 possibilities investigated

S = sample number; numbered 1 thru 16, three samples for each geometry with

α = 1/2, 1/3, 1/5

χ = thickness of sample (cm)

Σ = microscopic neutron cross-section (cm^{-1})

B = buildup factor

λ = path length in units of mean free path

a_i = regression analysis parameters

C_1 = center position of hole(1); radial distance from center of sample (inches)

D_1 = diameter of hole(1) in inches

D_T = diameter of sample (.755 inches)

INTRODUCTION

Two phase flow still remains a very difficult engineering problem. The lack of benchmark experiments with which to verify the theories is one of the problems. Different techniques to measure the void fraction have been devised over the years. However, they all have their drawbacks. Devices such as probes and isolating valves have been used but they have the disadvantage of interfering with the flow itself.

Pressurized water reactors require thick wall piping to contain the 1500 PSI pressure. This does therefore rule out methods of measuring void fraction using electromagnetic waves or charged particles like beta rays. Thus neutronic methods appear as appealing alternatives since their neutron cross-section in the wall as compared with the water is very low. Transmission techniques have been shown to predict voids in dynamic flows with a precision of the order of less than 6% but this method provides no information about the void distribution.

The object of this project is to investigate the neutron scattering method and attempt to determine the possibility of correlating the distribution of the voids with the angular scattering intensity of neutrons. We will represent voids in water by a solid plastic called PMMA for polymethylmethacrylic having the following chemical formula:

$$\left[-CH_2C(CH_3)\ (CO_2CH_3)-\right]_n$$

PMMA has a neutron absorption cross-section (Σ_a) of .019 inverse centimeters at .025 EV, as compared with .022 inverse centimeters for water. The thermal scattering cross-section for Lucite is 2.398 inverse centimeters as compared with 2.681 inverse centimeters for water. Since the cross-sections are very similar, we will use Lucite to simulate two phase water (liquid and steam) by drilling holes in the Lucite. This model certainly has limitations since it is a static situation while a flowing water and steam would be a dynamic situation. Nevertheless, this will provide a basis for assuming the role of void distribution which is basic to both the static as well as the dynamic case. Figure 1 provides a graphical display of the cross-sections of the Lucite targets while Table 1 lists their detailed numerical parameters.

The necessity of knowing the void fraction for reactor safety analysis of loss of coolant accidents has recently forced considerable research in void determination methods. In two phase flow it is possible to identify these main flow regimes:

(1) Bubble flow where discrete vapour bubbles are homogeneously distributed in a liquid continuum.

(2) Slug flow where the two phases segregate into liquid slugs and elongated vapour bubbles.

(3) Annular flow where a continuous gas core has forced the liquid phase into a thin film on the channel walls.

In our two dimensional model, regime (3) is the only one that can be exactly represented by drilling holes in a cylindrical piece of Lucite. Regime (1) is represented by drilling many smaller holes in the cylinder. This model should, however, be sufficient to investigate the magnitude of the effect of the voids distribution on neutron scattering.

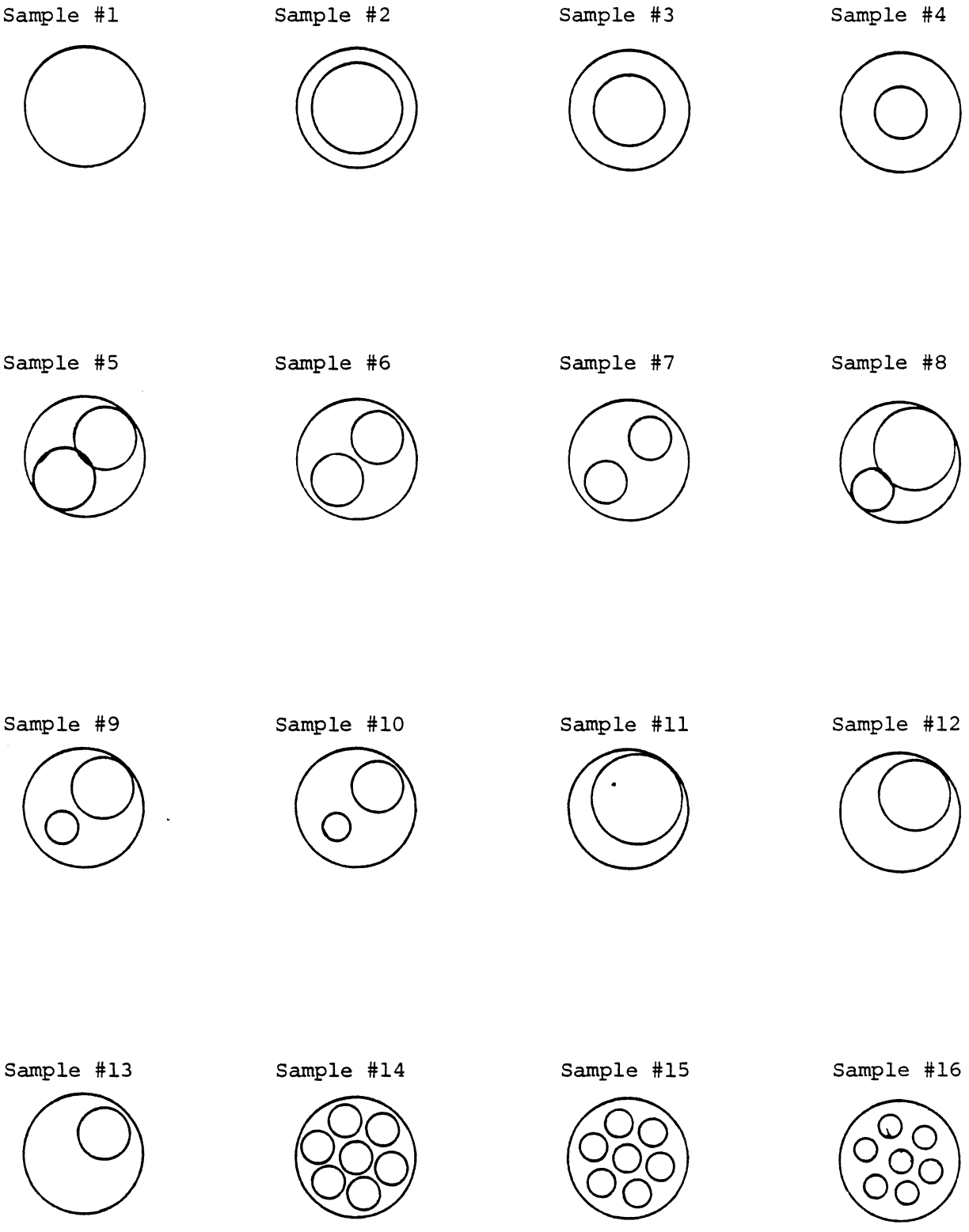

FIGURE 1: This is a full size illustration of the geometry of the samples used in this experiment

TABLE I: Physical parameters specifying the samples used in this experiment

Number	Number of Holes	Geometry Number G	Hole 1 Center C_1 (in)	Hole 1 Diam. D_1 (in)	Hole 2 Center C_2 (in)	Hole 2 Diam. D_2 (in)	$\alpha = \frac{D_1^2 + D_2^2}{D_T^2}$
1	0	Any	0	0	0	0	0
2	1	1	0	.532	0	0	.50=1/2
3	1	1	0	.440	0	0	.34=1/3
4	1	1	0	.337	0	0	.20=1/5
5	2	2	.174	.378	.185	.378	.50=1/2
6	2	2	.178	.303	.168	.303	.32=1/3
7	2	2	.176	.238	.151	.288	.20=1/5
8	2	3	.115	.242	.241	.472	.49=1/2
9	2	3	.122	.193	.214	.395	.33=1/3
10	2	3	.124	.151	.196	.303	.20=1/5
11	1	4	.078	.531	0	0	.49=1/2
12	1	4	.144	.4375	0	0	.34=1/3
13	1	4	.188	.339	0	0	.20=1/5
14	7	5	0	.201	.232	.201	.50=1/2
15	7	5	0	.161	.220	.161	.31=1/3
16	7	5	0	.128	.219	.128	.20=1/5

THEORY

When neutrons enter the cylindrical Lucite sample two main interaction processes may occur. They are absorption and scattering with the scattering cross-section being the largest. Since the size of the sample is much bigger than the mean free path of the neutrons, the diameter is about 5 times the mean free path, we expect that the neutrons will have had more than one interaction. For a thin sample, one where the dimension is smaller than a mean free path, the transmittance is given by the following:

$$T = \exp(-\Sigma\chi) \qquad \text{..... eq. (1)}$$

where: T = transmittance = R/R_o

Σ = the macroscopic neutron cross-section of the sample

χ = the thickness of the sample.

If we now allow the presence of voids in the sample we can correct equation (1) in the following way:

$$T = \exp(-\Sigma\chi(1-\alpha)) \qquad \text{..... eq. (2)}$$

where (α) is the void fraction and is defined as the ratio of the volume of the voids to the total volume of the sample.

If we now further allow the thickness (χ) of the sample to increase until it can no longer be considered to be thin with respect to the neutron mean free path, we then have to correct equation (2) with a build up factor (B) which will be a function of both the thickness of the sample and its void fraction. Therefore, equation (2) becomes:

$$T(\chi,\alpha) = B(\chi,\alpha)\exp(-\Sigma\chi(1-\alpha)) \qquad \text{..... eq. (3)}$$

The buildup factor (B) corresponds to the increase in the number of neutrons detected attributable to multiple scattering effects. Harms et al (3) have obtained a numerical expression for the buildup factor.

In our case here we will generalize the transmittance function (T) to be also a function of the detector angle (Ø) since all our samples are of the same size we will suppress its dependence on χ. Further parameters that should be included in the transmittance function are the neutron energy (E), the sample orientation (Θ) and the sample geometry (G). So our transmittance equation will become:

$$T(\alpha,\emptyset,\Theta,G) = B(\alpha,\emptyset,\Theta,G)\exp(-\lambda(1-\alpha)) \qquad \text{..... eq. (4)}$$

where ($\lambda = \Sigma\chi$) in units of mean free path.

Another function which might be of interest is the response function as defined by Sha et al (8). The response (RES) is the ratio of the transmittance at a given void to the transmittance with a non-voided sample. With other parameters unchanged we write this function as:

$$RES(\alpha,\emptyset,\Theta,G) = T(\alpha,\emptyset,\Theta,G) \;/\; T(\alpha=0,\emptyset,\Theta,G)$$

$$= \frac{R(\alpha,\emptyset,\Theta,G)}{R_o^{\alpha}} \div \frac{R(\alpha=0,\emptyset,\Theta,G)}{R_o^{o}}$$

$$= \frac{R(\alpha,\emptyset,\Theta,G)}{R(\alpha=0,\emptyset,\Theta,G)} \cdot \frac{R_o^{F}}{R_o^{\alpha}} \qquad \text{..... eq. (5)}$$

where (R_o^{α}) is the count rate when the detector is placed directly in the open beam with no sample at the time that $R(\alpha,\emptyset,\theta,G)$ was measured, while (R_o^{o}) is the count rate when the detector is placed directly in the open beam with no sample at the time that $R(\alpha = 0,\emptyset,\theta,G)$ was measured. If we assume that the reactor power fluctuation with respect to time is neglectable for the time intervals in which the measurements were made, then the ratio R_o^{o}/R_o^{α} is equal to 1 and:

$$RES(\alpha,\emptyset,\theta,G) = \frac{T(\alpha,\emptyset,\theta,G)}{T(\alpha=0,\emptyset,\theta,G)} = \frac{R(\alpha,\emptyset,\theta,G)}{R(\alpha=0,\emptyset,\theta,G)} \quad \text{..... eq. (6)}$$

For the previously defined functions to be independent of time as we have suggested they should be normalized by factors (R_o) which would have been obtained by real time monitoring. However, our experimental set-up did not allow us to do real time monitoring. Monitoring was only done once every hour or when it was suspected that there might have been a reactor power change. This procedure seemed adequate since results were reproduceable within the intrinsic ($\sqrt{N}$) error due to the statistical nature of the neutron beam.

Since the neutron interaction cross-section are energy dependent, the transmittance that we measure will also depend on the energy of the neutrons in the beam. Since cross-section generally decreases as the energy increases, the mean free path of the neutrons in the media will generally increase as the energy increases since the mean free path is the inverse of the macroscopic cross-section which in turn is proportional to the microscopic cross-section. This does imply that to obtain fewer interactions of the neutrons one would have to use neutrons of higher energy, or the energy of the neutrons chosen could depend on the size of the sample (or pipe) depending on how many neutron interactions are acceptable for statistical purposes.

Table (2) shows the total cross-sections of Lucite and water as functions of energy. For nuclear cross-section purposes, Lucite consists of the stoimetric ratio: $C_5H_8O_2$, while water is H_2O. Their microscopic cross-sections are therefore respectively given by the following expressions:

$$\sigma^L = 5\,\sigma^C + 8\,\sigma^H + 2\,\sigma^O$$

$$\sigma^W = 2\,\sigma^H + \sigma^O$$

Their macroscopic cross-sections are in turn given by:

$$\Sigma^L = n_1\,\sigma_1 + n_2\,\sigma_2 + n_3\,\sigma_3$$
$$= n\,\sigma^L$$

where n is the molecular density given by:

$$n = \frac{\rho N_o}{n} = \frac{\text{gm/cm}^3 \times \text{molecules/mole}}{\text{gm/mole}} = \frac{\text{molecules}}{\text{cm}^3}$$

$$n_L = \frac{1.185\ \text{gm/cm}^3 \times .60225 \times 10^{24}\ \text{molecule/mole}}{100.1183\ \text{gm/mole}} = .00713\ \text{molecule/cm}^3$$

$$n_W = \frac{1\ \text{gm/cm}^3 \times .60225 \times 10^{24}\ \text{molecule/mole}}{18.0153\ \text{gm/mole}} = .03343\ \text{molecule/cm}^3$$

For Lucite or water the total cross-section is the sum of the absorption cross-section and the scattering cross-section. However, the scattering cross-section is about one hundred times the absorption cross-section. Hence, we use:

$$\Sigma_t = \Sigma_a + \Sigma_s$$

$$\Sigma_s/\Sigma_a \simeq 100$$

$$\therefore\ \Sigma_t \simeq \Sigma_s$$

For pipes of diameters less than 45 cm, we can neglect absorption since this is its mean free path.

Table 2 lists the appropriate data for this comparison while Figure 2 provides a graphical display.

TABLE II: Cross-sections and mean free paths as a function of energy

E(eV)	σ_T^H(b)	σ_T^O(b)	σ_T^C(b)	σ_T^W(b)	σ_T^L(b)	Σ_T^W(cm^{-1})	Σ_T^L(cm^{-1})	λ^W(cm)	λ^L(cm)
.01	48	4.8	4.2	100.8	414.6	3.370	2.955	.297	.338
.25	38	4.2	4.8	80.2	336.4	2.681	2.398	.373	.417
.05	32	4.1	4.5	68.1	286.7	2.277	2.044	.439	.489
.1	27	3.9	4.8	57.9	247.8	1.936	1.766	.517	.566
1	20	3.8	4.7	43.8	191.1	1.464	1.362	.683	.734
10	19	3.75	4.6	41.75	182.5	1.396	1.301	.716	.769
10^2	20	3.7	4.5	43.7	189.9	1.461	1.354	.684	.739
10^3	20	3.7	4.5	43.7	189.9	1.461	1.354	.684	.739
10^4	18	3.3	4.3	39.3	172.1	1.314	1.227	.761	.815
10^5	12	3.7	4.3	27.7	124.9	.926	.890	1.080	1.124
10^6	4.2	5.8	2.7	14.2	58.7	.475	.418	2.105	2.392
10^7	.79	1.3	1.2	2.88	14.92	.096	.106	10.42	9.434
10^8	.70	.60	.47	2.0	9.15	.067	.065	14.93	15.38

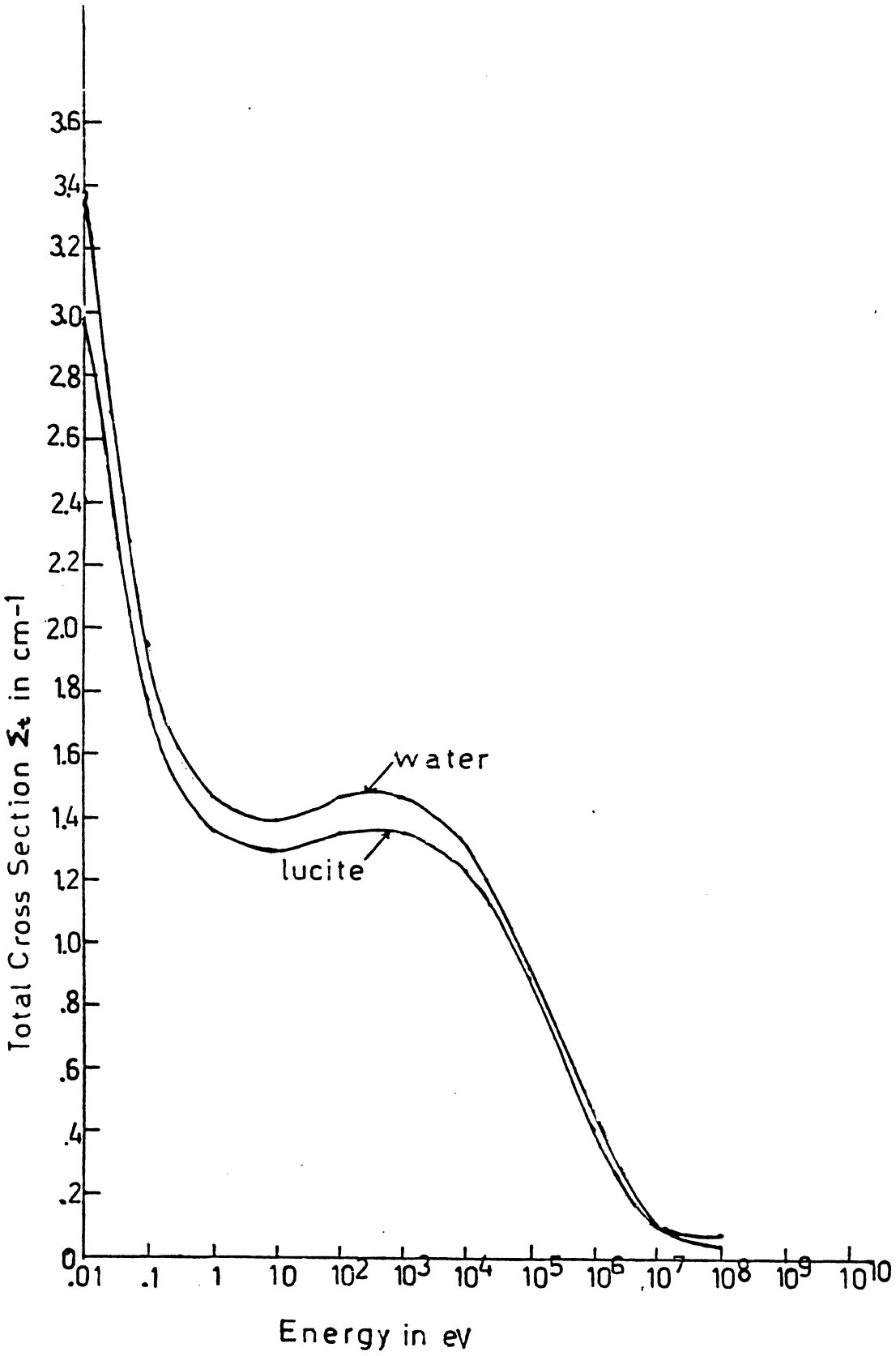

FIGURE 2: Graph of Total Cross-section (Σ_t) versus Energy

LITERATURE SURVEY

Relatively little work has been done in the detection of voids with scattered neutrons. The only reports in the literature are from J.C. Rousseau, et al, Centre D'etudes Nucleaire de Grenoble, France (7); J. Boisvert, Ecole Polytechnique de Montréal (16); S. Banerjee, et al, McMaster University, Hamilton, Ontario (9).

Rousseau, et al, (7) used as a neutron source the Siloette pool type reactor of the nuclear centre of Grenoble. A cadmium screen was placed in the beam to filter out thermal neutrons. Boisvert (16) used two Am-Be sources emitting 750,000 fast neutrons per second. Banerjee, et al, (9) used the McMaster pool type reactor to obtain a source of fast neutrons, again using a cadmium screen like Rousseau, et al, (7) to stop the thermal neutron. These three papers report good correlation between 90 degrees scattering and the void fraction for a given void fraction distribution.

A number of papers have been written on measuring void fractions by transmission either with thermal or fast neutrons. Three main groups can be classified:

(1) Thermalization of fast neutrons by hydrogeneous materials (water and Lucite are such materials).

(2) Attenuation of thermal neutrons by hydrogeneous materials (water and Lucite are such materials).

(3) Moderation and attenuation of fast neutrons by hydrogeneous materials.

The first method was employed by Semel, et al, (15) to detect moisture in a hydrogeneous media and by Jackson, et al, (11) to measure the void fraction in a steam-water flow.

The second method has been used extensively by Harms, et al, (3) and Moss, et al, (12) for void fraction determination.

The third method has been exploited by Sha and Bonilla (8) using an Sb-Be source to determine void fractions with dissolved boron in a 3 to 8 inches diameter pipe. According to Hahn (2) the above three methods can be implemented with range improvement when employing a Californium-252 source. Hahn concludes by saying: "the use of only thermal neutrons for void fraction determination should be avoided". This is due to the large build-up encountered when passing neutrons in a large diameter pipe. Neutron densitometers for measuring void fraction in steam-water flow have been built using fast neutrons isotopic sources. Estimation of the time-averaged void fraction have been made by Harms, et al, (6). However, the void fluctuation is very important and can introduce a significant bias in the void measurement as shown by Hancox, et al, (1). They further suggest a discrete sampling period technique with a gating interval much smaller than the dominant void fluctuation period.

Rousseau, et al, (7) has made some void measurements by neutron scattering using an epithermal beam of 10 neutrons per square centimeter of energy .625 eV and 5.5 KeV. This beam was obtained from the Siloette reactor and collimated through a .5 cm by 9 cm slit. Cylindrical samples made of aluminum represents the void in the water. These experiments were also duplicated by Banerjee, et al, (9) using similar samples and a fast neutron beam from the McMaster reactor. Rousseau, et al, (7) states that neutron transmission techniques is only interesting if the pipe diameter is less than 2 or 3 cm. Therefore, he went to a two boron proportional detectors arrangement. One placed above and one below a 10 cm pipe. This arrangement is like summing over Ø=45 to 135 degrees and here used for a very large pipe. Cadmium sleeves were used to completely cover the detectors so as to eliminate the counting of thermal neutrons. Rousseau, et al, (7) reports that the void distribution has negligeable effect on the counting rate at a given void fraction. This method was then used to measure the void as a function of time in blowdown tests. Banerjee, et al, (9) reports good agreement between the 90 degree scattering rate determined void with void determined by a quick closing valve method.

PROCEDURE

As mentioned above, cylinders of Lucite with holes of different sizes drilled in them were used as the target in these scattering experiments. Figure (1) shows the dimension of these analogues. The neutron beam was obtained from the McMaster University reactor. A quartz crystal is inserted in the neutron beam so as to scatter all the higher energy neutrons, leaving only thermal neutrons to pass through a 1.5 inch collimator. The beam then strikes the target which is centered by the method of maximum count. A BF_3 neutron detector was mounted on a rotating arm so as to rotate 180 degrees about the sample. See Figure (3) for a graphical representation of the experimental arrangement.

A high voltage power supply is connected to the detector. The detector output first goes through a preamplifier and then to a linear amplifier which is connected to a counter/timer.

A multichannel analyser was also connected to the output of the linear amplifier. By looking at the spectrum of counts versus energy it was possible to decide where to adjust the threshold of the counter so as to discriminate against amplified noise and counts due to gamma rays. The timer/counter threshold potentiometer was adjusted to give the same count as the integration over the thermal peak obtained on the multichannel analyser. A printout and a punched paper tape was also obtained for the spectrum data, Figure (3) displays in block diagram form the electronic circuitry.

The radial intensity distribution of the beam was also measured by mounting the BF_3 detector on a travelling stand and going horizontally across the beam. A plot of the beam versus position (χ) shows where in the beam the maximum count will center the sample, Figure (4). A series of measurements using an identical set-up of positioning of detector and sample demonstrated the statistical fluctuation nature of the count rate versus time. See Appendix (1).

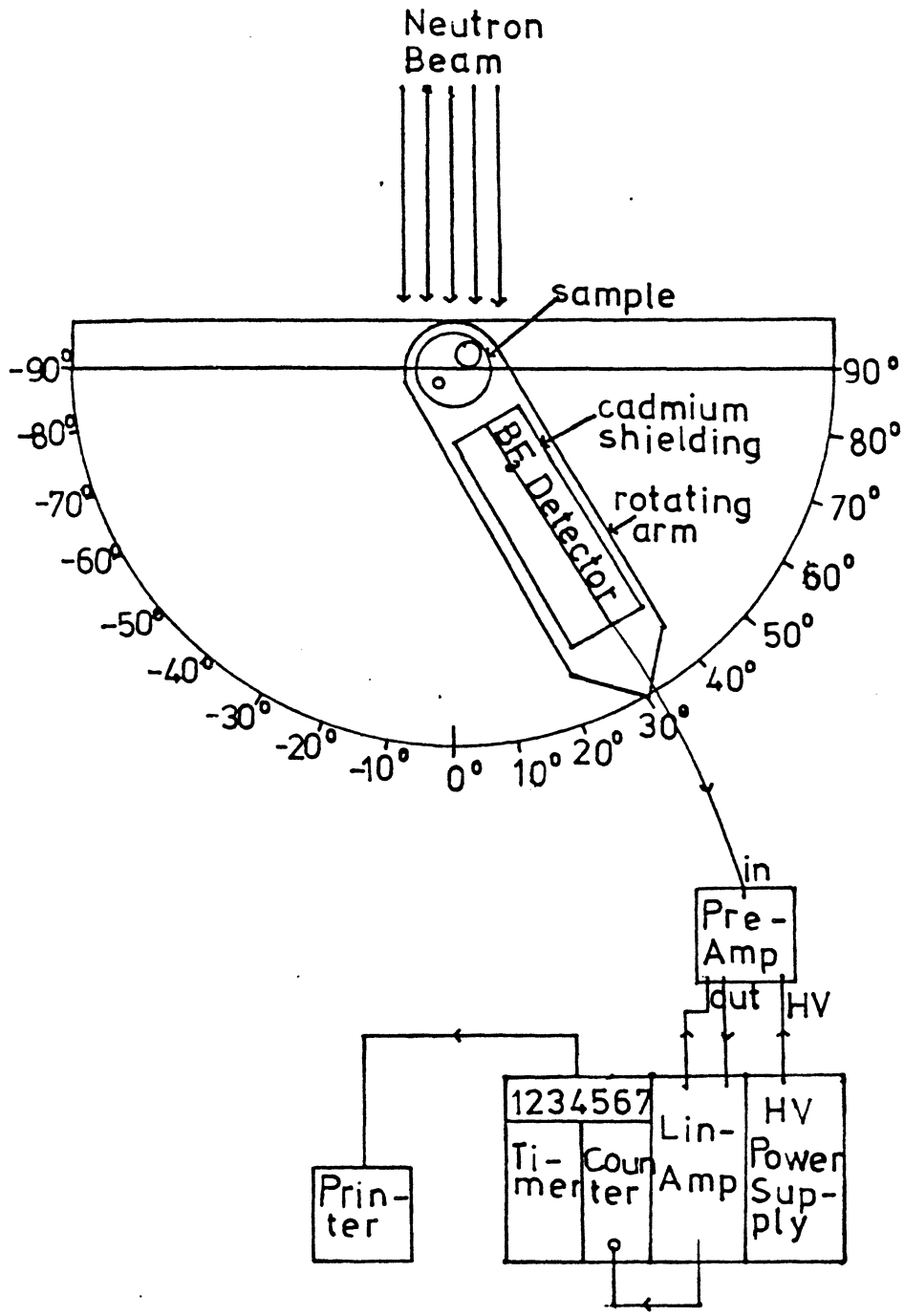

FIGURE 3: Diagram of Experimental Set-up

Before measurements were performed for different void fractions, a background reading was obtained with the beam opened but no sample. A background reading was also performed with the beam closed. The count rates obtained were sensibly the same except in the vicinity of $\emptyset$=0 degrees since the beam is well collimated and the cadmium sleeve covering the detector presents an aperture covering only a very small solid angle. Measurements were then performed for 10 different samples varying the detector angle ($\emptyset$) by steps of 10 degrees from 0 to 90 degrees.

Lucite samples with void fractions α =0,1/2,1/3,1/5 were prepared where (α =0) is a sample without any holes and the other samples have voids consisting of cylindrical holes. The samples have either a single hole, two holes or seven holes. The double hole samples have one hole being twice the diameter of the other.

The first set of measurements was performed leaving the BF_3 detector bare, but this led to very high background count rates, thus masking the phenomena under observation. A cadmium sleeve with a rectangular aperture of 1.3 cm by 0.7 cm was then used for the second set of data. The problem with this set-up was the detector could only see a very narrow portion of the sample such that if a void was situated behind that portion, its effect on the count rate would be negligeable. A third set of measurements were then obtained using a cadmium sleeve to shield the detector but maintaining a circular aperture the size of the detector. Graphics of the count rate versus the detector angle ($\emptyset$) were obtained using the Versatec plotting system of the McMaster University computing centre.

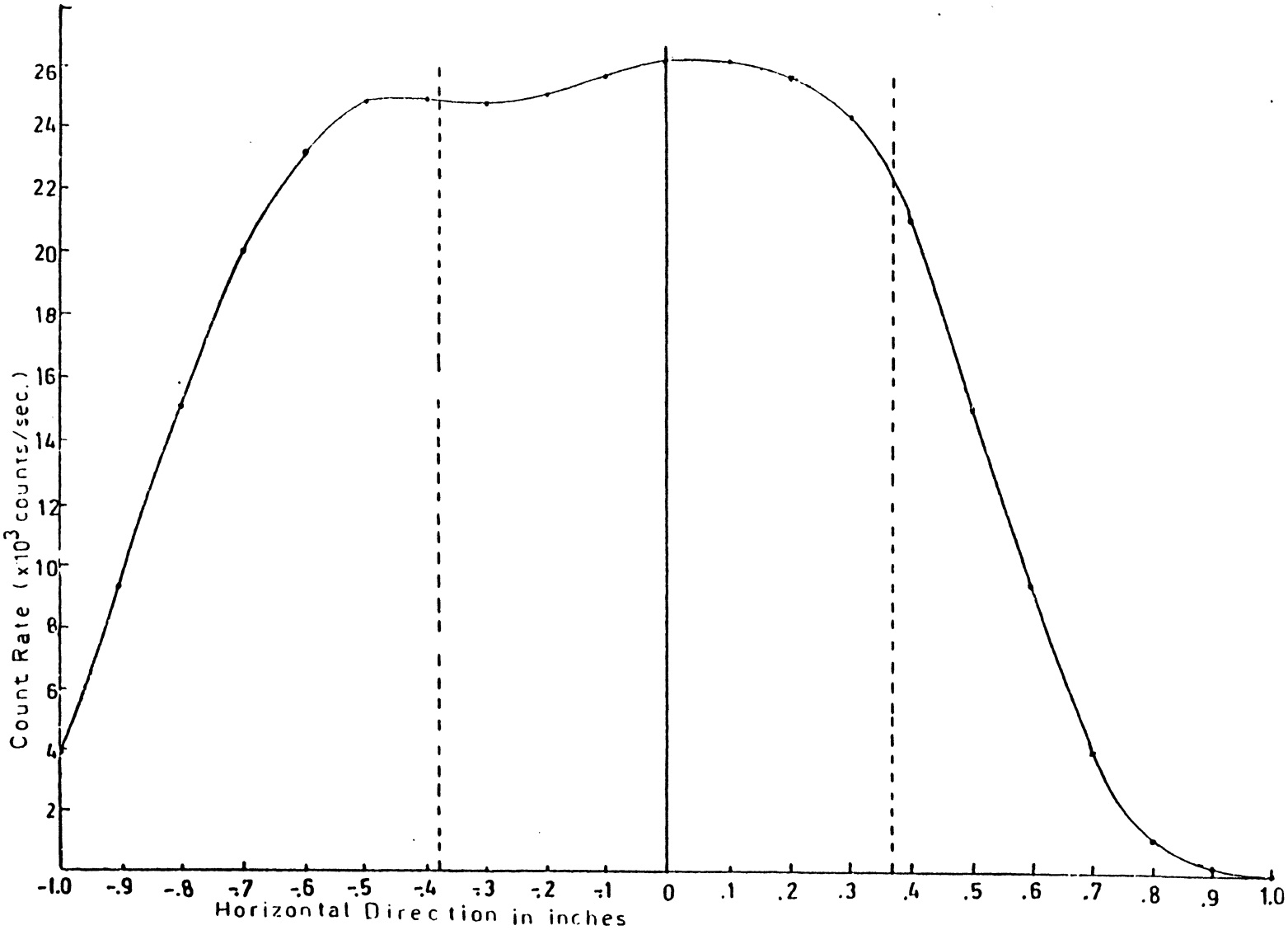

FIGURE IV: Graph of intensity of neutron beam versus horizontal direction

RESULTS AND DISCUSSION

The count rates as measured by the BF_3 detector were first corrected for background radiation at that angle. It was found that in the absence of a sample, the count rate for angles (Ø) greater than 20 degrees were essentially the same whether the neutron beam was opened or closed. Values with the beam open and no samples were thus considered as background radiation and were subtracted from the scattering count rates obtained later since they could not possibly be due to scattering. The count rates were also normalized by the value of the count rate when the detector was placed directly into the neutron beam. This is necessary due to the variations in power of the reactor from day to day. Also it would be meaningless to talk about an absolute count rate since it is both dependent on the geometry of the detector and the calibration of the electronic. However, the threshold of the counter was adjusted to give the same count as the integration over the thermal neutron peak on a tricon multichannel analyser.

We will consider only the data obtained with a cadmium sleeve on the detector and a circular opening the same size as the detector. Figures (4) to (23) show the transmittance versus the scattering angle (Ø) for all samples and all sample orientation (Θ). The transmittance refers to the count rate less the background rate which is the count rate obtained with the beam port opened and no sample; this difference is then normalized by the count rate for angle (Ø) equal zero degree and no sample (i.e. the detector straight into the beam) to take into account the variations in power of the reactor.

It was found that the larger the void the larger the count rate. It can also immediately be observed that the general tendancy is the larger the scattering angle (Ø) the larger the count. As for the effect on the count due to the orientation of the sample which is what the graphs (4) to (24) illustrate, it can be seen that it is very geometry dependent. Moreover the behaviour of the (Θ = 45) degrees and 135 degrees seems to be similar for small angle scattering (Ø = 20^{o}) and large angle scattering (Ø = 90^{o}) while the curves separate widely for intermediate scattering angles, likewise for Θ = 0^{o} and 90^{o}. For the geometries having unsymmetrical distributions (G=3,4 i.e. 8 values of Θ measured) we see that when the biggest part of the voids is towards the detector (Θ = $0,45,90,135^{o}$) the counts are much closer at small angle scattering while they spread out at larger angles (Ø = 90^{o}). The opposite can be said about the four other values of (i.e. Θ = $180,225,270,315^{o}$) when the voids are farther away from the detector. It is also striking that when the void fraction is smaller the difference between the different orientations of the samples are less pronounced. This observation is also valid for the differences between different geometries. However, the differences in count rates due to two holes of different sizes as opposed to the same size, for the same void fraction, are not that big. For the case of a many hole geometry representing nucleate bubbling, the effect of the orientation of the sample, as we would expect, then becomes almost undetectable. There is considerable crossing of the lines due to different orientations of the samples as the scattering angle increases showing the complicated nature of the neutron interaction processes inside the sample.

Figures (4) to (24) show the transmittance versus the angle ($\emptyset$) for different void fractions for the same geometry and same sample orientation. As mentioned above, it is observed that the larger the void the larger the count rate for small scattering angles. Thereafter some crossing occurs to end with the opposite relation at $\emptyset$=90 degrees for most of the time. Again the processes of absorption and scattering are competing for the net effect on the neutron count rate.

The Figures (24) to (49) are transmittance versus void fraction (α), with the geometry and orientation (Θ) of the sample. The first feature to note in these graphs is that the larger the void fraction the more isotropic the count becomes. Also, the count rate increases with the void fraction for small angle scattering while the inverse trend dominates for $\emptyset$=90 degrees. This leads to crossing of the curves for different scattering angle, but in such an irregular pattern that it is not possible to determine the void fraction by looking at the intersection of those lines like I had hoped to. The consistency of the $\emptyset$=20 degrees curve as the geometry and the orientation of the samples is changed is remarkable.

When plotting the transmittance for $\emptyset$=0 versus the void fraction (α) for different orientations (Θ) of the same geometry (G), it can be seen that the effect of the distribution of the holes is very large, even larger than the differences between different void fractions. It is useful to note that for the geometries having unsymmetrical distributions (G=3,4) the graph showing the first four orientations (Θ =0,45,90,135^{o}) is quite identical to graph having orientations (Θ = 180,225,270,315^{o}) as far as transmission is concerned. This is what might be expected if the sample were well centered in the neutron beam. It can again be seen that for the samples with seven holes the difference in count rate due to the different orientations is much less prominent.

It is useful to note that the Θ=0 degree orientation spreads out from the other orientations, probably due to the fact that there is almost an open passage for the transmission of neutrons at this direction. However, for geometry G=3, consisting of one off-center hole, the maximum transmittance is when the hole is off to one side. The explanation that the sample is not centered in the beam can be ruled out, since this phenomena is observed for both (Θ =90 and 270) degrees. In this set of experiments the lowest transmission is when the off center hole is directly in the beam (i.e. Θ=0 and 180°).

If, instead of plotting simply the transmittance on the Y axis we plot the response function, then the results look much more informative. The response function is defined by Sha, et al, (8) in the following way:

$$RES = T_\alpha / T_F = \frac{R_\alpha - R_b}{R_F - R_b} \cdot \frac{R_T^F}{R_T^\alpha}$$

where R_T^F/R_T^α takes care of power variations between the measurement of sample (1) (α =0=F) and the voided sample. The trend of the response when plotted as a function is downward (negative slope) as opposed to the trend of the corrected rate as a function of (Ø). Again the slope is steeper for a higher void fraction, with the range overlapping for different orientations (Θ).

As mentioned ealier in the graphs of (T) versus (Ø), the response for Θ = 45 and 135 are similar for small and large angle scattering while it spreads out for intermediate value of (Ø), similar observations can be made for the response of Θ = 0 and 90°. There is again considerable crossing of the response lines for different orientations (Θ). For the geometry G=5, the response is much less dependent on the orientation (Θ), and a much better defined function of (α).

The graphs of RES versus (α), figures (70) to (95), look very interesting. One first notes that the lines are much straighter. For low angle scattering the slope is positive while for higher angles the slope is almost zero, even slightly negative for $\emptyset$ = 90 degrees. We could not expect this linear increase of the response with respect to (α) to go on all the way to the limiting case of α =1, where the scattering would obviously have to be zero since there is no material to scatter. There must therefore be a value of where the response will be a maximum. The general trend of the response line as a function of (α) to be straight lines of varying slope for different scattering angles. It should be possible to predict the void fraction of samples in the range α =0 to .5 from the curves for low angle scattering. It would also be interesting to measure the voids of samples of .5 $<\alpha<$ 1.0 to find where the maximum in the response occurs.

For scattered neutrons to be a good void fraction measurement technique we would want a function of the scattering yielding a void fraction measurement which would be independent of the geometry of the voids and of their distribution. Moreover it would be useful if it was also independent of the scattering angle. However, the graphical representation shows a clear distinction for both the transmittance and the response function between the different geometries used and also between different scattering angles.

REGRESSION ANALYSIS

Emperical formulas for the response as a function of void fraction (α) and detector orientation (ϕ) have been fitted to our data using the computer library routine UWHAUSS. The formula chosen was of the following form:

$$R(\alpha,\phi) = a_1 + a_2\,\alpha + a_3\phi + a_4\,\alpha\phi + a_5\,\alpha^2 + a_6\phi^2$$

The computer program starts from initial guesses for the (a_i) and works its way through the data adjusting the a_i for the best least square fit. Table (3) shows the values found for (a_i, i=1,6) for our 25 effectively different sample geometries. It can be seen that $a_1 \simeq 1$ which is what we would expect from the definition of the response function for (α =0) with no voids in the sample and (ϕ=0) the detector aligned with the neutron beam direction. The angle ϕ is best expressed in radians so that the variable will remain in the range of 0 to about 1 just like the void fraction variable. This allows for easier comparison of the parameters found for the different terms of the model.

In every case the Sum of the Squares After Regression (SSAR) was recorded. It is a very good indicator of how well it was possible to fit the model under study to the data points. Different models were first tried before the one mentioned above. For instance, a model where the variable ϕ was inserted inside a sin function gave an SSAR of 2.85 which is 60 times larger than what was obtained with the straight polynomial, thus indicating that introducing a sin function is not a good choice on the basis of our data. The model was fitted to the data letting ϕ vary over both ranges (0^o,90^o) and (20^o,90^o). For the first range the SSAR was 23 times larger than for the second. This shows clearly that our model holds much better for the range where the detector sees only scattered neutrons and no transmitted ones.

TABLE III: Results obtained after regression analysis with library routine UWHAUSS

MODEL:

$$R(\alpha,\phi) = a_1 + a_2\,\alpha + a_3\phi + a_4\,\alpha\phi + a_5\,\alpha^2 + a_6\phi^2 \qquad NOB = 32$$

#	G	θ	a_1	a_2	a_3	a_4	a_5	a_6	SSAR	SSAR/NOB	S
1	1	0	1.089	2.133	-.2745	-1.631	.3609	.1569	.02923	.00091	.030
2	2	0	1.158	2.298	-.4061	-1.379	-1.512	.2023	.1048	.00328	.057
3	2	45	1.035	1.487	-.1337	-1.274	1.108	.08167	.028206	.00088	.030
4	2	90	.9489	2.019	+.05794	-1.580	.04645	-.01136	.05190	.00162	.040
5	2	135	1.251	1.735	-.6212	-1.083	-.21111	.3158	.13622	.00426	.065
6	3	0	1.117	2.795	-.3210	-1.747	-1.019	.1724	.04235	.00132	.036
7	3	45	.9899	2.458	-.004646	-1.533	.08225	.01114	.01466	.00046	.021
8	3	90	.9467	2.786	.09431	-1.818	-.4976	-.03777	.04039	.00126	.035
9	3	135	1.114	2.217	-.3118	-1.544	-.05494	.1674	.03703	.00116	.034
10	3	180	1.177	2.334	-.4656	-1.564	-.8775	.244	.05166	.00161	.040
11	3	225	1.160	1.502	-.4223	-1.139	.08906	.2241	.030216	.00094	.031
12	3	270	1.092	1.929	-.2747	-1.377	-.5103	.1570	.02435	.00076	.028
13	3	315	1.159	2.032	-.4215	-1.332	-.1106	.2244	.04421	.00138	.037
14	4	0	1.107	2.444	-.2686	-1.910	.6913	.1420	.02694	.00084	.029
15	4	45	.9425	3.460	.1210	-1.818	-1.237	-.05251	.02663	.00083	.029
16	4	90	.8894	3.354	.2889	-1.949	-1.084	-.1530	.06311	.00197	.044
17	4	135	1.198	2.774	-.469	-2.059	-.1117	.2335	.05473	.00171	.041
18	4	180	1.315	1.753	-.789	-1.686	.6502	.4112	.06332	.00198	.044
19	4	225	1.240	.8466	-.6424	-1.265	1.269	.3519	.05379	.00168	.041
20	4	270	1.128	.5837	-.3973	-1.238	1.796	.2404	.06872	.00215	.046
21	4	315	1.155	1.618	-.4354	-1.723	1.323	.2477	.04611	.00144	.038
22	5	0	1.075	1.497	-.2376	-1.293	.6283	.1406	.02334	.00073	.027
23	5	45	1.047	1.621	-.1747	-1.436	.8216	.1115	.03665	.00115	.034
24	5	90	1.020	1.457	-.1030	-1.307	.8172	.07345	.02267	.00071	.027
25	5	135	1.066	1.485	-.2161	-1.345	.9310	.1324	.02925	.00092	.030

MODEL:

$$R = R(\alpha,\phi,i) = a_1 + a_2\,\alpha + a_3\phi + a_4\,\alpha\phi + a_5\,\alpha^2 + a_6\phi^2 + a_7 i + a_8 i^2$$

#	NOB	φ	a_1	a_2	a_3	a_4	a_5	a_6	a_7	a_8	SSAR	SSAR/NOB	S
1	750	0, π/2	.6794	1.441	.7469	-1.122	.3047	-.376	-.02038	.1250	28.75138	.0383	.196
2	600	π/9, π/2	.9747	2.569	-.3178	-1.655	-.4	.2019	.00840	.1230	7.399409	.0123	.11

TABLE III: Continued

MODEL:

$R(\alpha,\phi) = a_1 + a_2\,\alpha + a_3\phi + a_4\alpha\phi$ NOB = 32; $\phi = (20^\circ, 90^\circ)$ in degrees

#	G	θ	a_1	a_2	a_3	a_4	SSAR	$\frac{SSAR}{NOB}$	S
1	1	0	.9592	2.312	.0004671	-.02846	.04807	.00150	.039
2	2	0	1.046	1.549	.0003103	-.02406	.1916	.00599	.077
3	2	45	.9421	2.036	.0004025	-.02223	.06523	.00204	.045
4	2	90	.9562	2.042	.0006308	-.02758	.05204	.00163	.040
5	2	135	1.017	1.631	-.0002612	-.0189	.1996	.00624	.079
6	3	0	1.014	2.29	.001759	-.03048	.088704	.00277	.053
7	3	45	.9792	2.498	.0002921	-.02676	.01429	.00045	.021
8	3	90	.9892	2.540	.0003805	-.03173	.04791	.00150	.039
9	3	135	.9854	2.244	.0001678	-.02695	.054587	.00171	.041
10	3	180	1.015	1.900	.00004917	-.02738	.109407	.00342	.058
11	3	225	.987	1.546	.0001395	-.01988	.06176	.00193	.044
12	3	270	.9868	1.676	.0004666	-.02404	.04670	.00146	.038
13	3	315	.9913	1.978	.0001611	-.02325	.075933	.00237	.049
14	4	0	.9802	2.786	.00007109	-.03333	.05232	.00164	.040
15	4	45	1.017	2.848	.0003531	-.03174	.06932	.00217	.047
16	4	90	1.036	2.817	.00008386	-.03401	.1092	.00341	.058
17	4	135	1.023	2.718	-.0003621	-.03593	.08907	.00278	.053
18	4	180	.9841	2.075	6.944×10^{-5}	-.02943	.1802	.00563	.075
19	4	225	.937	1.475	.0005803	-.02208	.1745	.00545	.074
20	4	270	.895	1.473	.00112	-.0215	.1918	.00599	.077
21	4	315	.9296	2.274	.0007028	-.03007	.1317	.00412	.064
22	5	0	.9505	1.808	.000566	-.0226	.04624	.00144	.038
23	5	45	.9397	2.027	.0006874	-.02506	.06249	.00195	.044
24	5	90	.9417	1.861	.0006639	-.02282	.04152	.00130	.036
25	5	135	.9392	1.946	.0006639	-.02348	.06338	.00198	.044

MODEL:

$R(\alpha,\phi) = a_1 + a_2\alpha + a_3\phi + a_4\alpha\phi$ for S = #1,2,3,4

#	G	θ	θ_1	θ_2	θ_3	θ_4	ϑ	S	SSAR	$\frac{SSAR}{NOB}$
1	1	0	.9370	1.326	.000813	-.01356	$0^\circ,90^\circ$	.166	1.09977	.02749
2	1	0	.9592	2.312	.0004671	-.02846	$20^\circ,90^\circ$	.039	.04807	.00150
3	1	0	.9592	2.312	.02675	-1.631	$\pi/9,\pi/2$	.039	.04807	.00150
4	1	0	.6299	1.498	2.744	1.906	$\pi/9,\pi/2$	.298	2.8526	.08914

TABLE III: Continued

MODEL:

$$R(\alpha,\phi) = a_1 + a_2\,\alpha + a_3\phi + a_4\,\alpha\phi; \quad NOB = 32; \quad \phi = \left(\frac{\pi}{9}, \frac{\pi}{2}\right)$$

#	G	θ	a_1	a_2	a_3	a_4	SSAR	$\frac{SSAR}{NOB}$	S
1	1	0	.9592	2.312	.02675	-1.631	.04807	.00152	.039
2	2	0	1.046	1.549	-.01777	-1.379	.1916	.00599	.077
3	2	45	.9421	2.036	-.02306	-1.274	.06523	.00204	.045
4	2	90	.9562	2.042	.03613	-1.580	.05204	.00163	.040
5	2	135	1.017	1.631	-.01496	-1.083	.1996	.00624	.079
6	3	0	1.014	2.29	.01007	-1.747	.088704	.00277	.053
7	3	45	.9792	2.498	.01672	-1.533	.01429	.00045	.021
8	3	90	.9892	2.540	.02178	-1.818	.04791	.00150	.039
9	3	135	.9854	2.244	.009602	-1.544	.054587	.00171	.041
10	3	180	1.015	1.900	.002813	-1.554	.109407	.00342	.058
11	3	225	.987	1.546	.007998	-1.139	.06176	.00193	.044
12	3	270	.9896	1.676	.02673	-1.377	.04670	.00146	.038
13	3	315	.9913	1.978	.009227	-1.332	.075933	.00237	.049
14	4	0	.9802	2.786	.004051	-1.910	.05232	.00164	.040
15	4	45	1.017	2.848	.02021	-1.818	.06932	.00217	.047
16	4	90	1.036	2.817	-.004825	-1.949	.1092	.00341	.058
17	4	135	1.023	2.718	-.02077	-2.059	.08907	.00278	.053
18	4	180	.9841	2.075	.0003889	-1.686	.1802	.00563	.075
19	4	225	.937	1.475	.03325	-1.265	.1745	.00545	.074
20	4	270	.895	1.473	.06415	-1.238	.1918	.00599	.077
21	4	315	.9296	2.274	.04025	-1.723	.1317	.00412	.064
22	5	0	.9505	1.808	.03242	-1.293	.04624	.00144	.038
23	5	45	.9397	2.027	.03938	-1.436	.06249	.00195	.044
24	5	90	.9417	1.861	.03803	-1.307	.04152	.00130	.036
25	5	135	.9392	1.946	.03803	-1.345	.06338	.00198	.044

TABLE III: Continued

MODEL:

$$R(\alpha,\phi) = a_1 + a_2\,\alpha + a_3\phi + a_4\,\alpha\phi \qquad \phi = \left[0^\circ, 90^\circ\right] \qquad NOB = 40$$

#	G	θ	a_1	a_2	a_3	a_4	SSAR	$\frac{SSAR}{NOB}$	S
1	1	0	.937	1.326	.000813	-.01356	1.09977	.02749	.166
2	2	0	.653	2.12	.00251	-.03351	3.062987	.07657	.277
3	2	45	.9494	1.032	.0002949	-.007027	.9678825	.02420	.156
4	2	90	.9366	1.256	.000949	-.01581	.9175	.02294	.151
5	2	135	.9809	.8464	.0002979	-.007061	.9164	.02291	.151
6	3	0	.9241	1.784	.001587	-.02323	1.7103	.04276	.207
7	3	45	.9588	1.283	.0006101	-.008338	1.4410	.03602	.190
8	3	90	.962	1.34	.0008147	-.0136	1.5602	.03901	.198
9	3	135	.9669	1.114	.0004576	-.009811	1.2704	.03176	.178
10	3	180	.9273	1.616	.001427	-.0234	1.3317	.03329	.182
11	3	225	.973	.8927	.0003599	-.01006	.5800	.01450	.120
12	3	270	.961	1.052	.0008718	-.01473	.6822	.01706	.131
13	3	315	.9689	1.026	.0005124	-.00846	.9979	.02495	.158
14	4	0	.9631	1.495	.0003428	-.01377	1.6406	.04102	.203
15	4	45	.9701	1.574	.001077	-.01249	1.8999	.04750	.218
16	4	90	.989	1.676	.0006406	-.01682	1.7057	.04264	.206
17	4	135	.9832	1.499	.0002568	-.01751	1.6877	.04219	.205
18	4	180	.9627	1.202	.0003457	-.01625	1.0000	.02500	.158
19	4	225	.9515	1.023	.0003774	-.01539	.5351	.01338	.116
20	4	270	.9513	1.159	.000267	-.01705	.5505	.01376	.117
21	4	315	.9543	1.308	.0003361	-.01551	.9706	.02426	.156
22	5	0	.9508	1.121	.000573	-.01225	.3912	.01478	.122
23	5	45	.9526	1.103	.0004991	-.01106	.8005	.02001	.141
24	5	90	.9474	1.088	.0005916	-.0117	.6466	.01616	.127
25	5	135	.9481	1.085	.0005366	-.01045	.7126	.01782	.133

TABLE III: Continued

MODEL:

$$R(\alpha,\phi) = 1 + a_1 \alpha^2 + a_2 \alpha + a_3 \alpha\phi$$

$$\phi = \left[\frac{\pi}{9}, \frac{\pi}{2}\right] \qquad NOB = 32$$

#	G	θ	a_1	a_2	a_3	SSAR	$\frac{SSAR}{NOB}$	S
1	1	0	.4042	2.035	-1.562	.04602	.00144	.038
2	2	0	-1.401	2.261	-1.424	.1323	.00413	.064
3	2	45	1.151	1.399	-1.214	.0335	.00105	.032
4	2	90	.1123	1.881	-1.487	.0547	.00171	.041
5	2	135	-.1811	1.750	-1.122	.1989	.00622	.079
6	3	0	-.9797	2.741	-1.721	.06124	.00191	.044
7	3	45	.1032	2.401	-1.490	.0153	.00048	.022
8	3	90	-.4671	2.710	-1.782	.0422	.00132	.036
9	3	135	.08758	2.170	-1.519	.0548	.00171	.041
10	3	180	-.8242	2.288	-1.556	.0891	.00278	.053
11	3	225	.1132	1.465	-1.119	.0617	.00193	.044
12	3	270	-.4966	1.853	-1.309	.04097	.00128	.036
13	3	315	-.08589	1.992	-1.308	.07582	.00237	.049
14	4	0	.6645	2.454	-1.899	.03963	.00124	.035
15	4	45	-1.253	3.422	-1.766	.02908	.00091	.030
16	4	90	-1.095	3.374	-1.961	.0778	.00243	.049
17	4	135	-.1098	2.824	-2.112	.08947	.00280	.053
18	4	180	.6288	1.768	-1.685	.1688	.00527	.073
19	4	225	1.233	.7902	-1.179	.1331	.00416	.064
20	4	270	1.740	.4652	-1.072	.11216	.00351	.059
21	4	315	1.280	1.550	-1.619	.08738	.00273	.052
22	5	0	.6371	1.410	-1.209	.0375	.00117	.034
23	5	45	.8196	1.525	-1.334	.0471	.00147	.038
24	5	90	.8109	-1.367	-1.209	.0261	.00082	.029
25	5	135	.9186	1.400	-1.247	.0427	.00133	.036

Regression parameter fits were also made using all the data of all the different geometries. The model used was of the following form:

$$R(\alpha,\phi,\xi) = a_1 + a_2\,\alpha + a_3\phi + a_4\,\alpha\phi + a_5\,\alpha^2 + a_6\phi^2 + a_7\xi + a_8\xi^2$$

where ξ is an eccentricity factor defined as the area of voids included on the side of the detector of a diameter line on the sample which is parallel to the face of the detector, over the total void area (see Figure 3). The area of a circular void delimited by such a diameter line can be shown to be given by:

$$A = 1/2\ R^2 - E\sqrt{R^2-E^2} - R^2 \sin^{-1}(E/R)$$

where R is the radius of the circular void and $E = C \sin(1/2-\theta-\phi)$; here where C is the distance from the center of the sample to the center of the void. Theta (θ) and phi (ϕ) are respectively the sample orientation and the detector angles as defined earlier in this report. Table (1) which was read in the computer program under the name MA, shows the data for C's and D's for the different samples used in this series of experiments.

The above response function model was fitted with its eight parameters to the data for the sixteen samples, for both detector angle range (0,1/2) and (1/9, 1/2) radians. The values obtained for the parameters in the second case are given by the following set of coefficients:

$a_1 = 0.9747$
$a_2 = 2.569$
$a_3 = -.3178$
$a_4 = -1.655$
$a_5 = -.40$
$a_6 = .2019$
$a_7 = .008405$
$a_8 = .1280$

Again it can be seen that a_1, the constant factor is close to one. The parameter in the eccentricity (ξ) term is very small, indicating little linear dependence on (ξ) as we defined it. However, a stronger dependence is shown on ξ^2 by a_8.

CONCLUSION

While it is possible to detect voids using scattered neutrons, it is concluded that an accurate measurement of the void fraction with this technique is not readily possible. It is seen that the response function is very much a function of the geometry of the voids, and the orientation of the sample. However, it can be seen from both the figures and the regression analysis parameters that the response does not depend very much on the scattering angle as long as this does not get in the transmission range. The isotropy of the response is more obvious in the many holes samples which are more symmetrical.

Since these experiments show a strong influence of the void distribution on the neutron scattering in a static case, we can extrapolate that the results could not be better in a dynamic situation where the void distribution is continuously changing.

These measurements were made with thermal neutrons, for which the mean free path is much smaller than the size of the sample, therefore the neutrons counted have usually had more than one interaction in the sample. However, the same problem will be encountered if one was to go to bigger sample section and higher energy neutrons since the mean free path could still be smaller than the size of the sample. It should also be realized when comparing the counts at different angle (Ø) that the average distance that the neutrons have to travel through the sample without being absorbed after having been scattered is not the same.

The regression analysis results show that for a given void geometry (fix G and θ) the response function can be approximated by:

$$Res = 1 + a\alpha$$

or the void fraction is given by:

$$\alpha = \frac{Res - 1}{a}$$

where a is an emperical constant depending on the geometry of the voids.

We conclude that the void fraction can be correlated to the thermal neutron scattering in the case of uniformly distributed voids like bubble flow or in the case of known void distributions, like in laminar flow.

APPENDIX 1

The total count rate varies with time. This is due to both variations in power of the reactor due to oscillations in its control system and the statistical nature of the fission process itself. The fluctuations in the full count rate of the beam port were therefore investigated. This is of upmost importance to this experiment since it imposes a limitation on our results. We have to compare count rates for different samples and different orientations which were measured at different times. The full count rate was measured about once every 2 to 3 hours during experimentation and then used to normalize the results in the transmittance function. For the response function measurements made at some small intervals of time to each other were directly compared. These results therefore rely on the fact that the total power of the beam to be nearly constant. A more sophisticated experiment should involve real time monitoring of the full beam and constant normalization.

Table (4) shows two series of count rates measured consecutively for periods of 100 seconds in the first series and for periods of 1,000 seconds in the second series. The standard deviation (S) is computed for both series from its definition:

$$S = \sqrt{\frac{\sum_{i=1} (\chi_i - \chi)^2}{n-1}}$$

It is then compared with the error (E) which is given by:

$$E = \sqrt{R/t}$$

This error (E) simply follows from the result that $\sqrt{N}$ is the standard deviation for a normal distribution where N is total number of counts.

TABLE 4: Fluctuation of Beam Port Intensity

SERIES A (T = 100 sec.)

Rate	Dev.	$(\text{Dev.})^2$
841	0	0
838	3	9
836	5	25
834	7	49
839	2	4
839	2	4
835	6	36
845	4	16
847	5	25
847	5	25
842	1	1
839	1	1
841	0	0
841	0	0
843	2	5
846	5	25
843	2	4
Mean: 841	3	228 TOTAL

$$S = \sqrt{\frac{228}{17-1}} = 3.775$$

$$E = \sqrt{R/t} = \sqrt{\frac{841}{100}} = 2.9$$

SERIES B (T = 1000 sec.)

Rate	Dev.	$(\text{Dev.})^2$
872.2	.67	.4489
871.5	1.37	1.8769
872.5	.37	.1369
872.6	.27	.0729
874.1	1.23	1.5129
873.7	.83	.6889
875.8	2.93	8.5849
873.6	.73	.5329
869.8	3.07	9.4249
Mean: 872.87	1.27	23.29 TOTAL

$$S = \sqrt{\frac{23.28}{9-1}} = 1.706$$

$$E = \sqrt{R/t} = \sqrt{\frac{872.87}{1000}} = .934$$

For the series of 100 second periods rates S was found to be 3.775 while E was 2.9. The 1000 second periods rates series S was found to be 1.706 while E was .934. The standard deviation computed from its definition is larger in both cases than what is found by assuming a normal distribution. This indicates that the intensity distribution might not be necessarily a normal distribution but might also be a result of fluctuations in power of the whole reactor. Therefore, real time monitoring is advisable, just increasing the counting times might not improve the results as it would if it were a real normal distribution. However, one should realize the limitation of this indication from Table (4) due to its small number of samples. S and E would only be theoretically equal for a large number of samples. It can be seen for the 100 second period series that S and E are closer than for the other series. The 100 second period series has more samples than the other series. However, both S and E are much smaller for the longer counting time (T) of 1000 seconds.

APPENDIX 2

Following is four sets of graphs for the data obtained using a cylindrical cadmium sleeve over our BF_3 detector. Figures 5 to 23 are the transmittance (background corrected count rate for given parameters normalized by full beam count rate) versus the scattering angle (Ø). Figures 24 to 48 are the Transmittance (T) versus the void fraction (α) where samples of the same geometry are grouped together for the same orientation. Figures 49 to 67 are the Response (count rate at given parameter normalized by the count rate for a non-voided sample and the same scattering angle Ø) versus scattering angle Ø for all samples and all orientations. Figures 68 to 91 are the Response (R) versus the void fraction (α). In these figures each graph has samples of the same geometry (G) and all for the same orientation Θ.

These graphs were generated using the Versatec Plotter of the McMaster University computing center. A fortran program called PLOTER was written to process the data and produce the graphs. It has the ability to sort the data to plot it against different parameters according to a prescribed order.

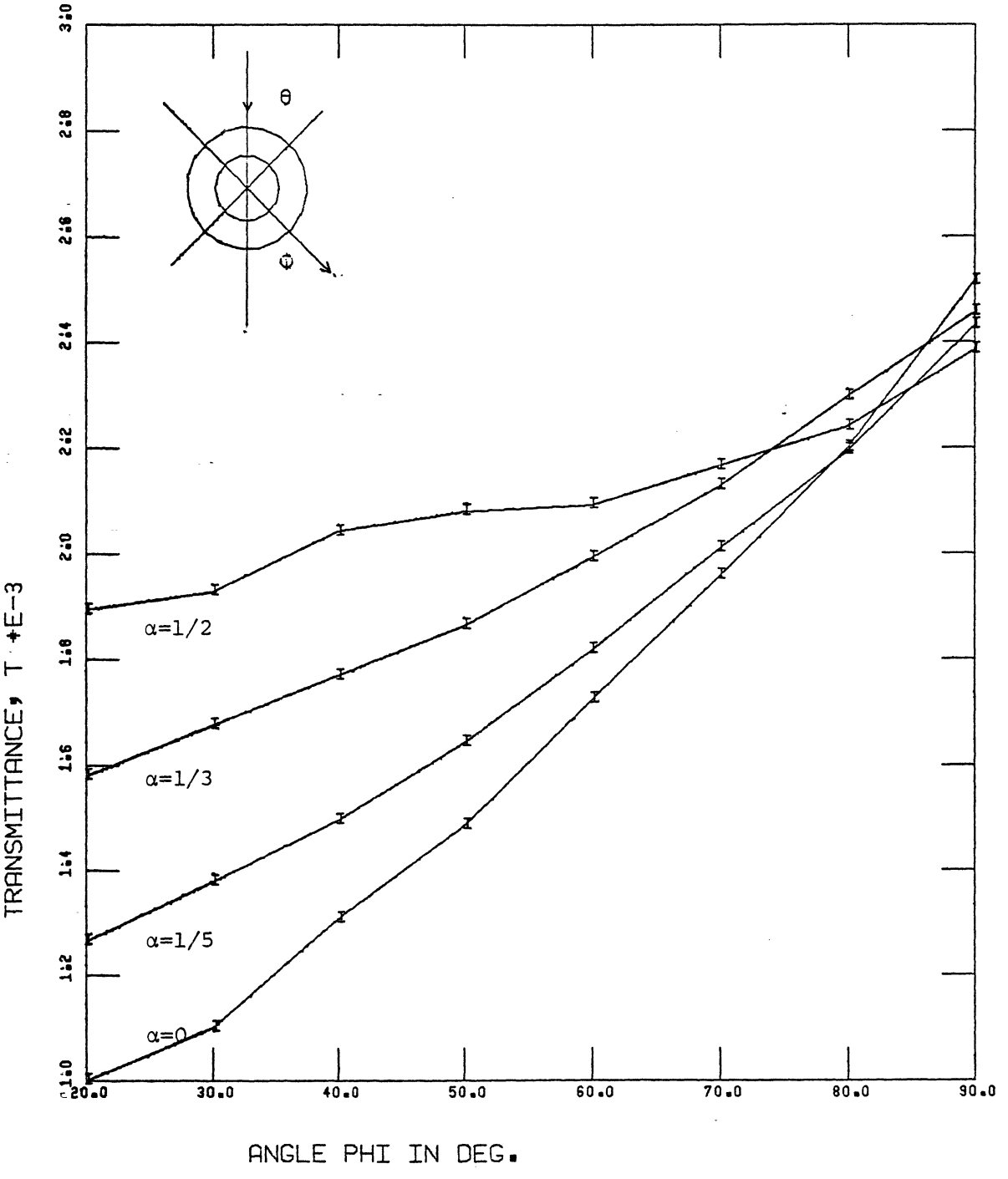

FIGURE 5: Transmittance versus Ø
For Samples #1,2,3,4

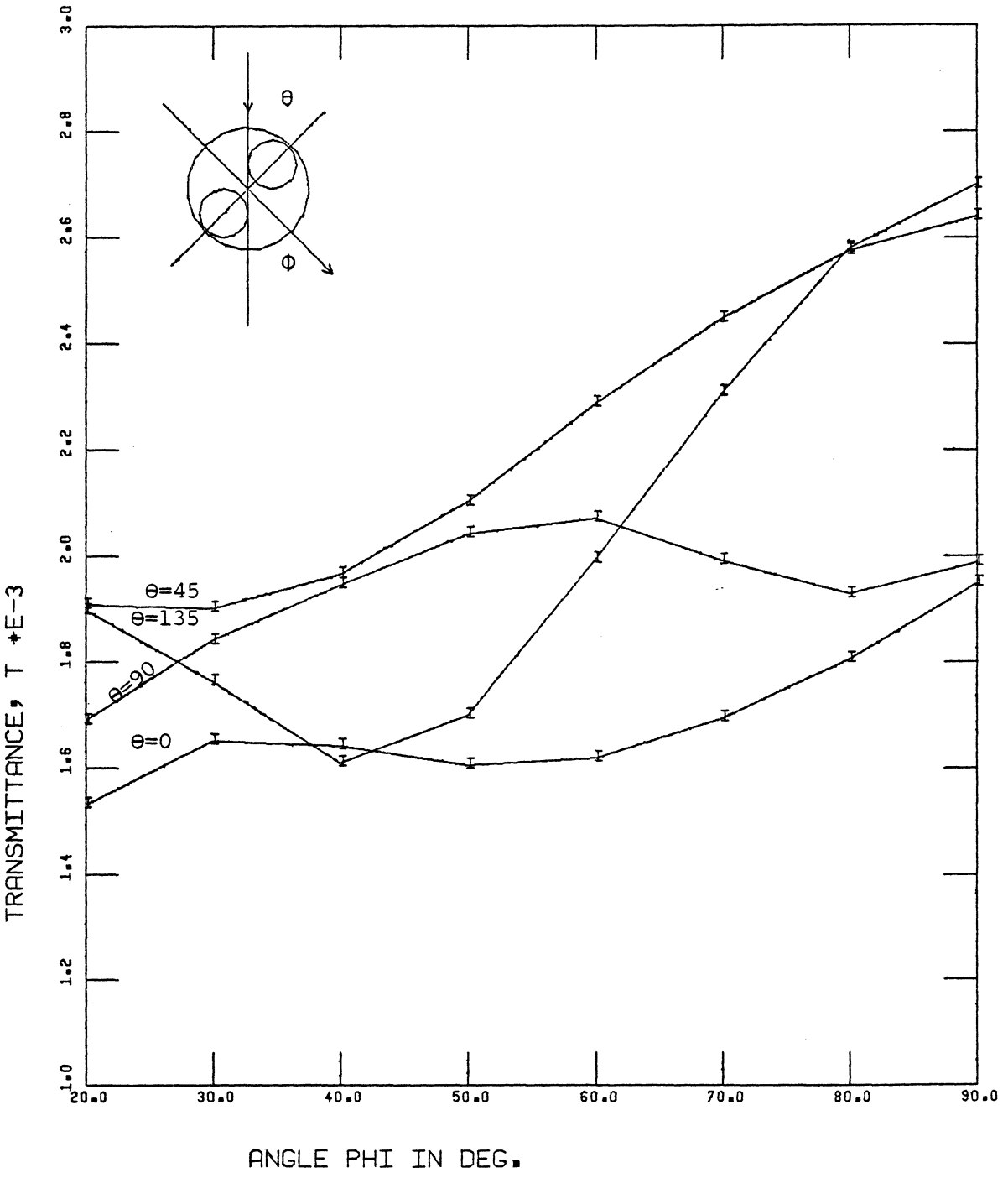

FIGURE 6: Transmittance versus Ø
For Samples #5; θ = 0,45,90,135°

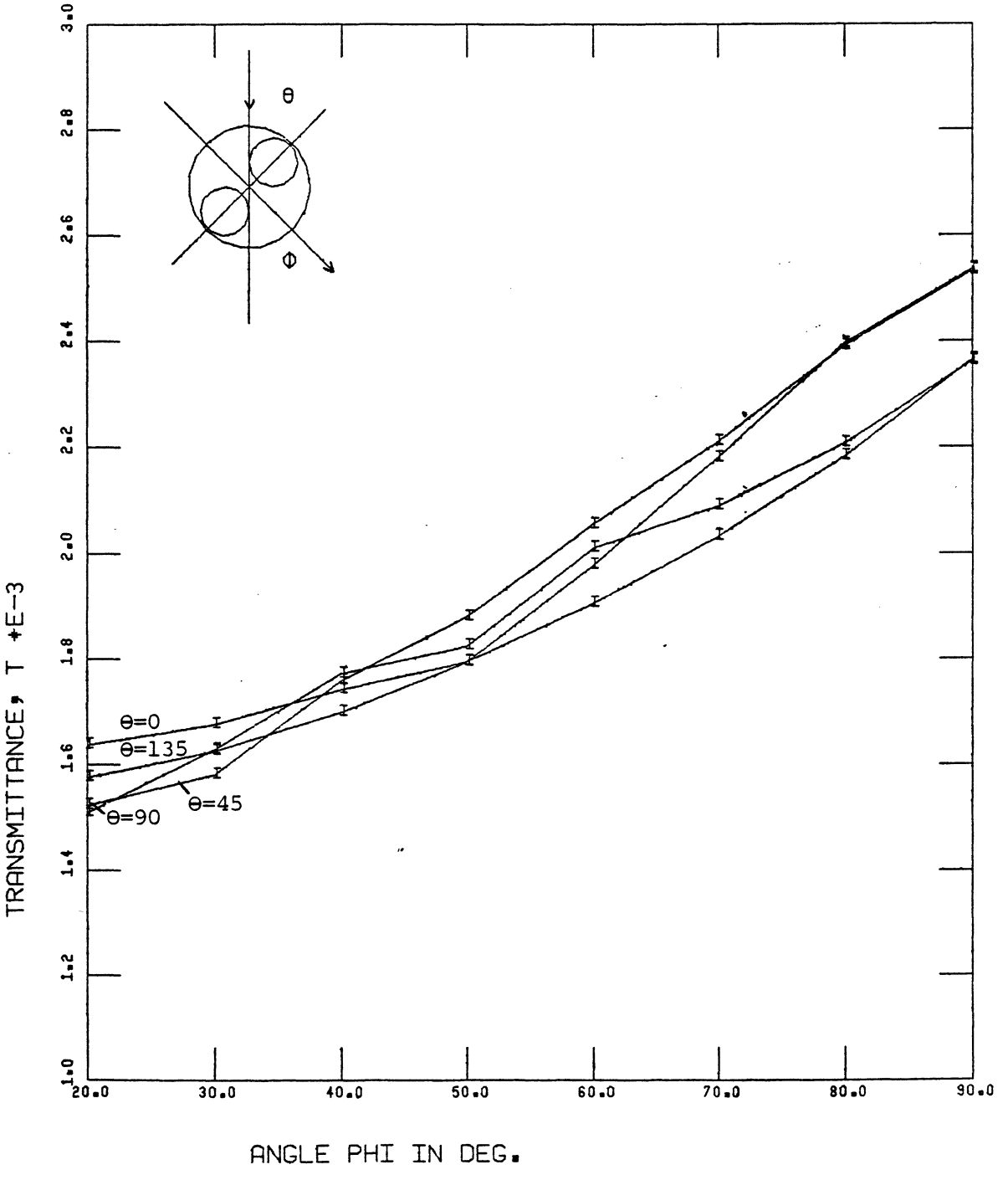

FIGURE 7: Transmittance versus Ø
For Sample #6; θ = 0,45,90,135°

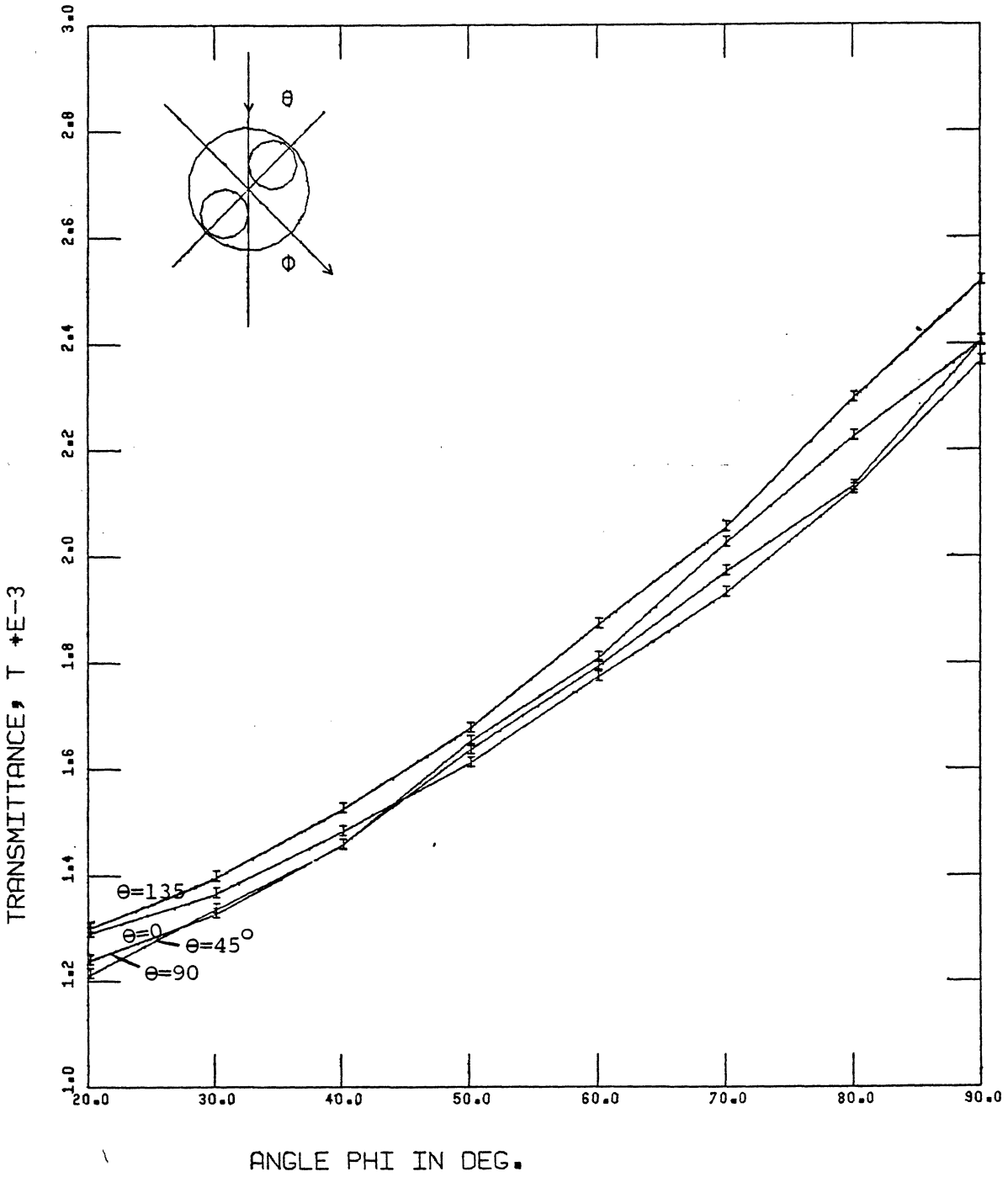

FIGURE 8: Transmittance versus Ø
For Sample #7; θ = 0,45,90,135°

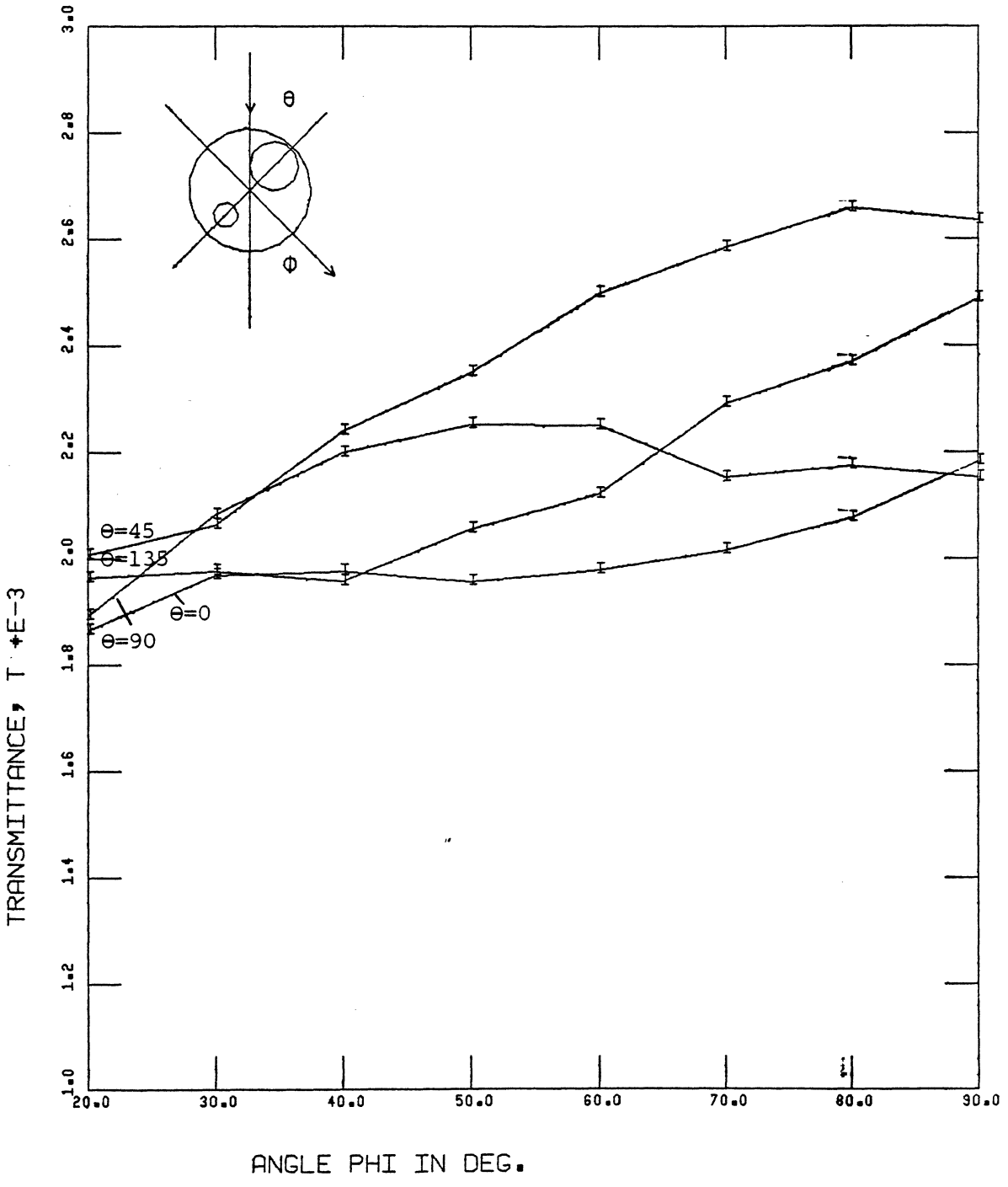

FIGURE 9: Transmittance versus Ø
For Sample #8; θ = 0,45,90,135°

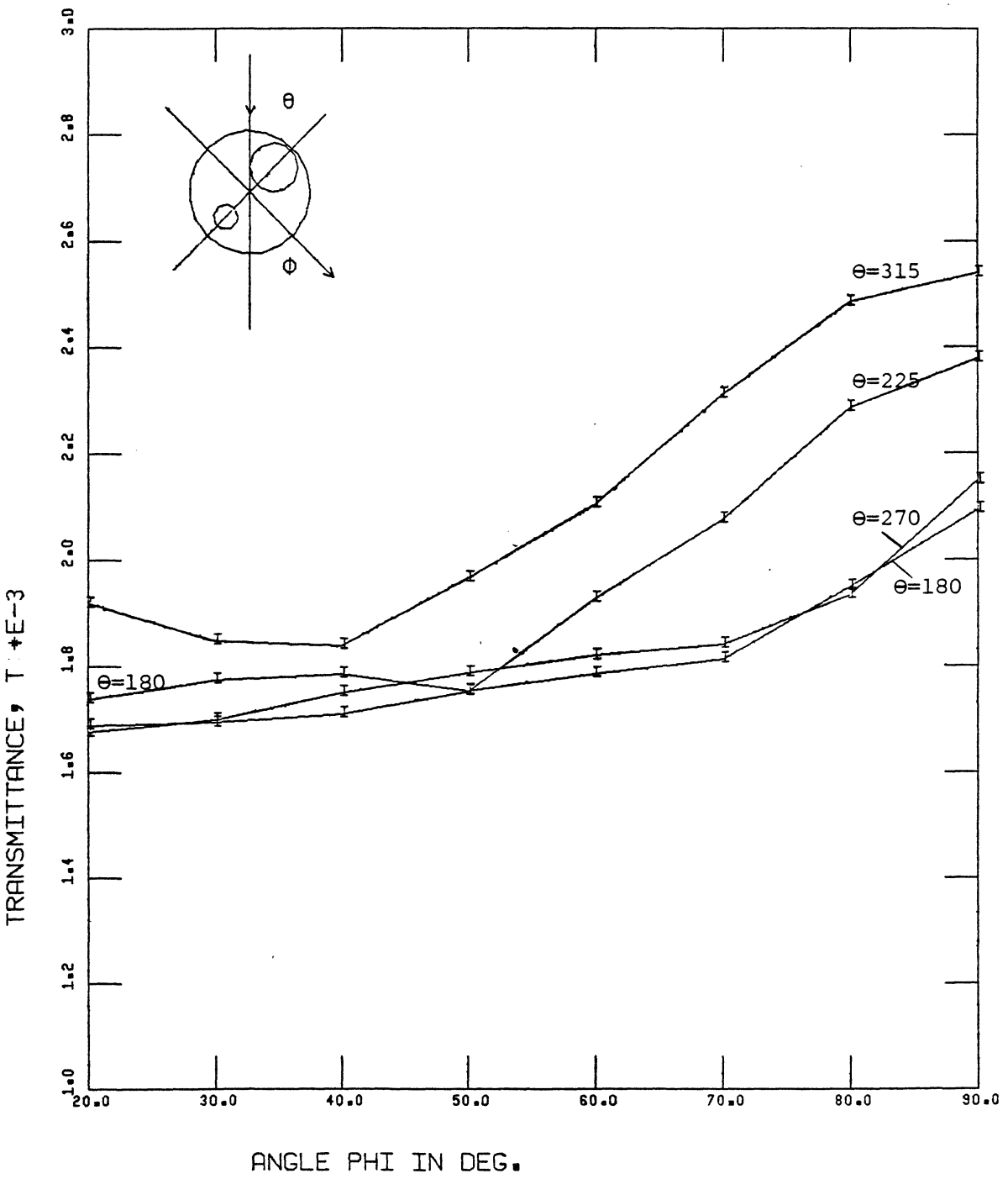

FIGURE 10: Transmittance versus Ø
For Sample #8; θ = 180,225,270,315°

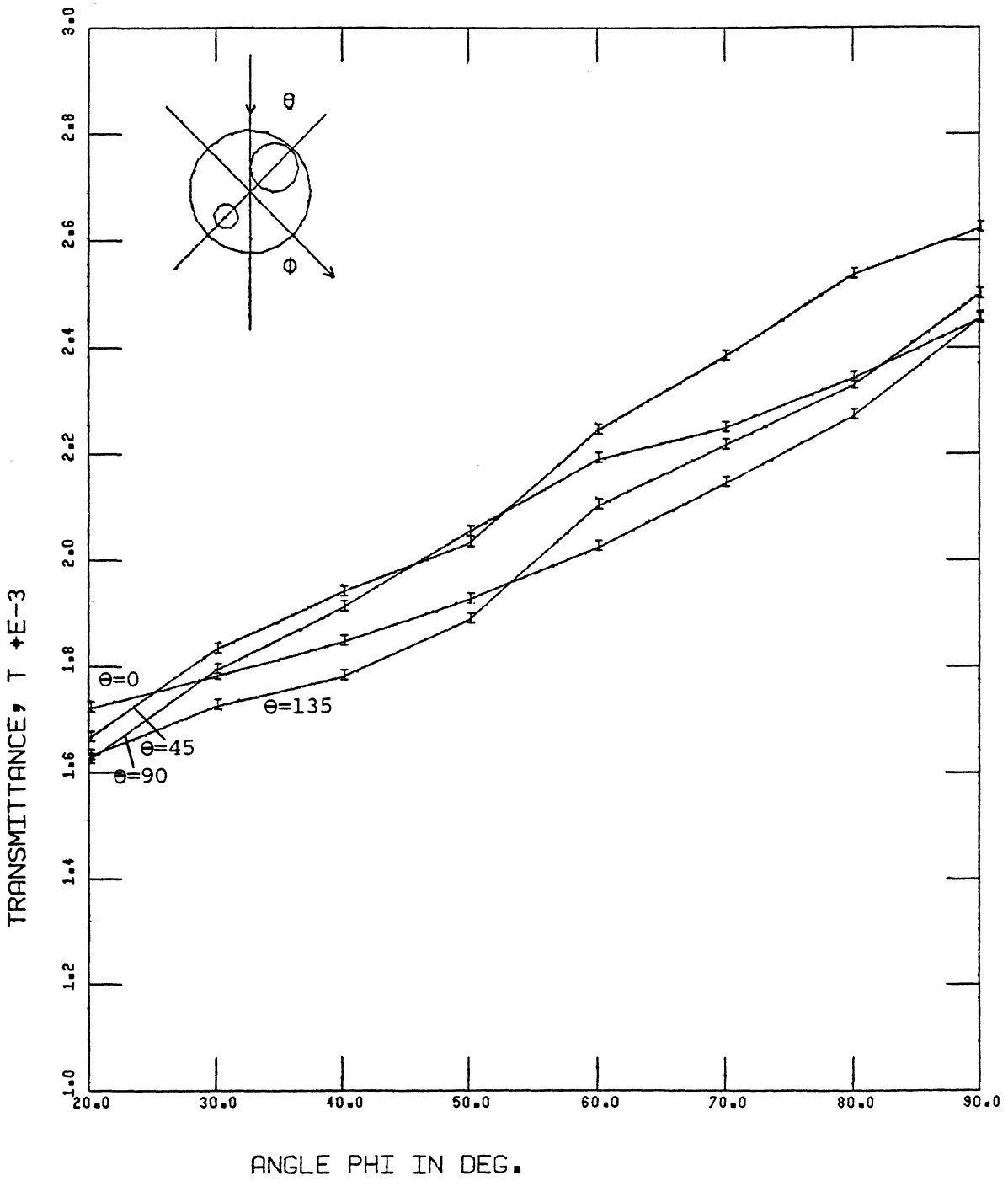

FIGURE 11: Transmittance versus Ø
For Sample #9, θ = 0,45,90,135°

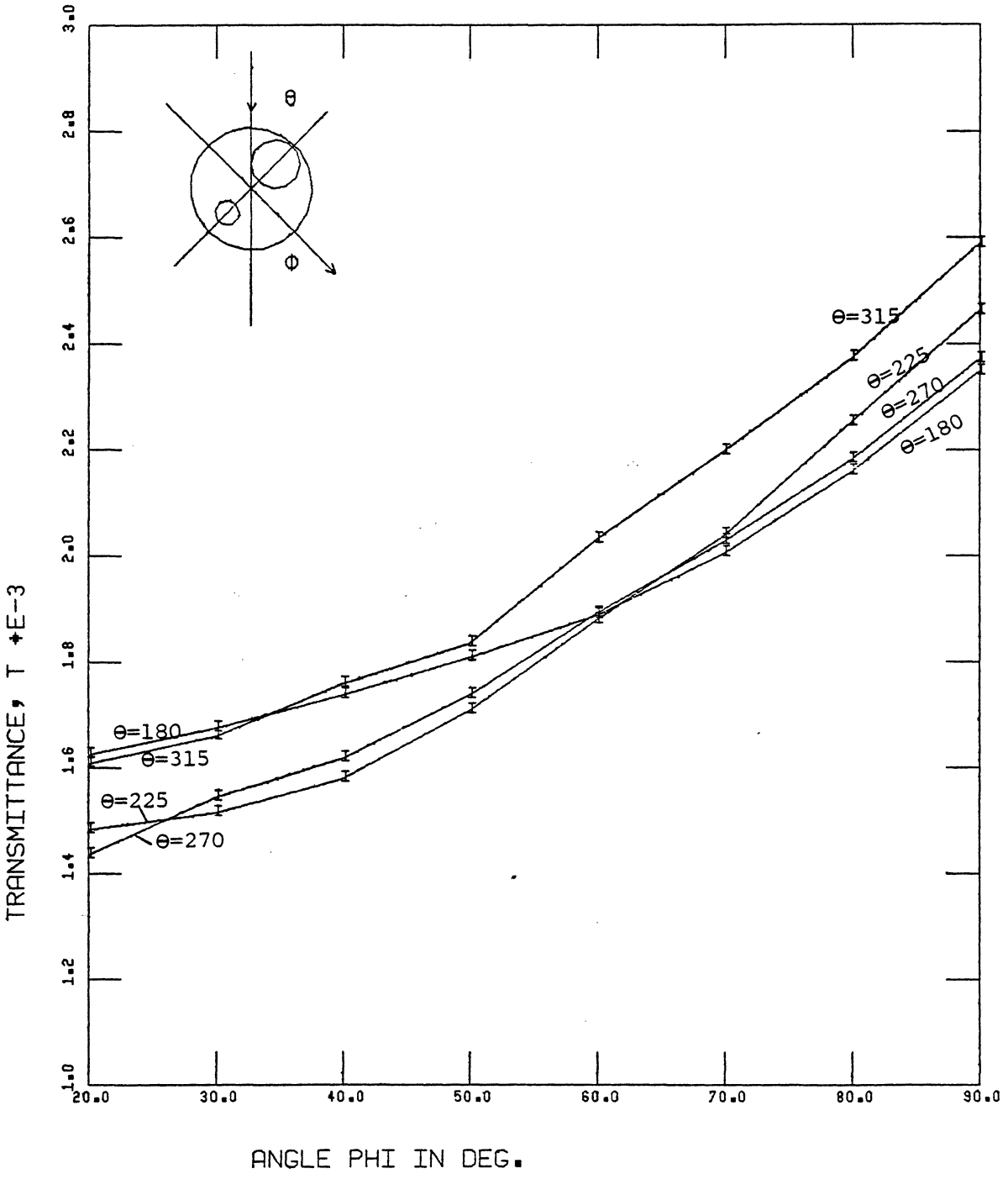

FIGURE 12: Transmittance verus Ø
For Sample #9; θ = 180,225,270,315°

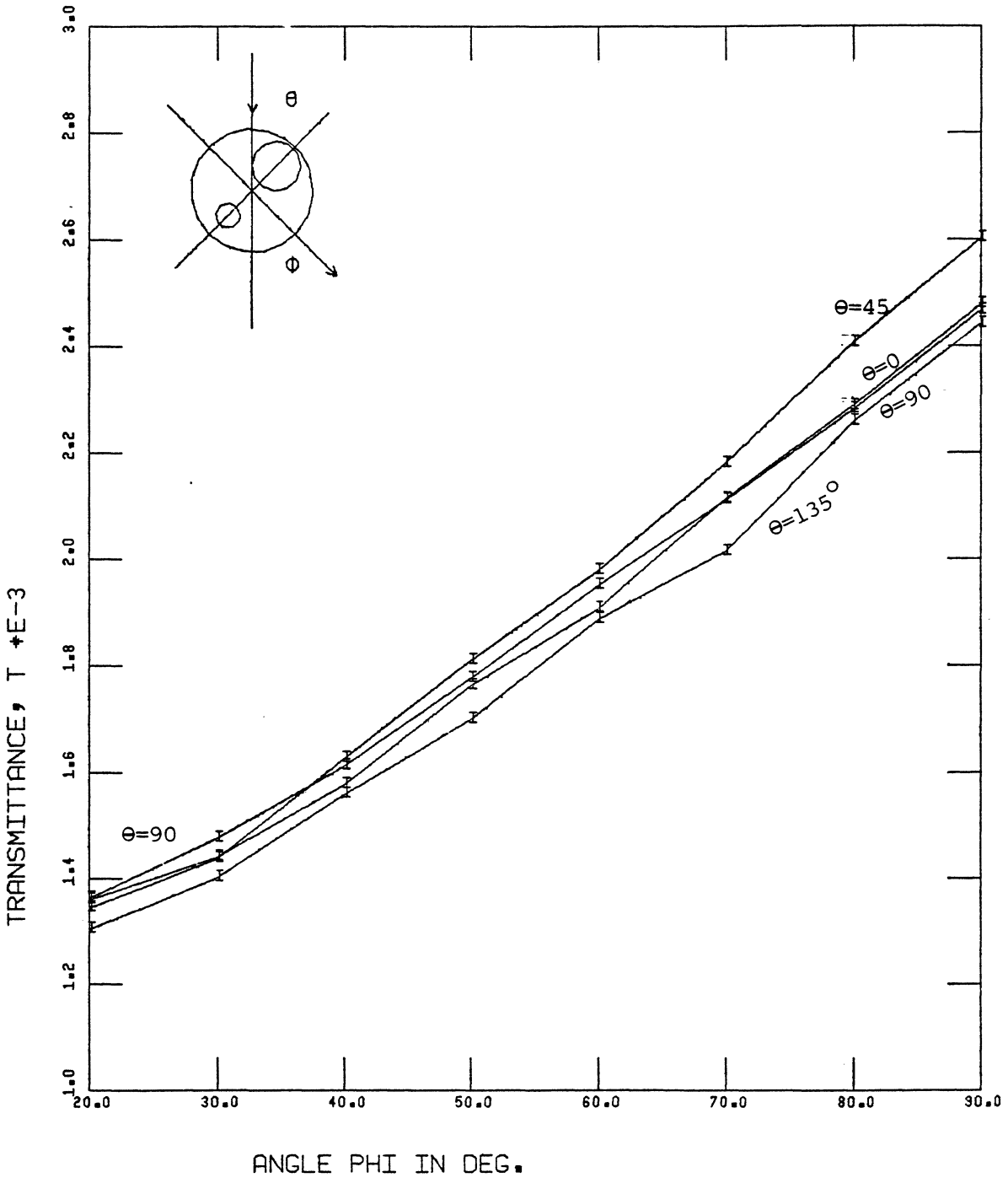

FIGURE 13: Transmittance versus Ø
For Sample #10; Θ = 0,45,90,135°

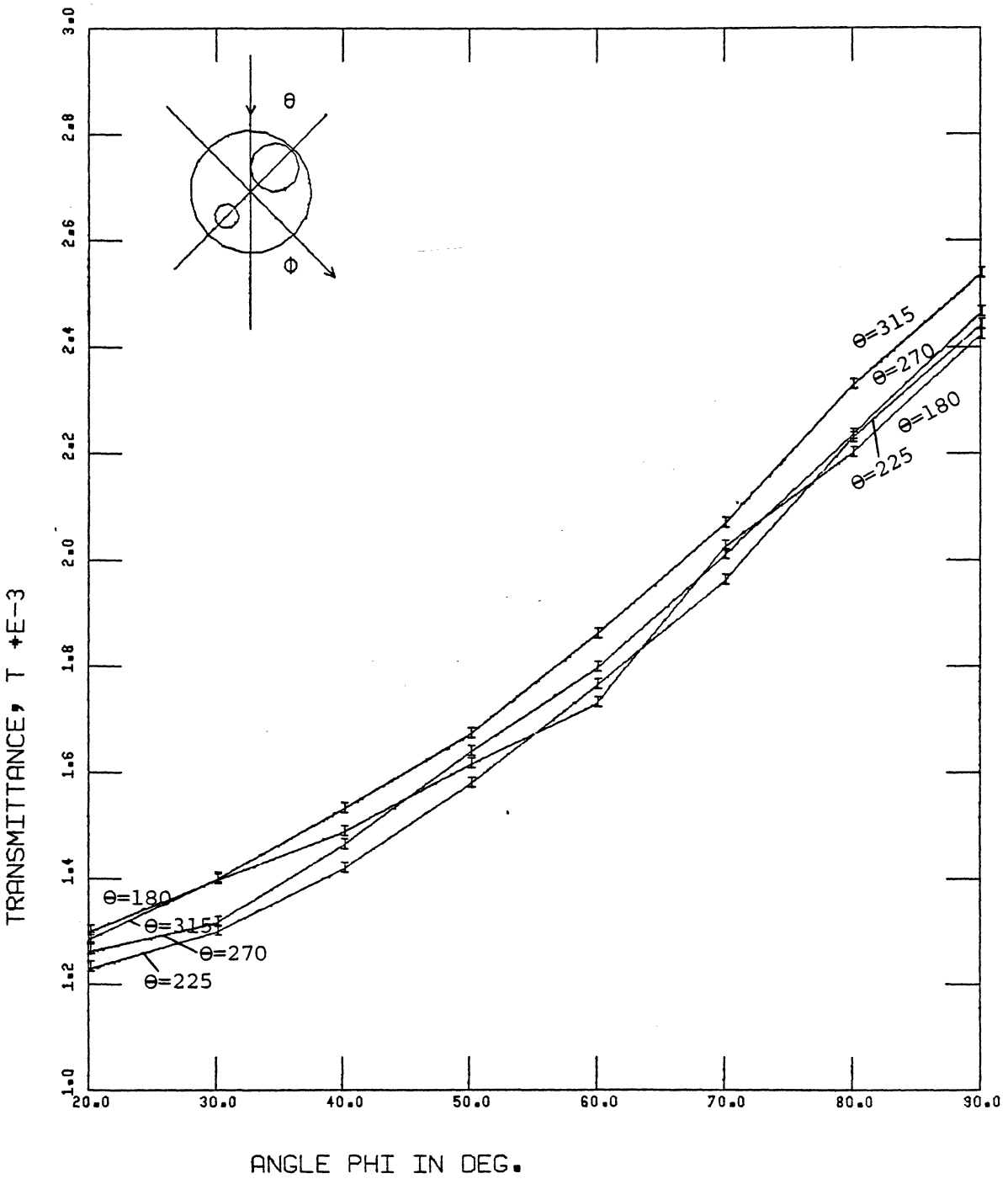

FIGURE 14: Transmittance versus Ø
For Sample #10, Θ = 180,225,270,315°

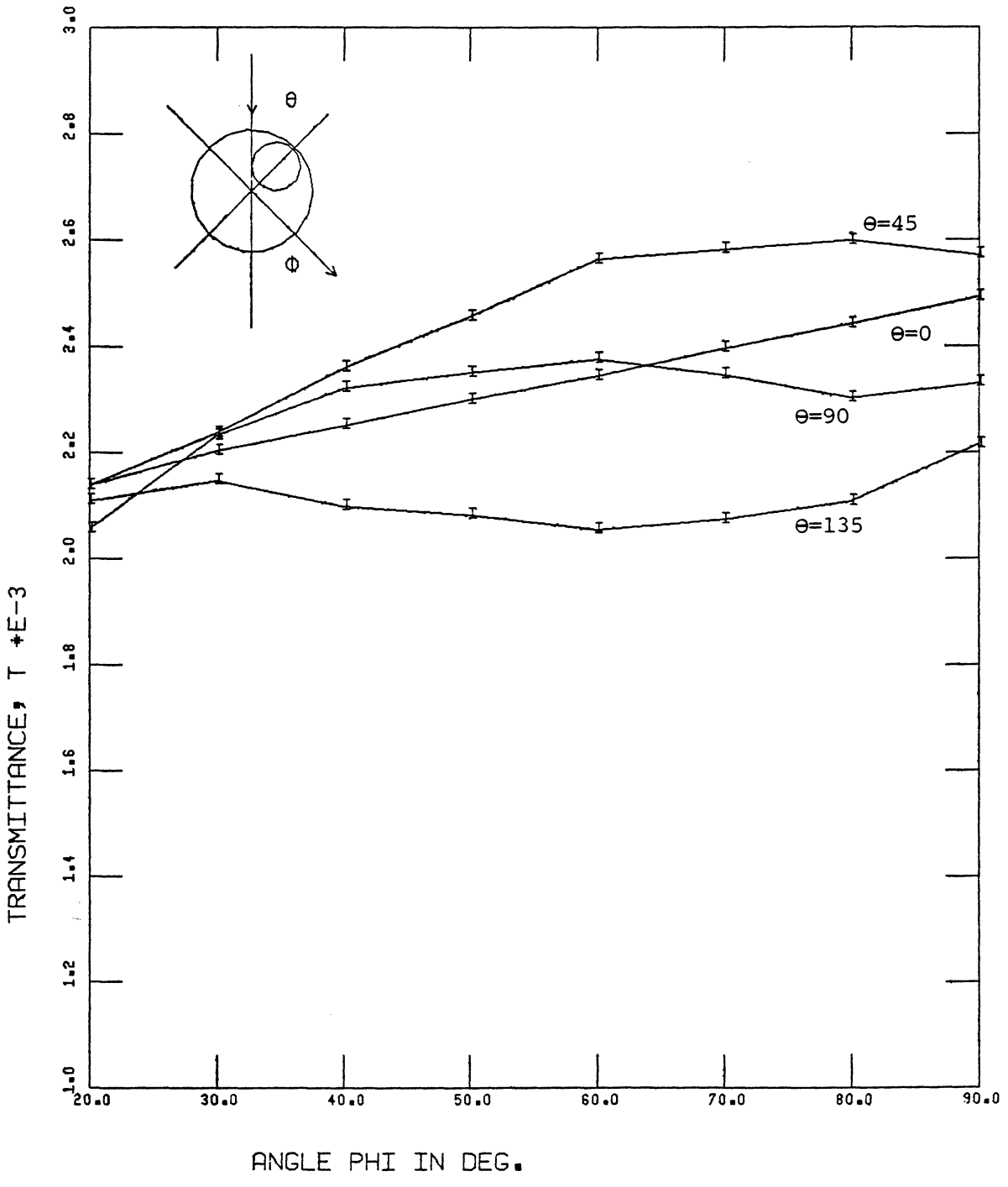

FIGURE 15: Transmittance versus Ø
For Sample #11, θ = 0,45,90,135°

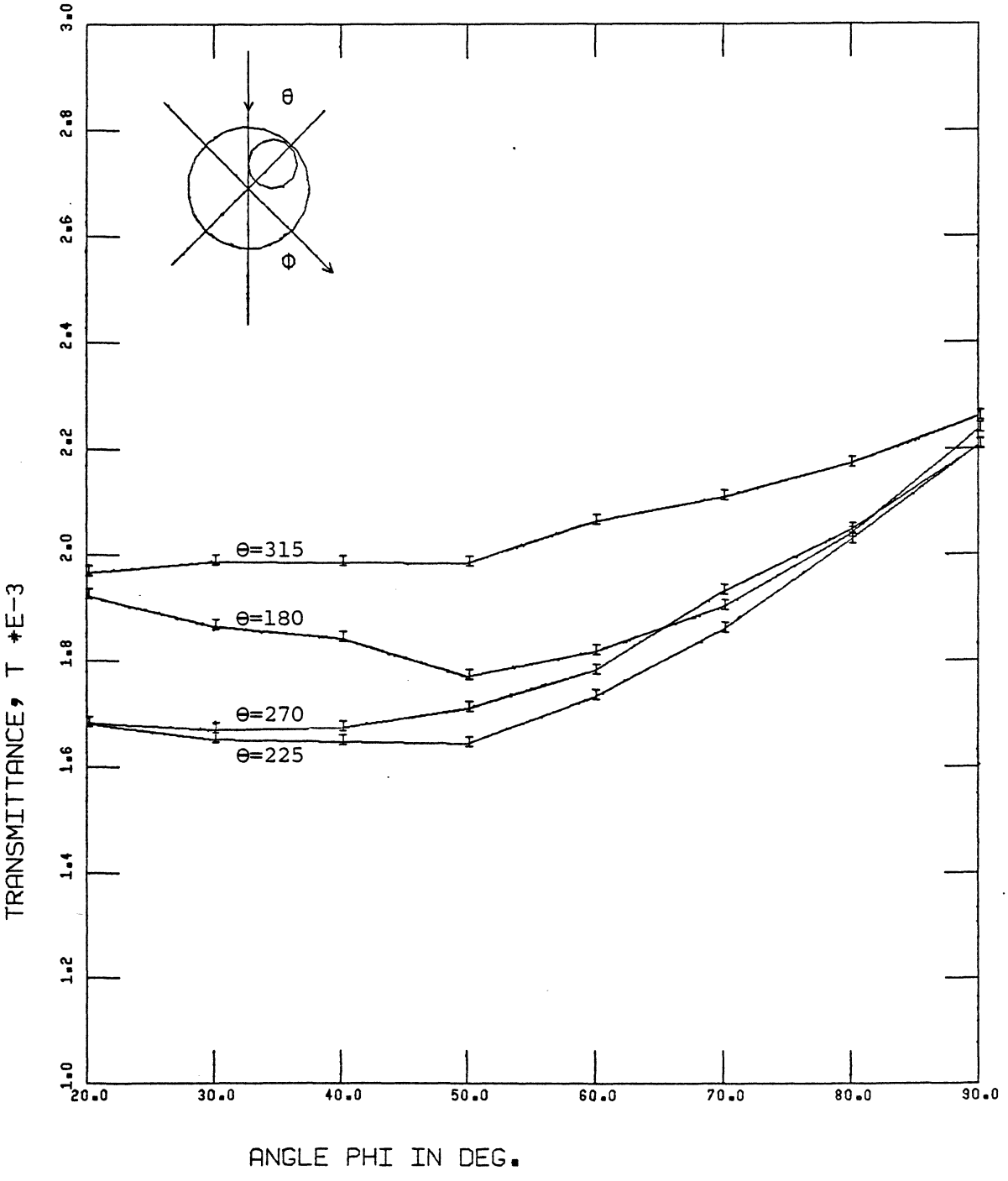

FIGURE 16: Transmittance versus Ø
For Sample #11; Θ = 180,225,270,315°

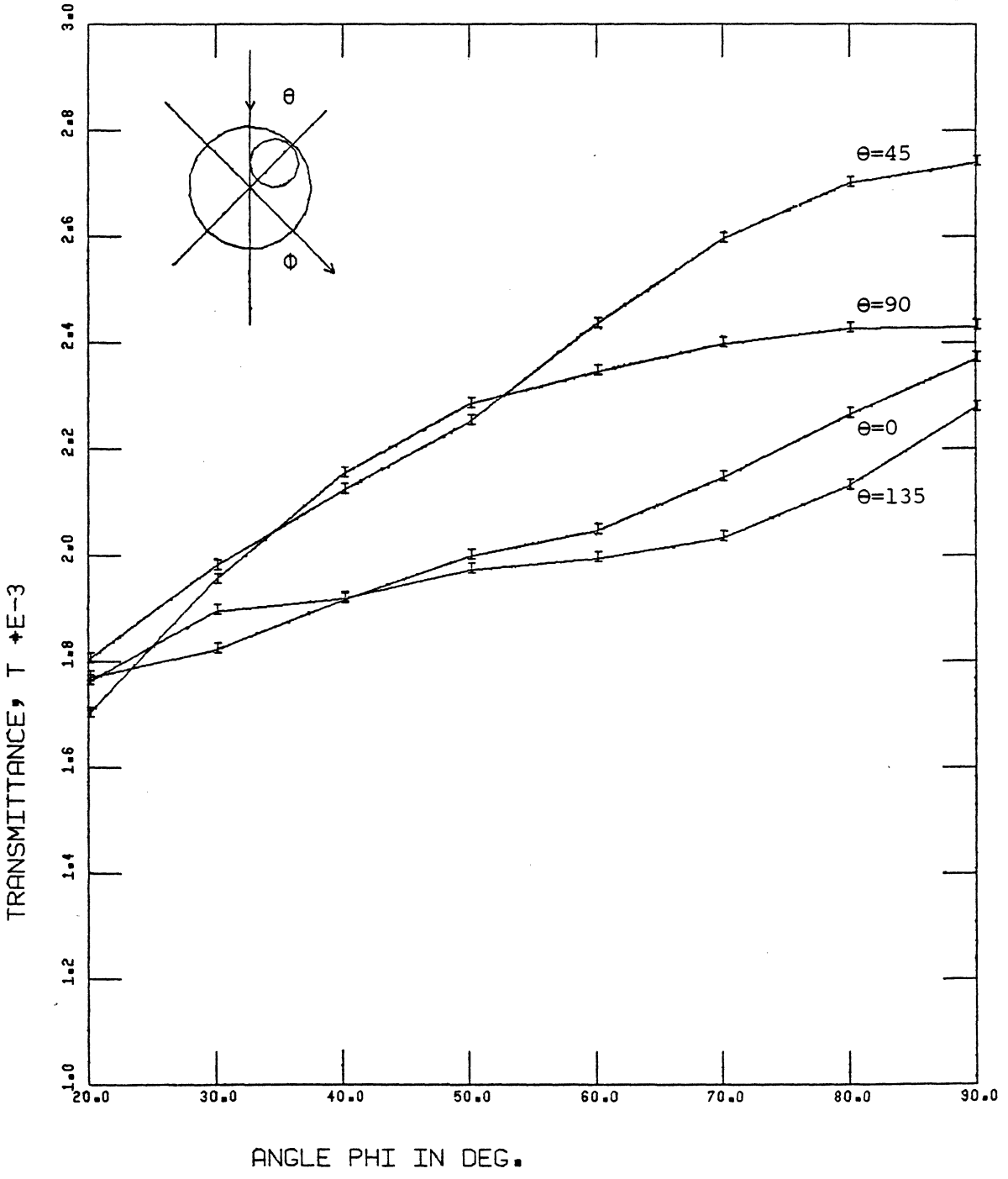

FIGURE 17: Transmittance versus Ø
For Sample #12; θ = 0,45,90,135°

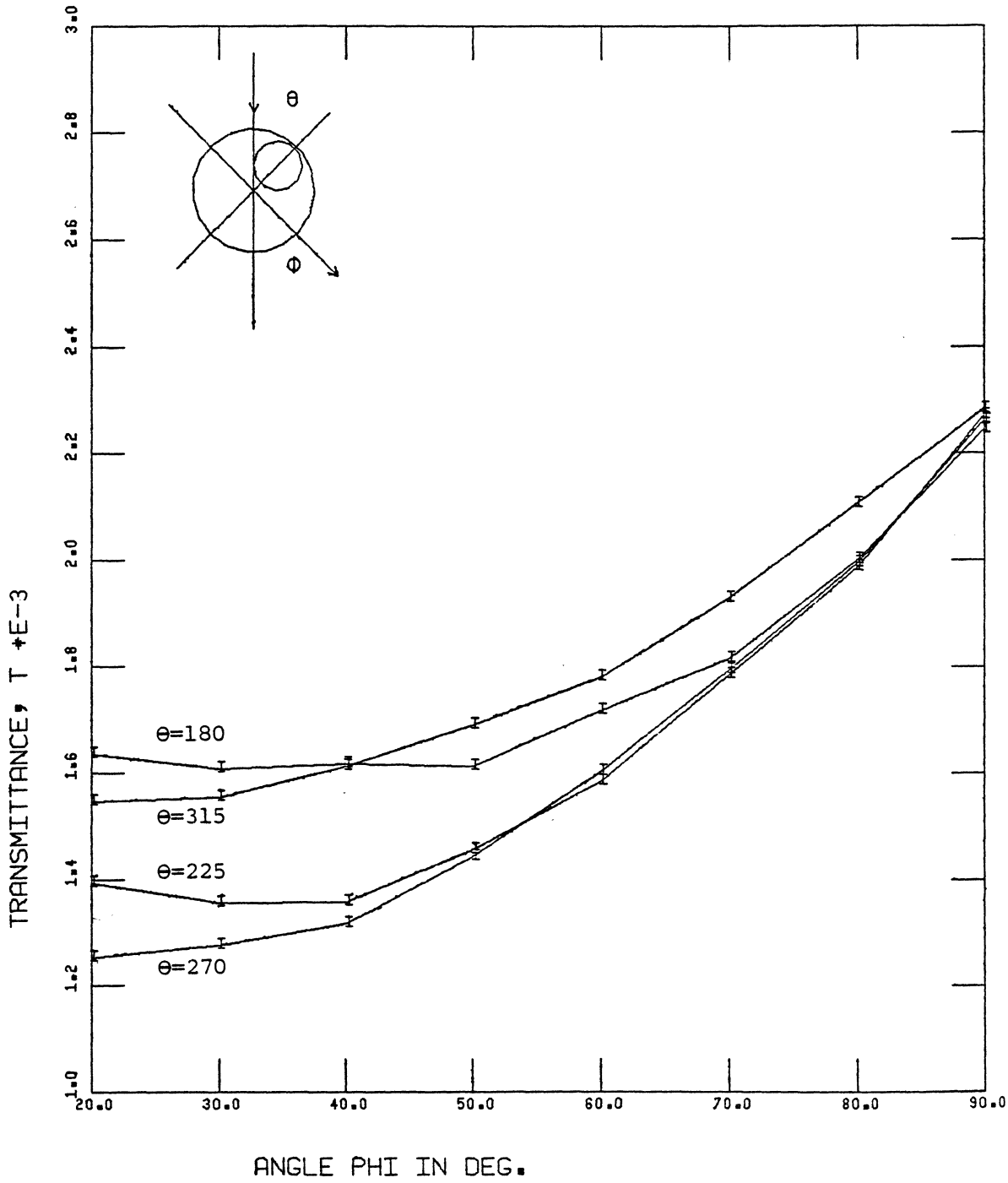

FIGURE 18: Transmittance versus Ø
For Sample #12; θ = 180,225,270,315°

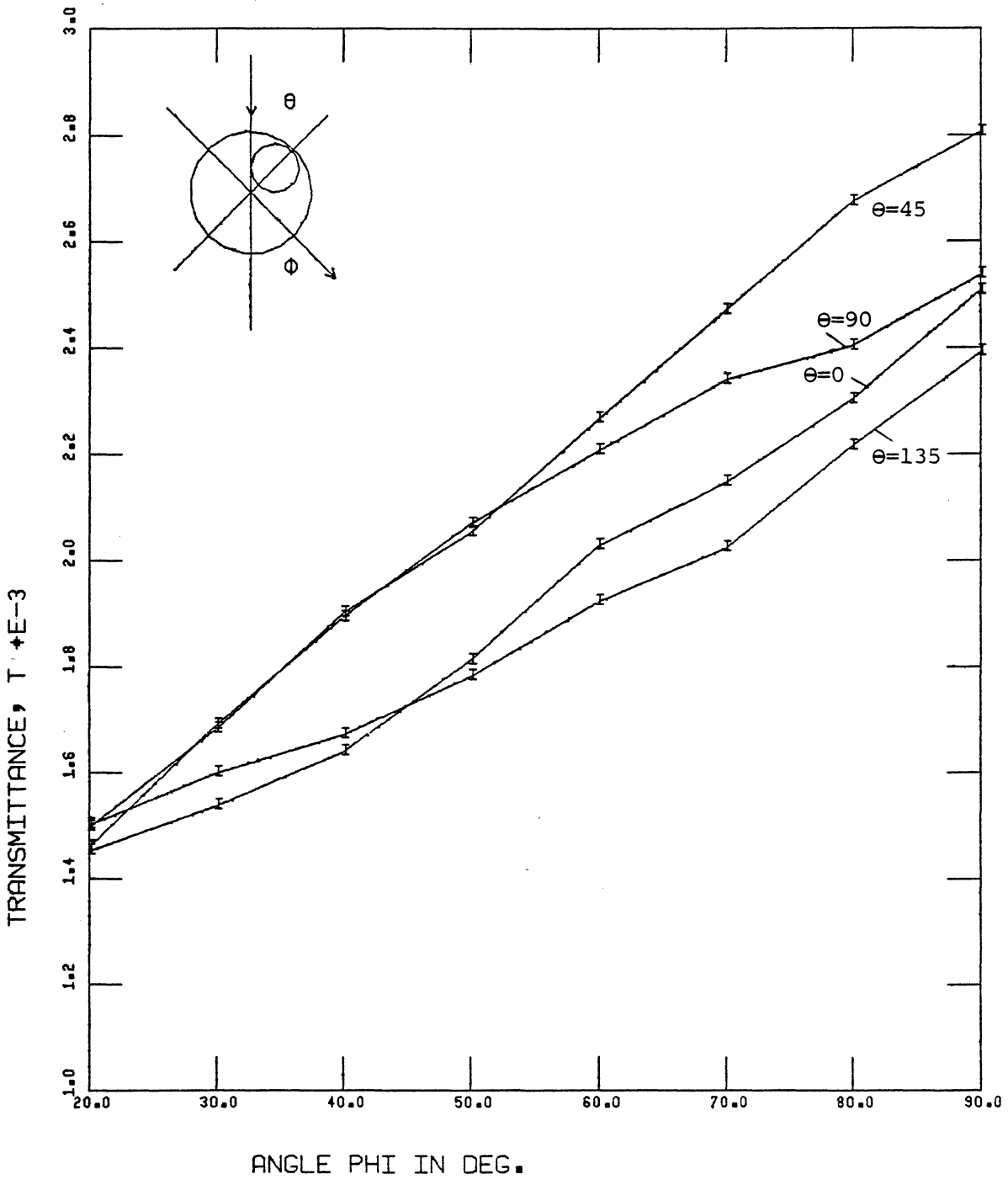

FIGURE 19: Transmittance versus Ø
For Sample #13, θ = 0,45,90,135°

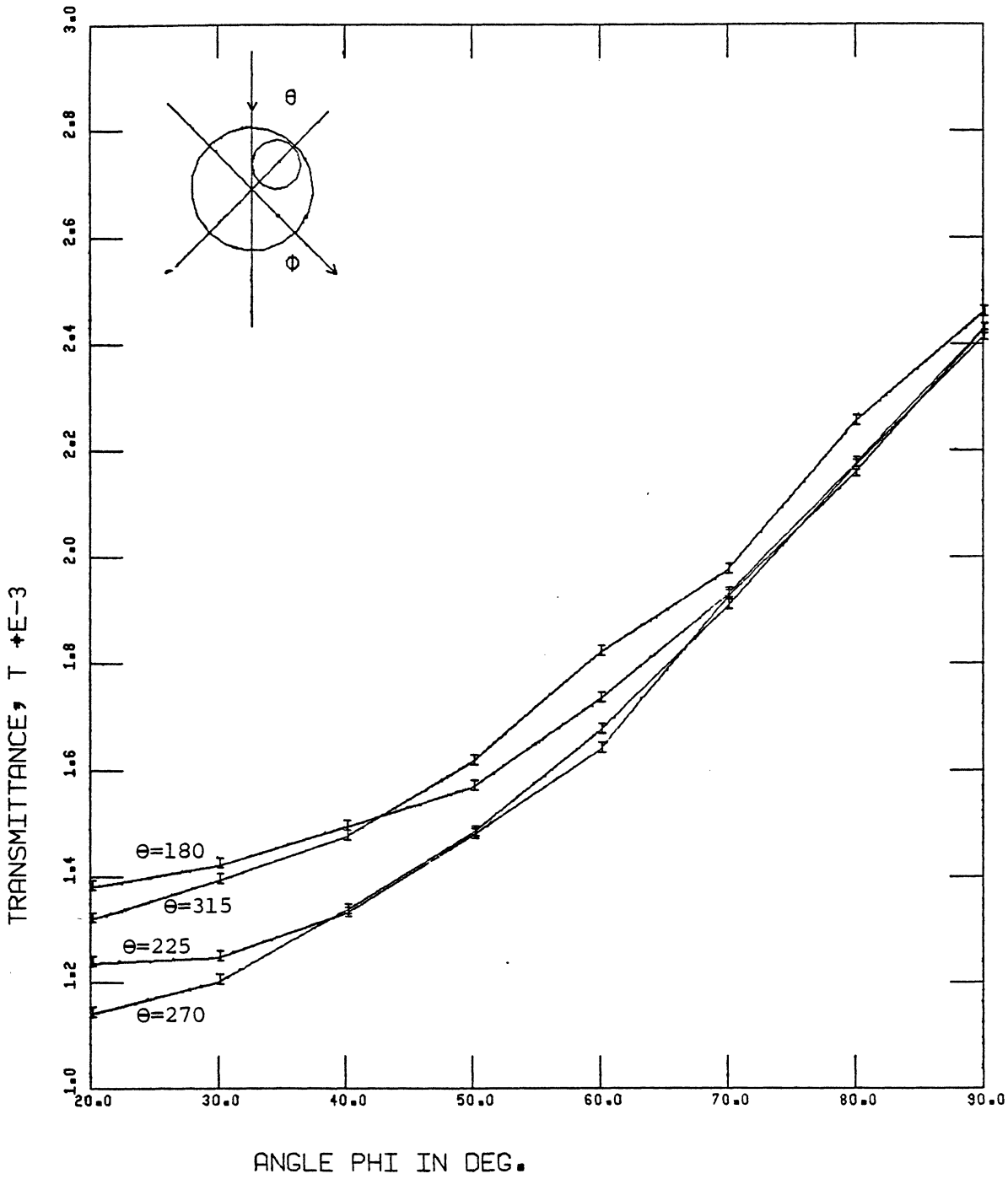

FIGURE 20: Transmittance versus Ø
For Sample #13; θ = 180,225,270,315°

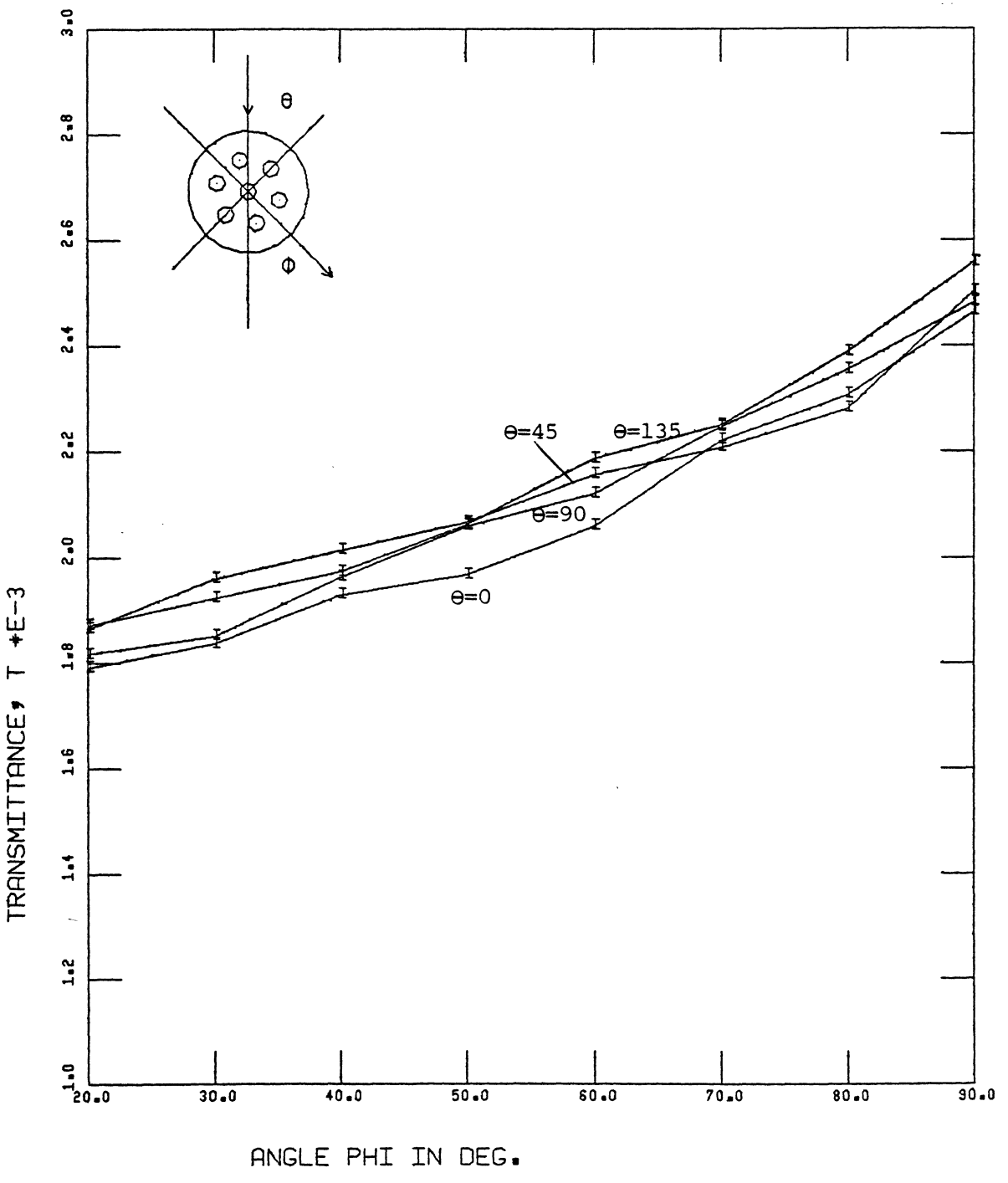

FIGURE 21: Transmittance versus Ø
For Sample #14, θ = 0,45,90,135°

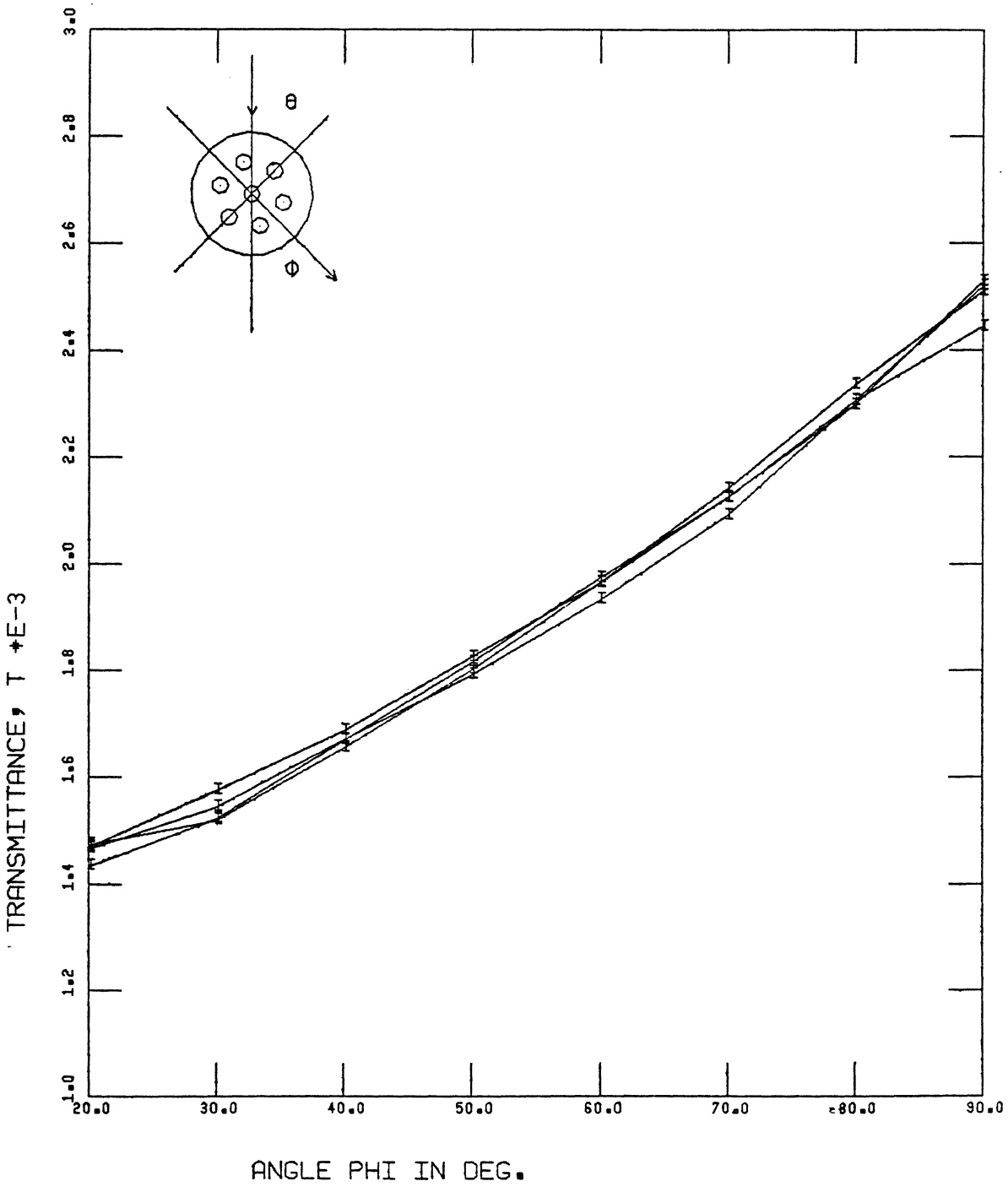

FIGURE 22: Transmittance versus Ø
For Sample #15; Θ = 0,45,90,135°

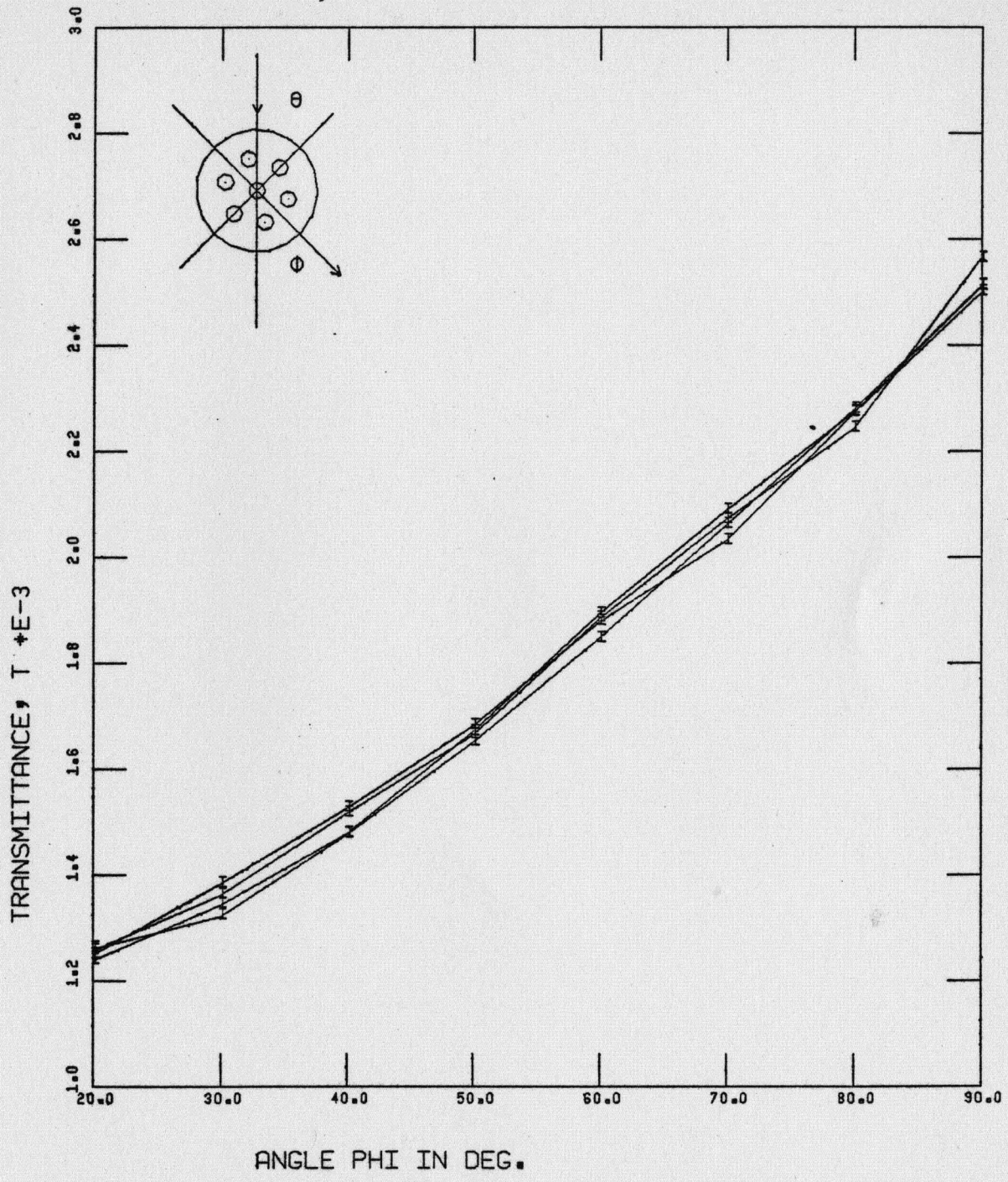

FIGURE 23: Transmittance versus Ø
For Sample #16; Θ = 0,45,90,135°

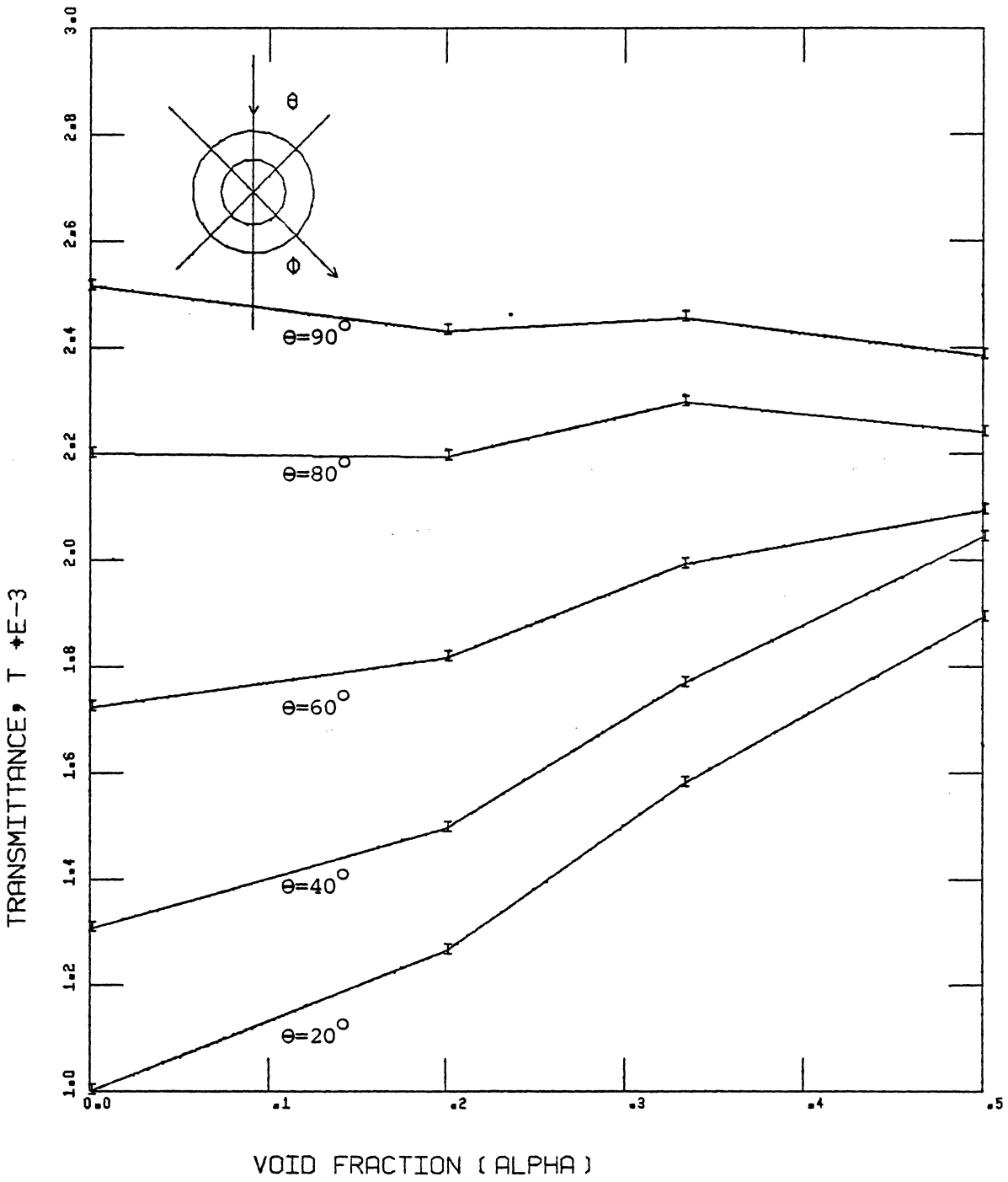

FIGURE 24: Transmittance versus
For Sample #1,2,3,4; $\theta = 0^{\circ}$

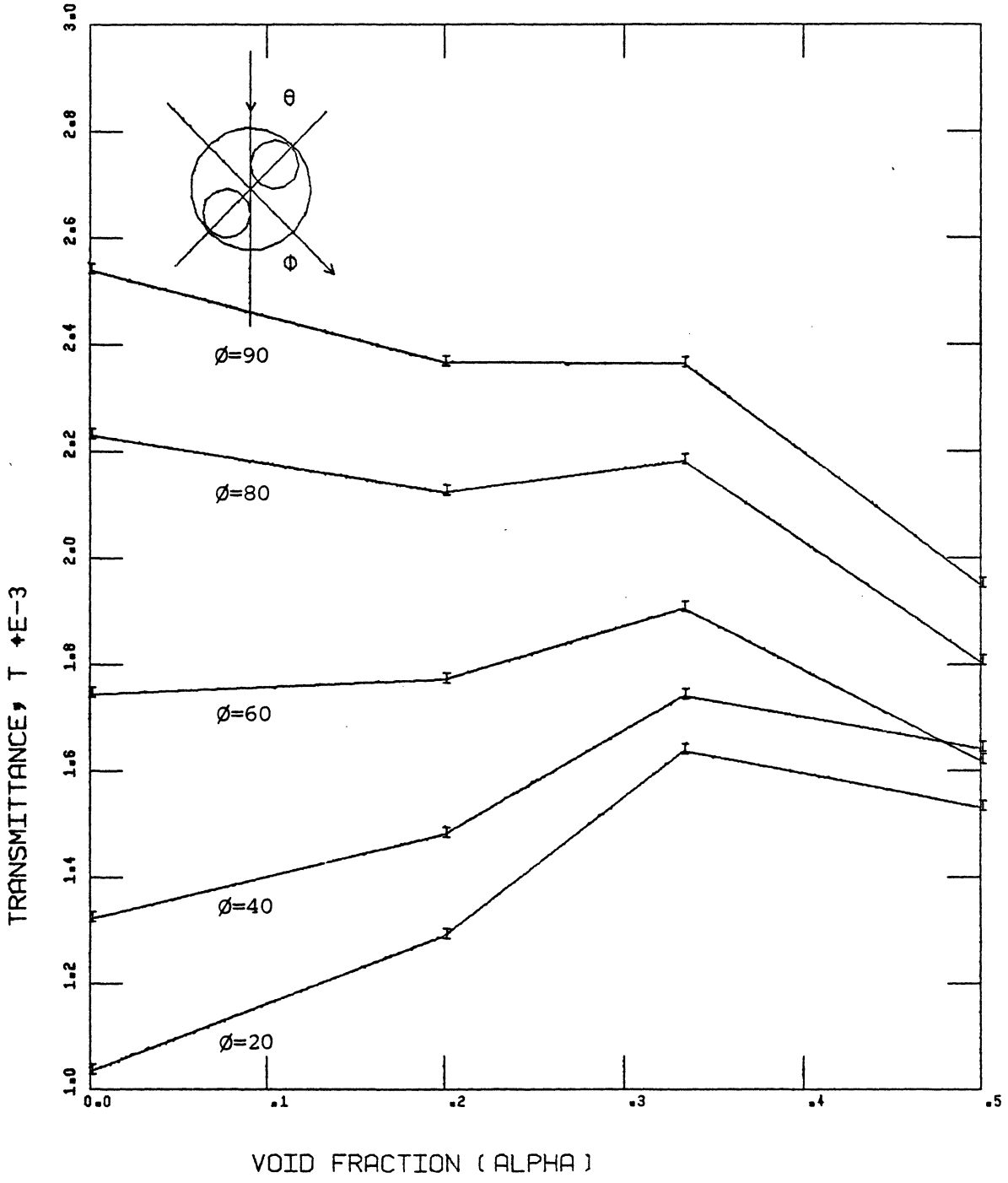

FIGURE 25: Transmittance versus
For Sample #1,5,6,7; $\theta = 0^{\circ}$

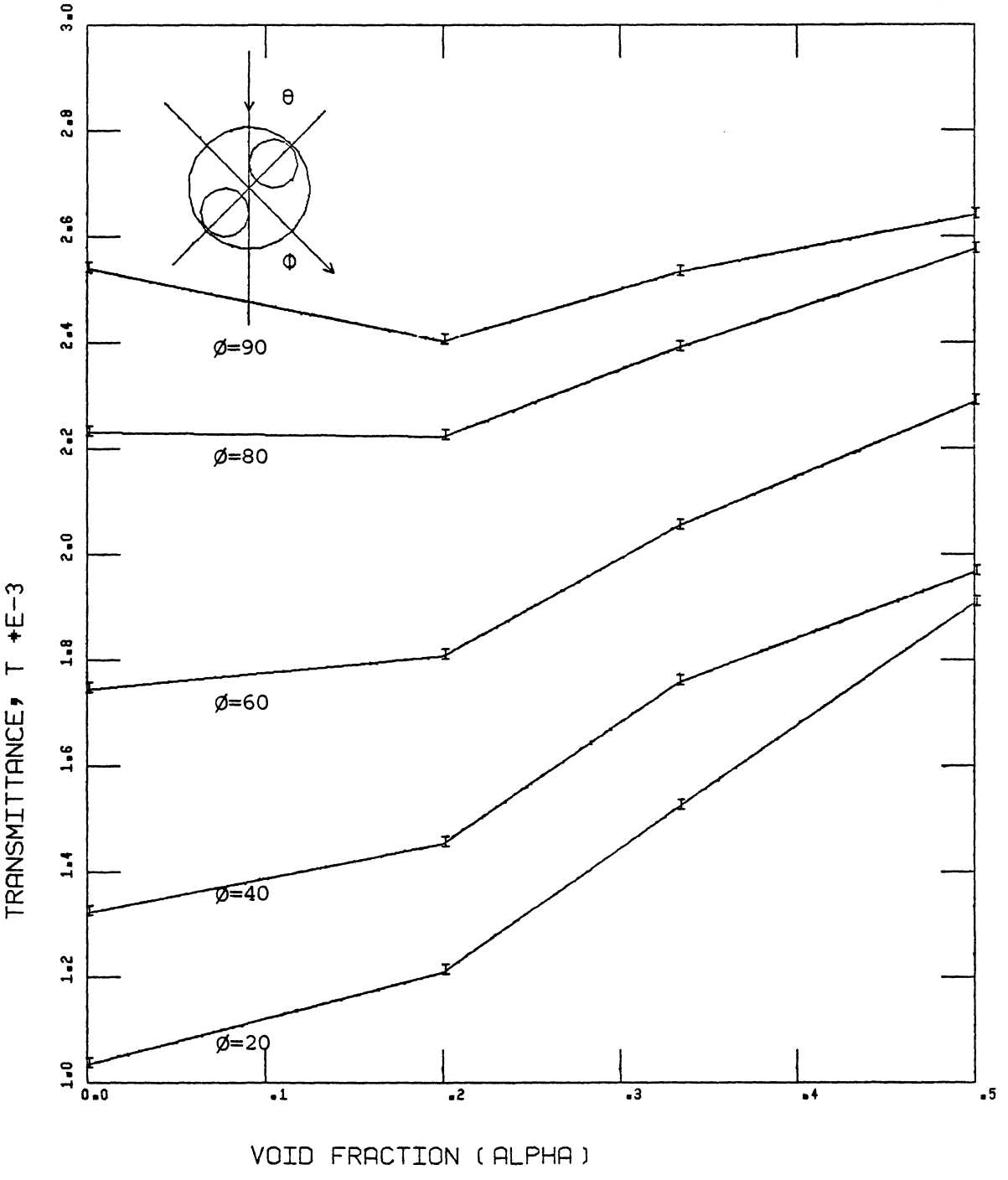

FIGURE 26: Transmittance versus
For Sample #1,5,6,7; $\Theta = 45^{\circ}$

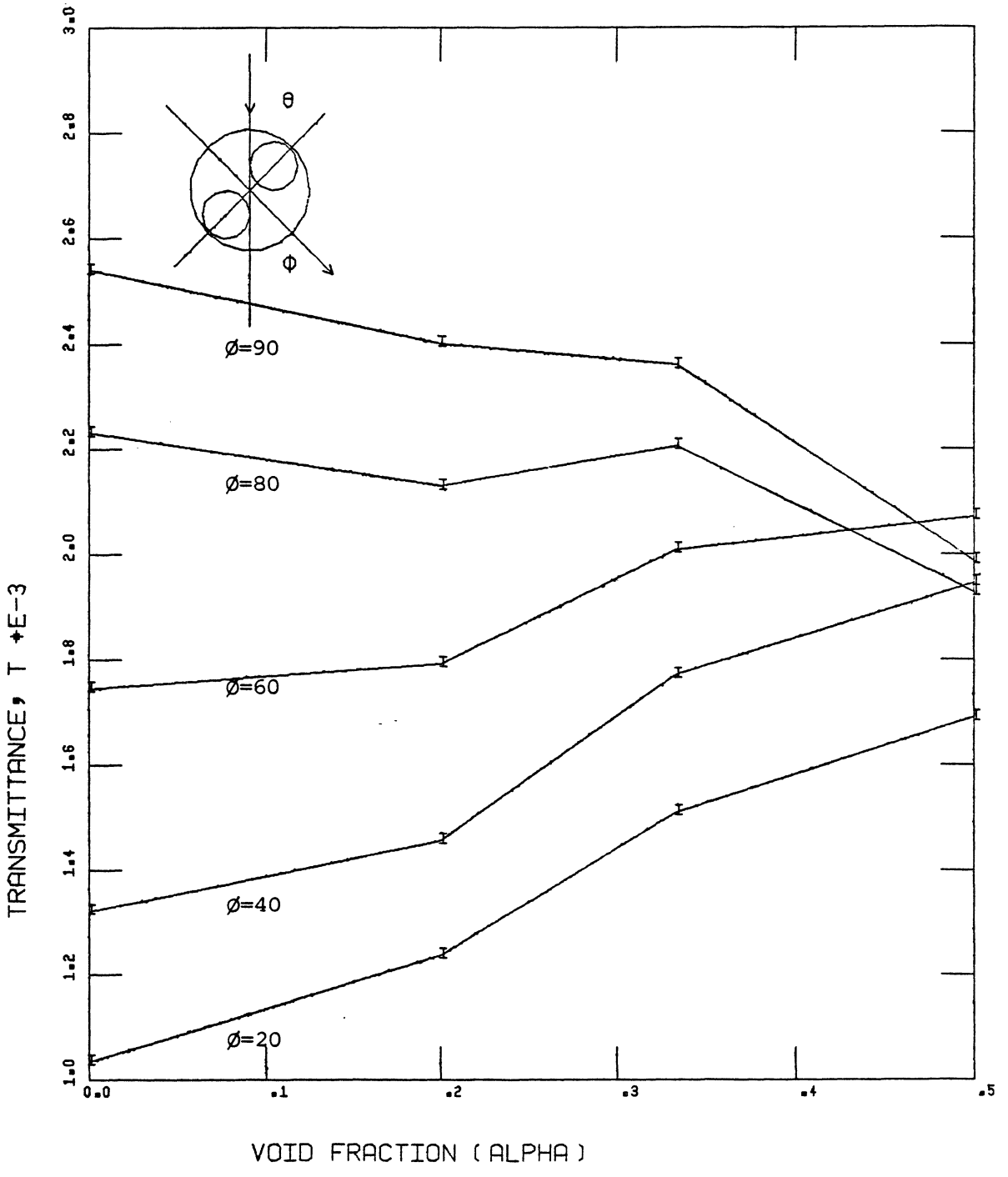

FIGURE 27: Transmittance versus
For Sample #1,5,6,7; $\Theta = 90^{o}$

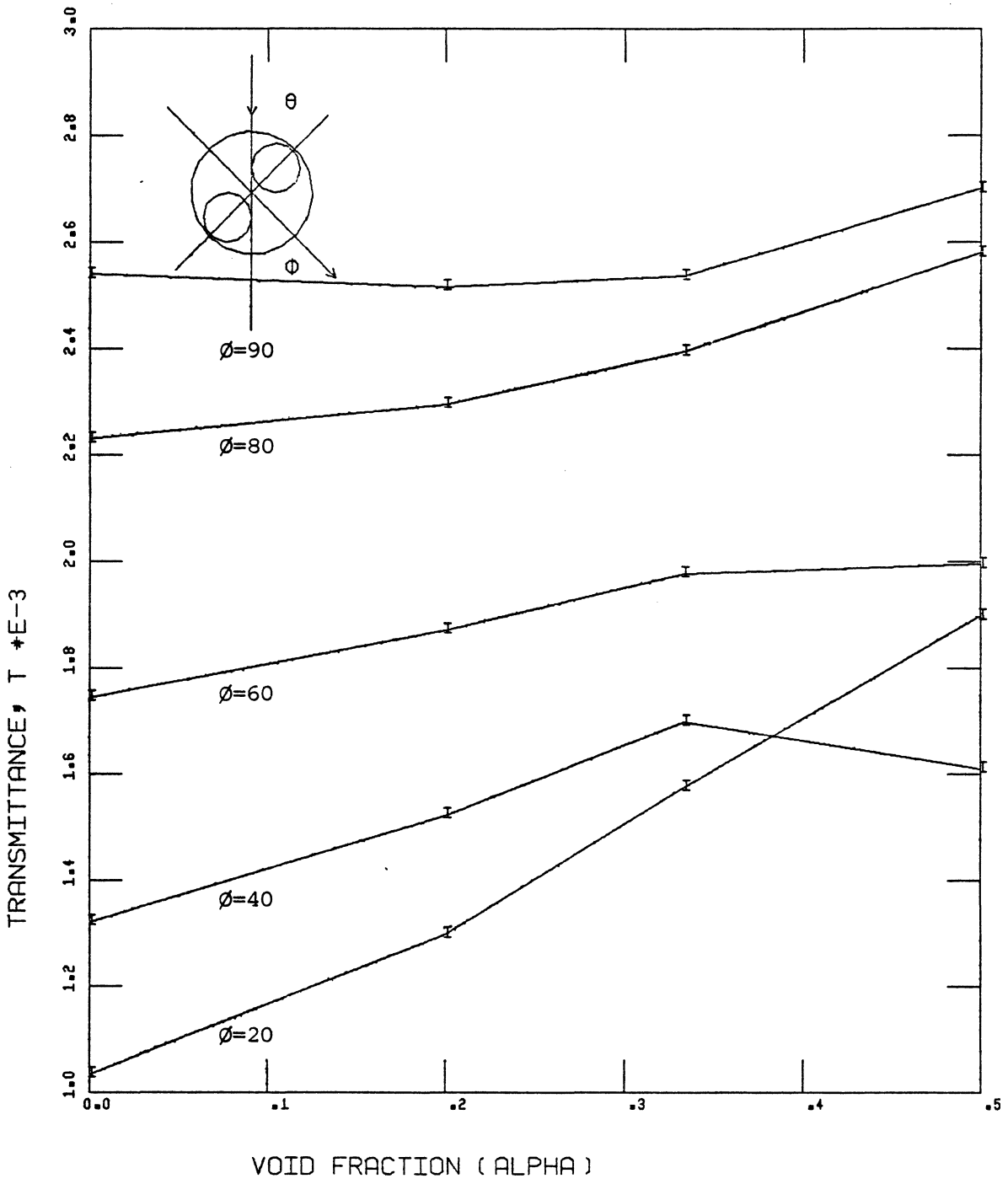

FIGURE 28: Transmittance versus
For Sample #1,5,6,7; $\theta = 135^{o}$

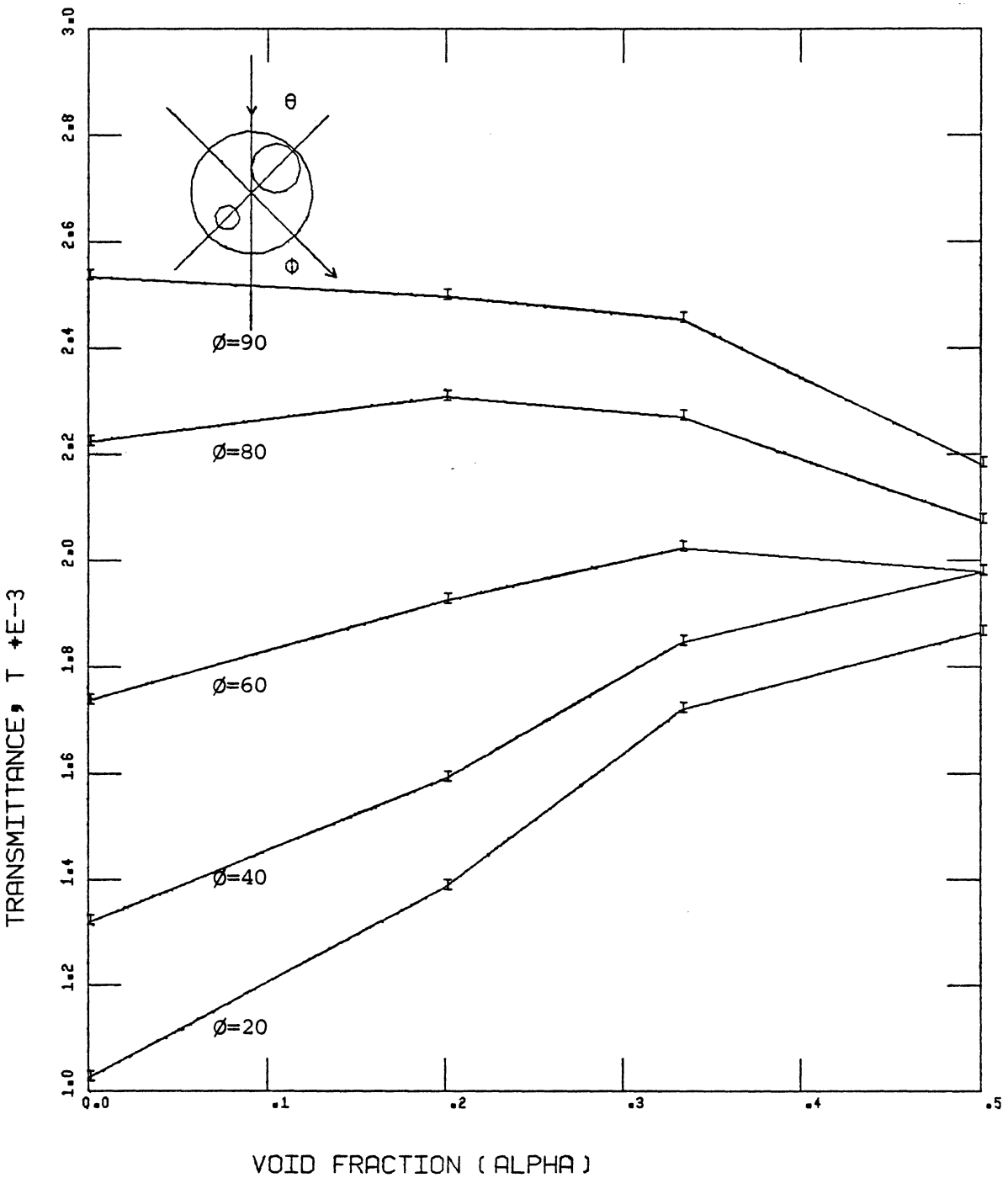

FIGURE 29: Transmittance versus
For Sample #1,8,9,10; $\theta = 0^{\circ}$

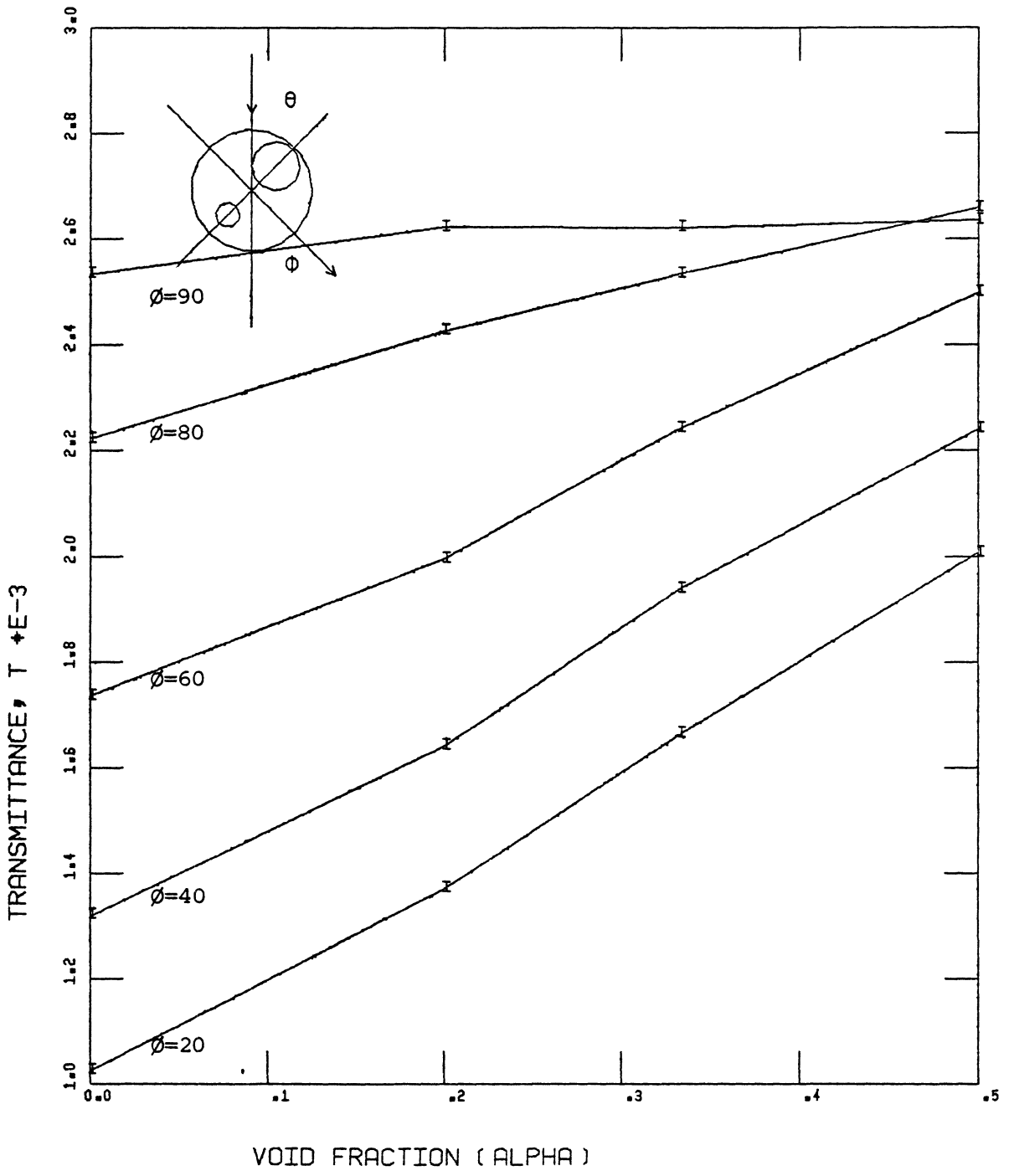

FIGURE 30: Transmittance versus
For Sample #1,8,9,10; $\Theta = 45^{\circ}$

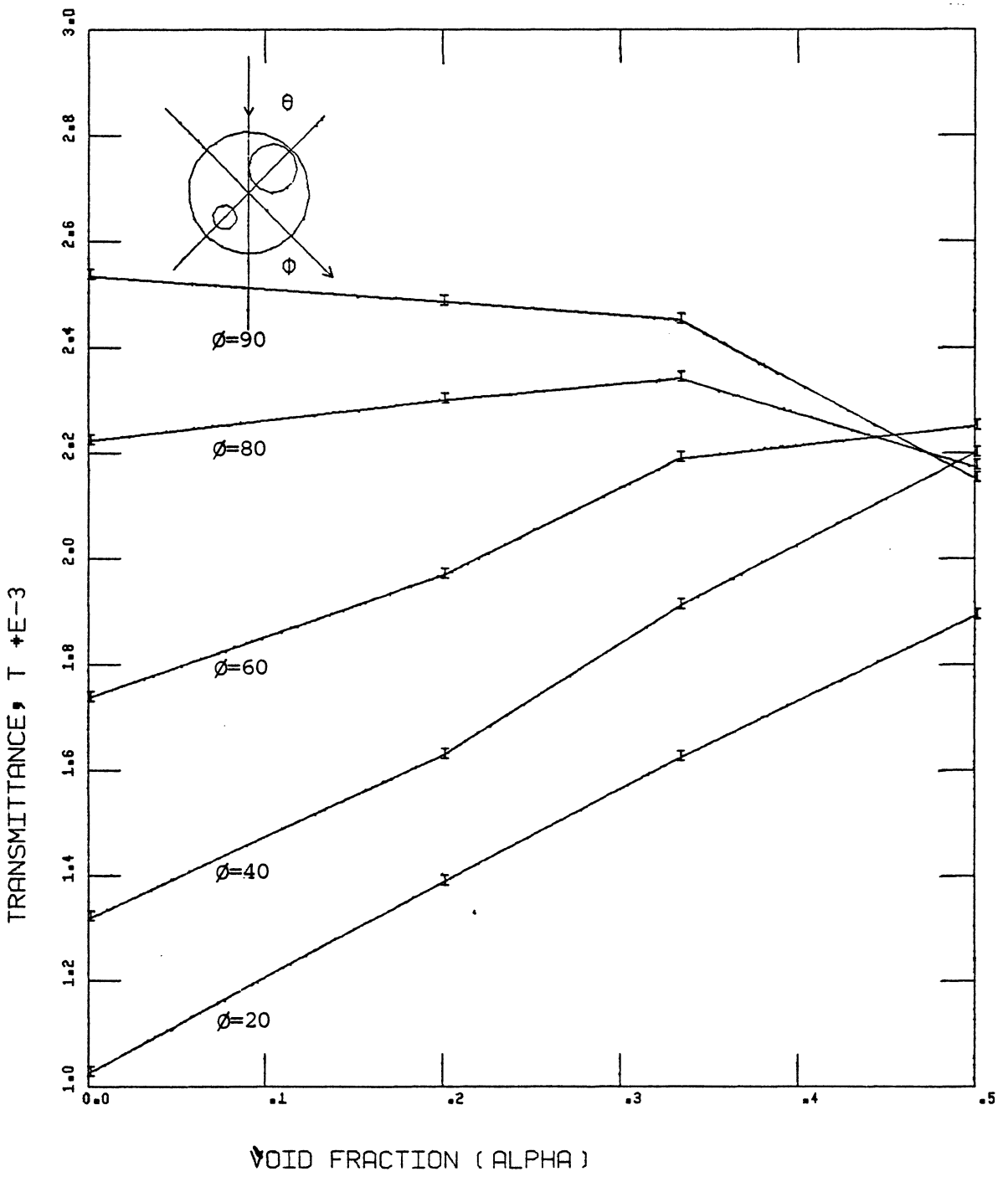

FIGURE 31: Transmittance versus
For Sample #1,8,9,10; $\Theta = 90^{\circ}$

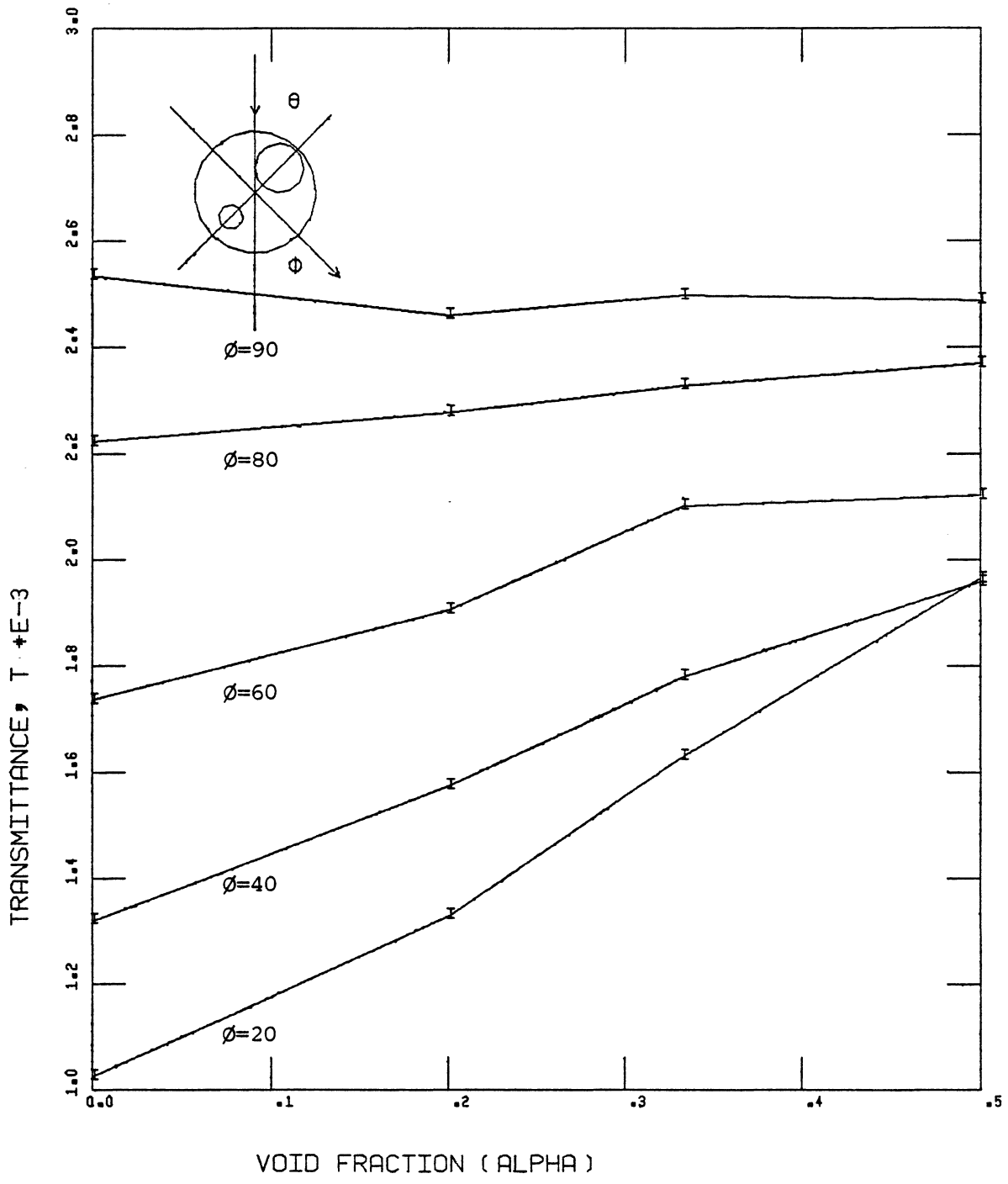

FIGURE 32: Transmittance versus
For Sample #1,8,9,10; $\theta = 135^{\circ}$

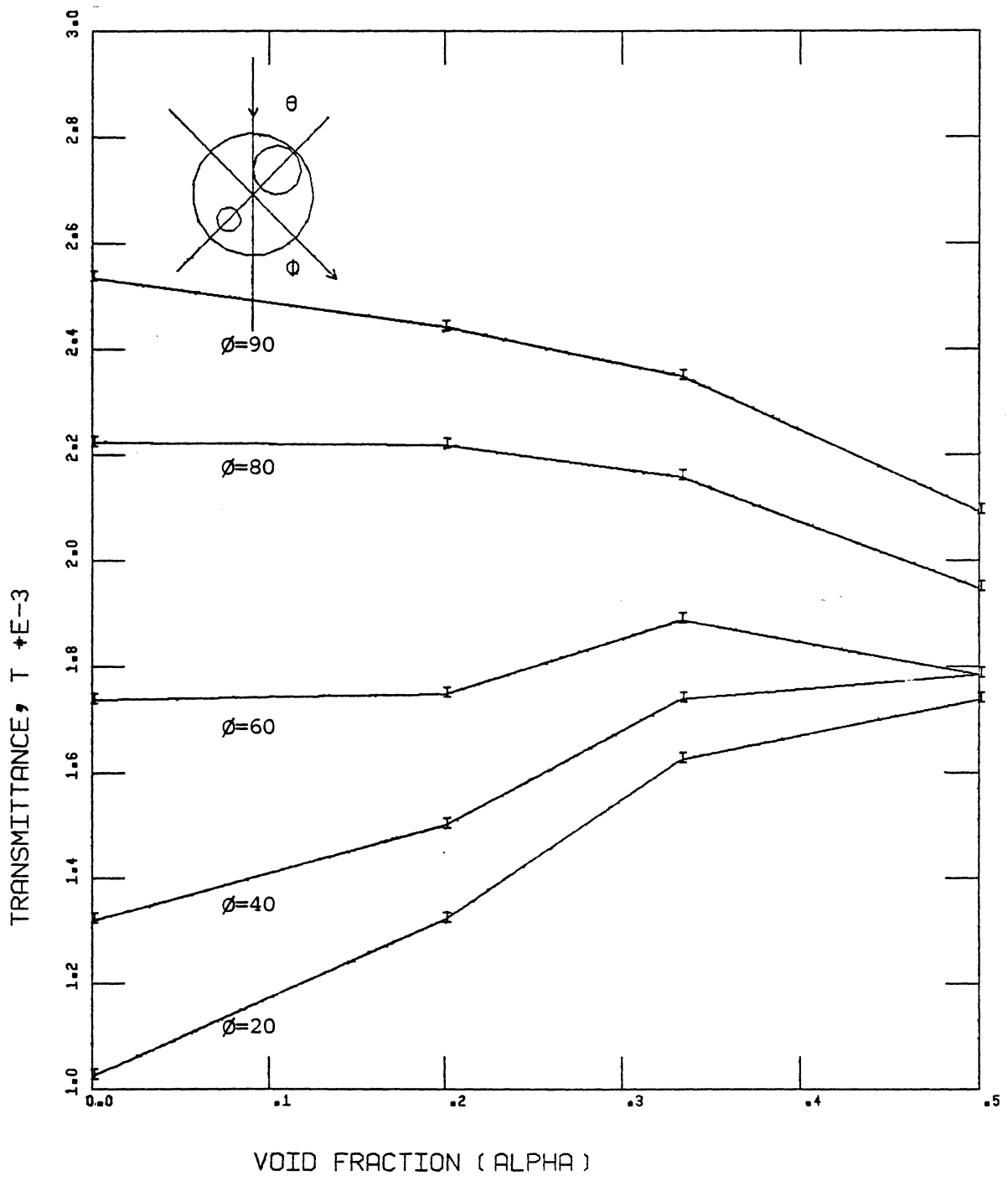

FIGURE 33: Transmittance versus
For Sample #1,8,9,10; $\theta = 180^{\circ}$

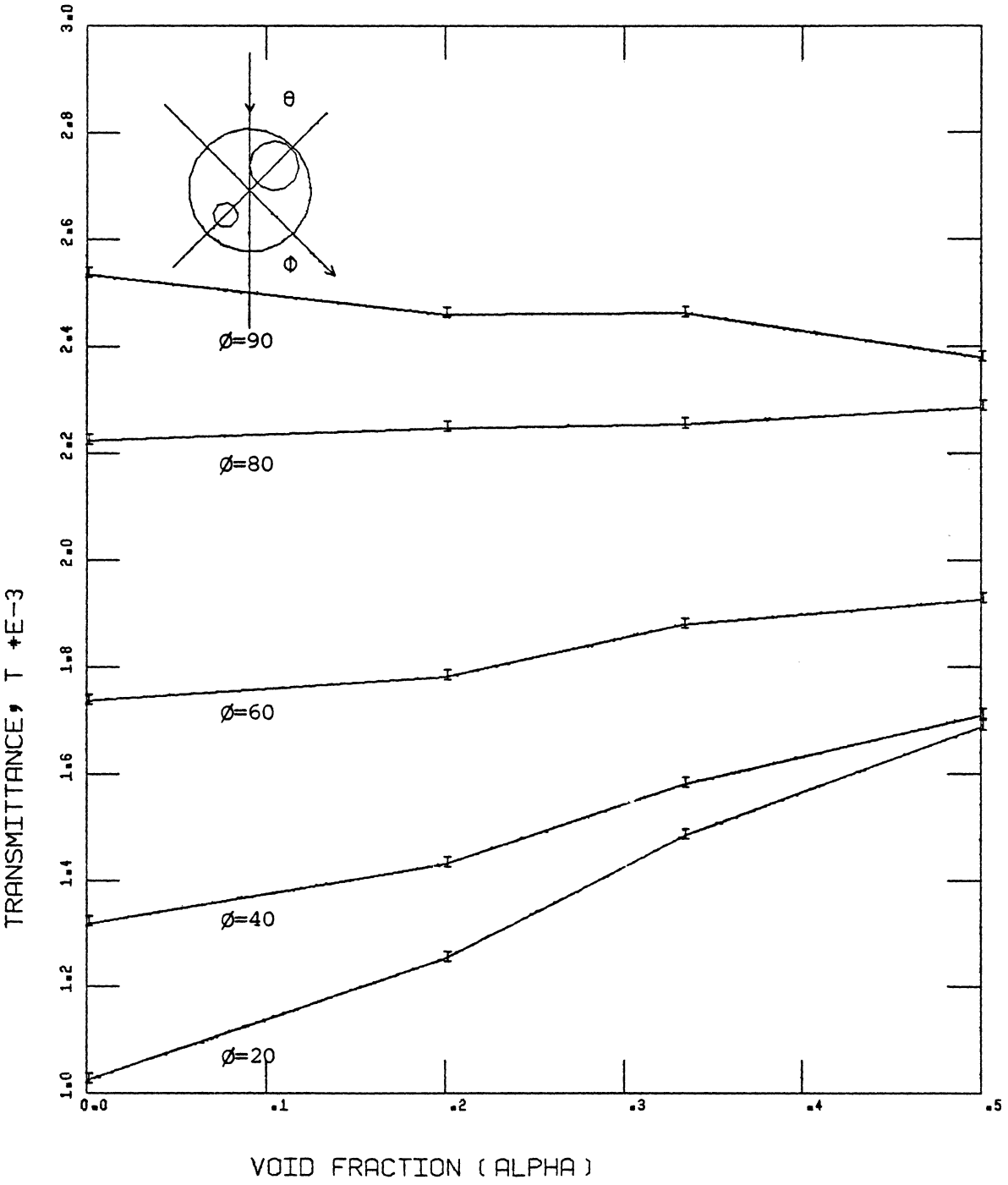

FIGURE 34: Transmittance versus
For Sample #1,8,9,10; $\theta = 225^{\circ}$

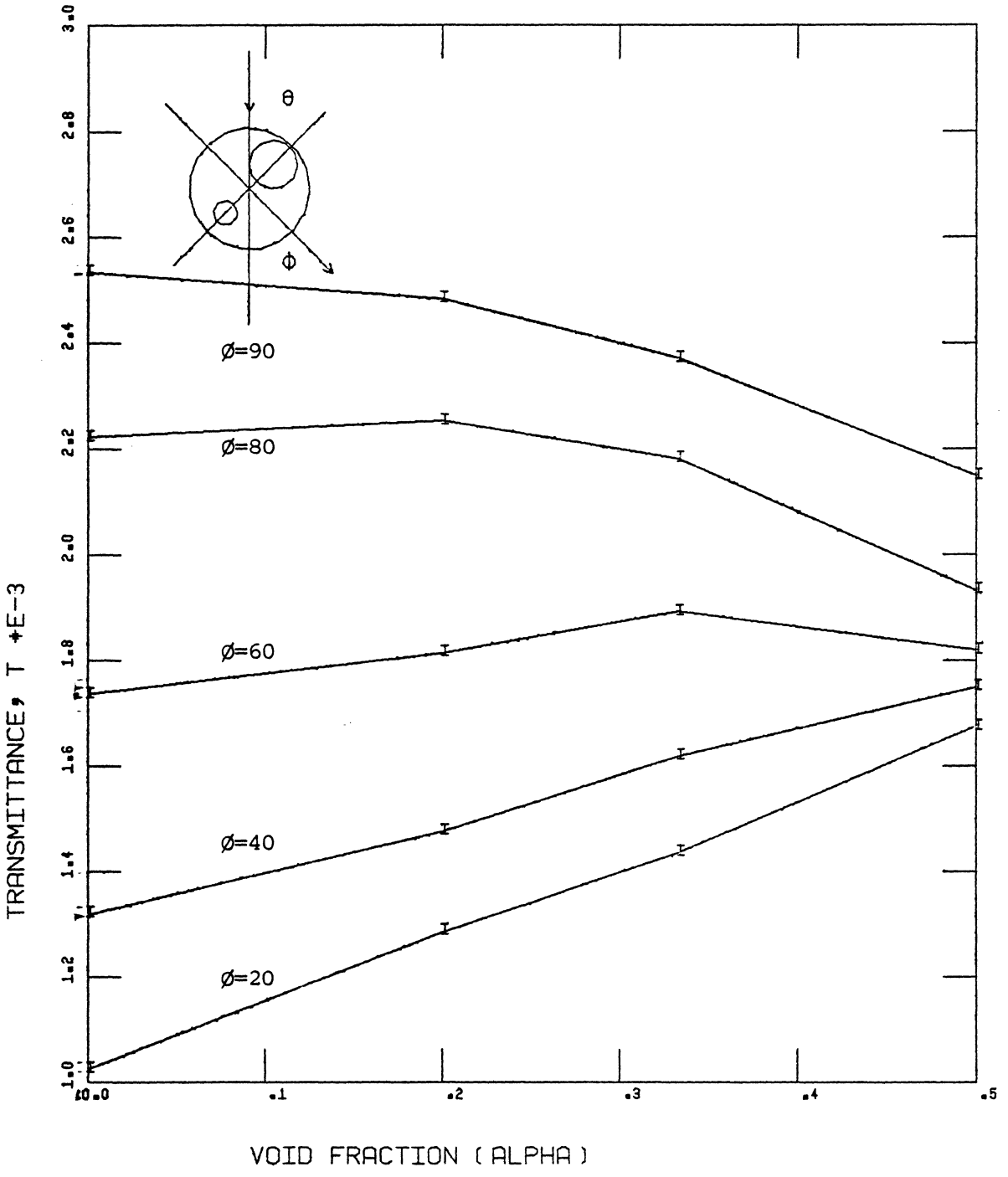

FIGURE 35: Transmittance versus
For Sample #1,8,9,10; $\theta = 270^{\circ}$

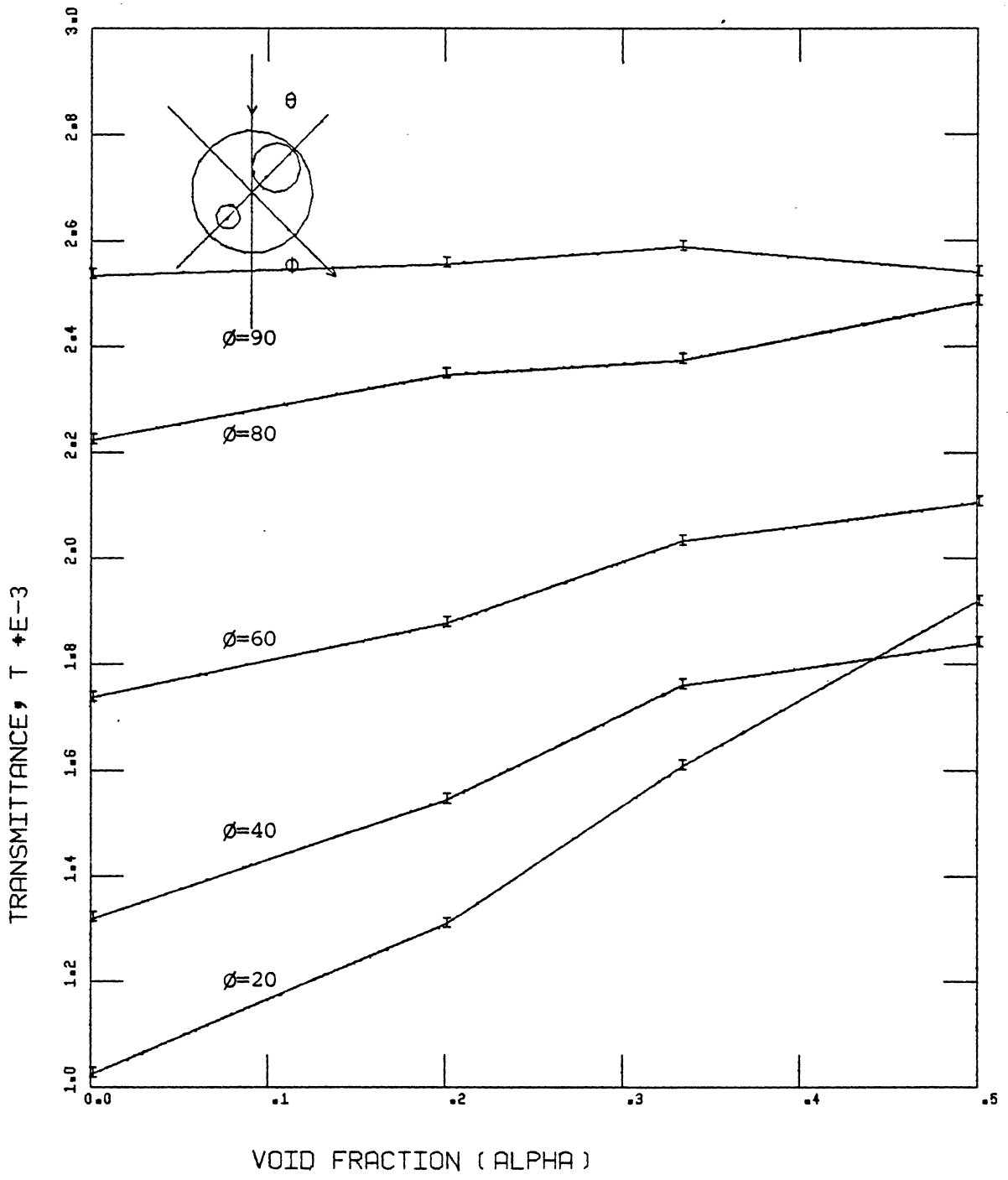

FIGURE 36: Transmittance versus
For Sample #1,8,9,10; $\theta = 315^{\circ}$

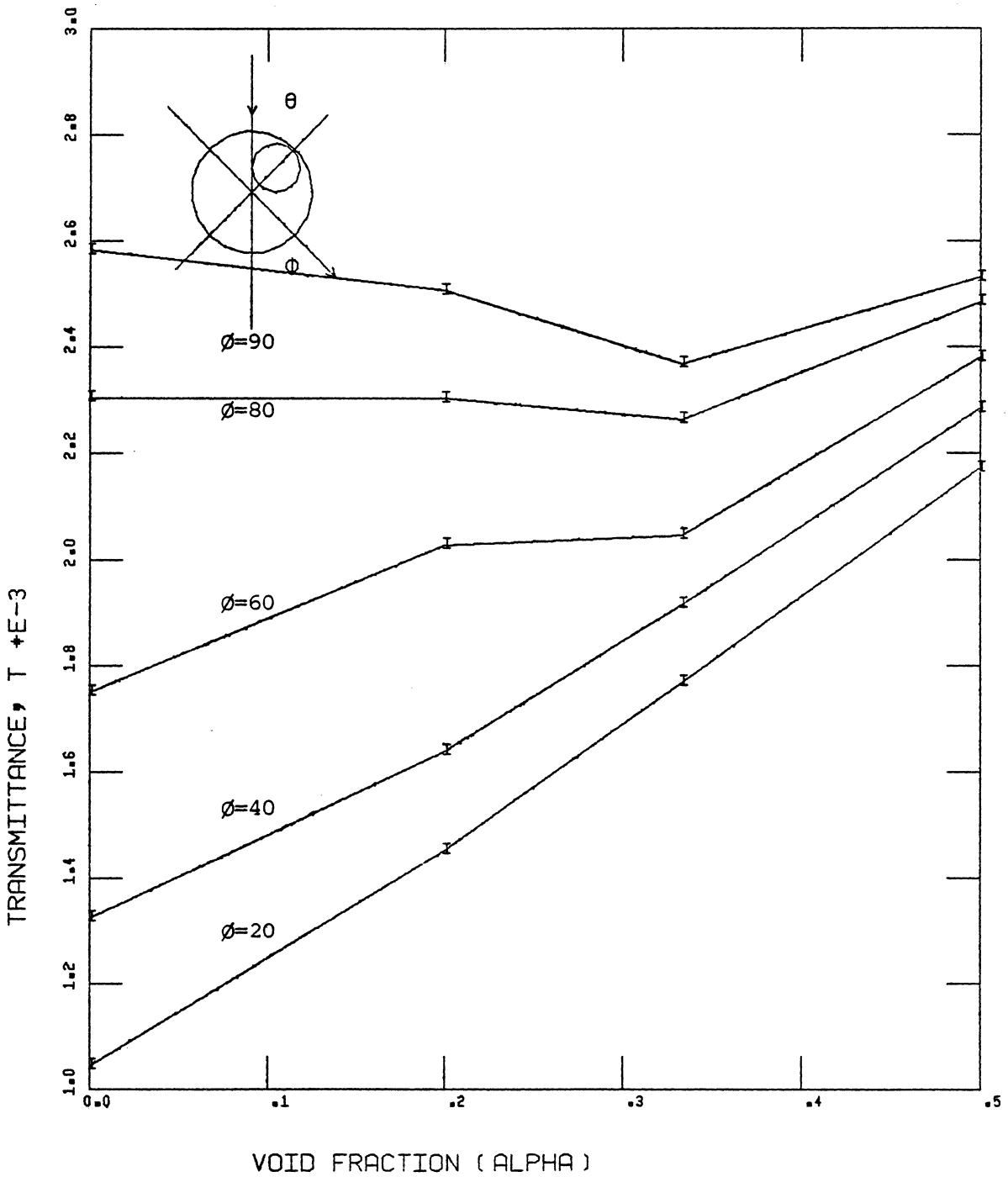

FIGURE 37: Transmittance versus
For Sample #1,11,12,13; $\Theta = 0^{\circ}$

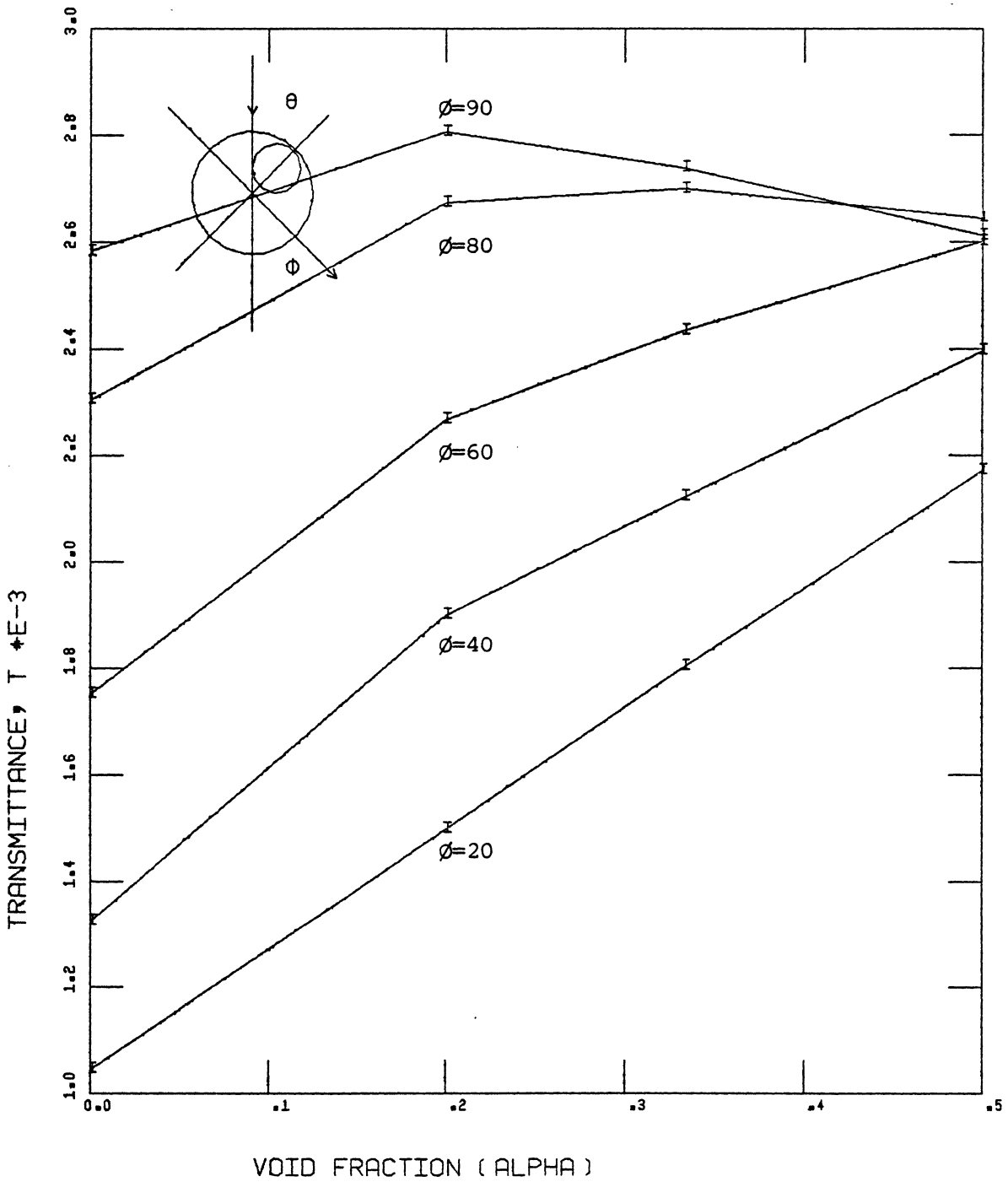

FIGURE 38: Transmittance versus
For Sample #1,11,12,13; $\theta = 45^{o}$

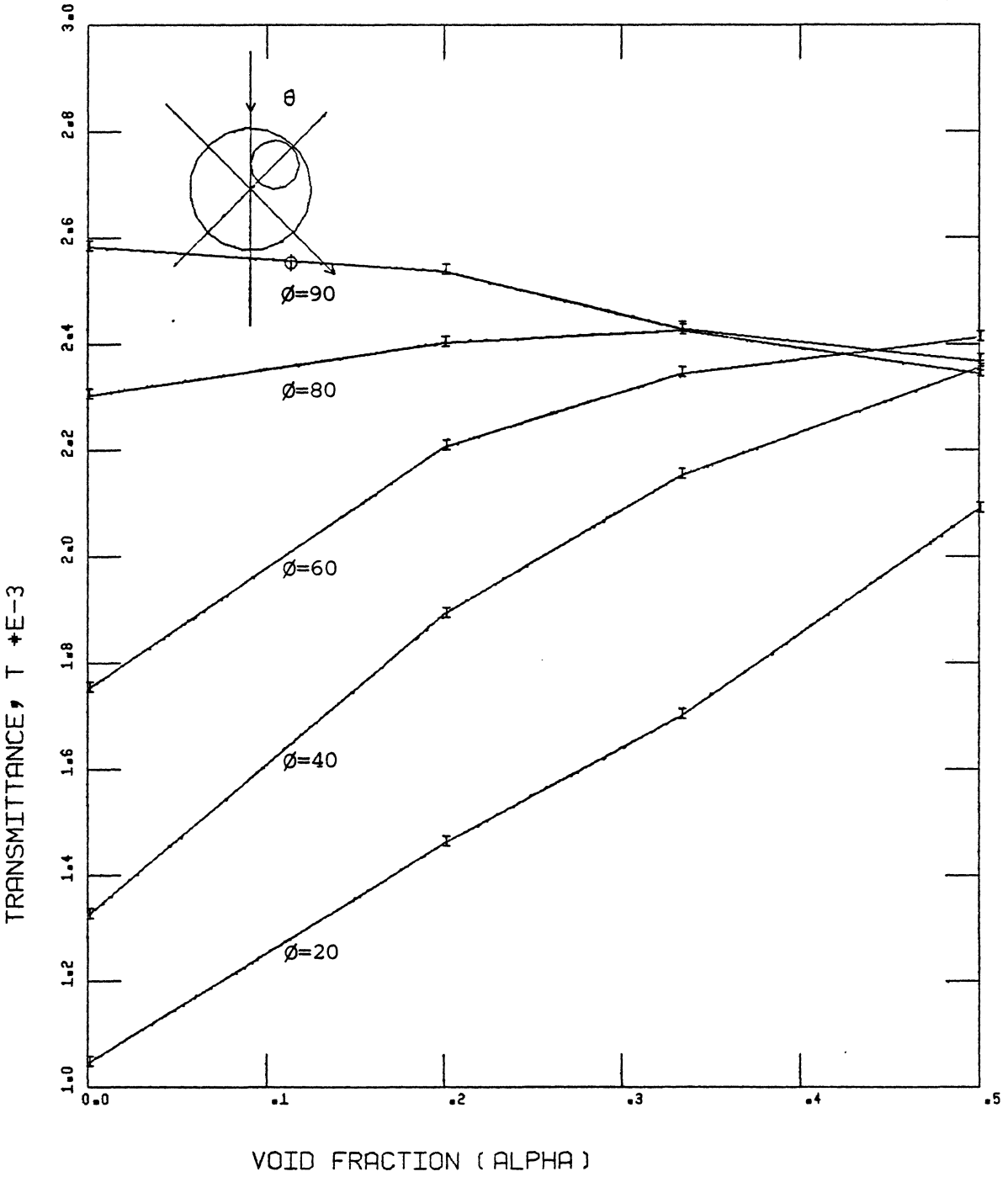

FIGURE 39: Transmittance versus
For Sample #1,11,12,13; $\theta = 90^{\circ}$

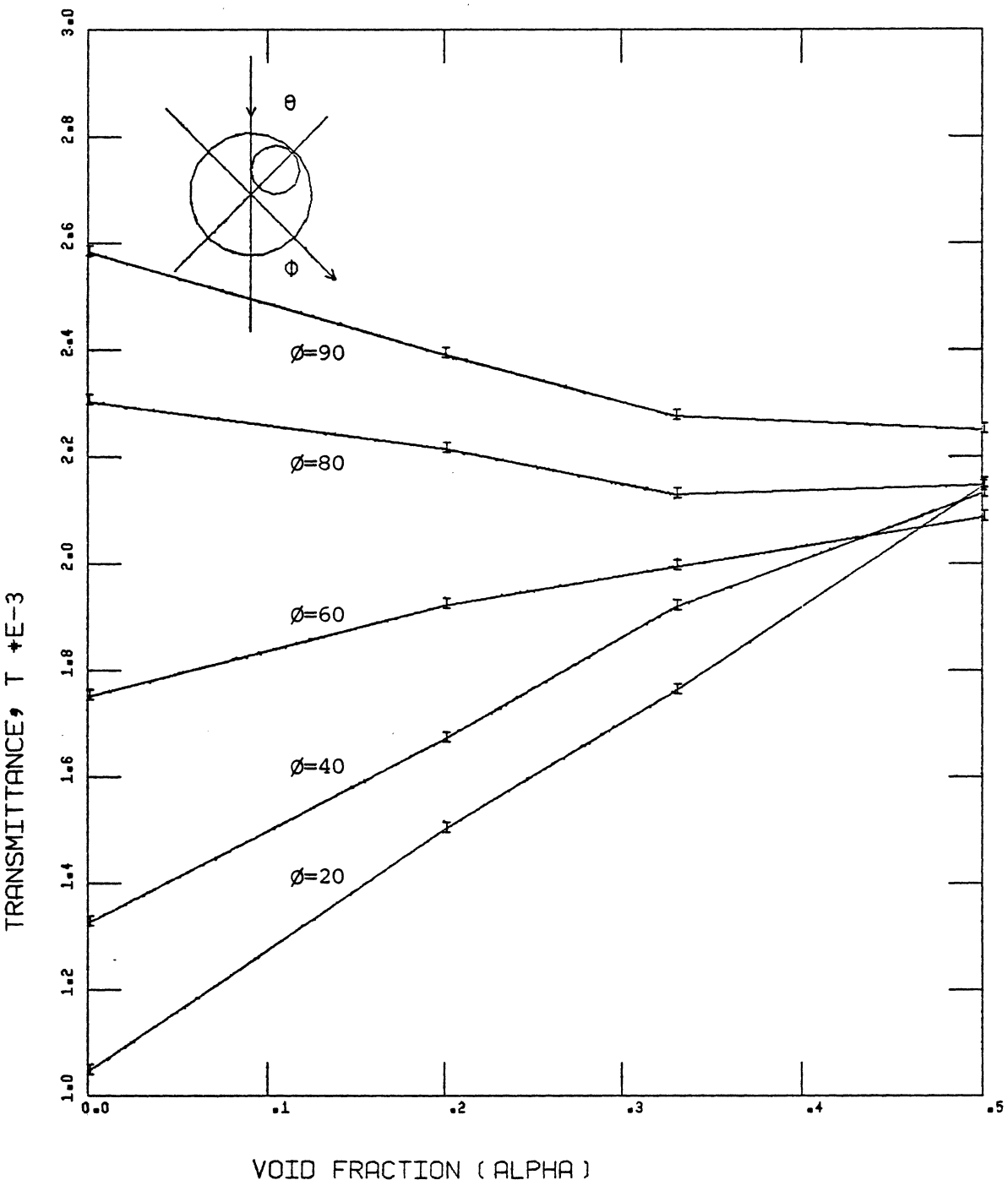

FIGURE 40: Transmittance versus
For Sample #1,11,12,13; $\Theta = 135^{\circ}$

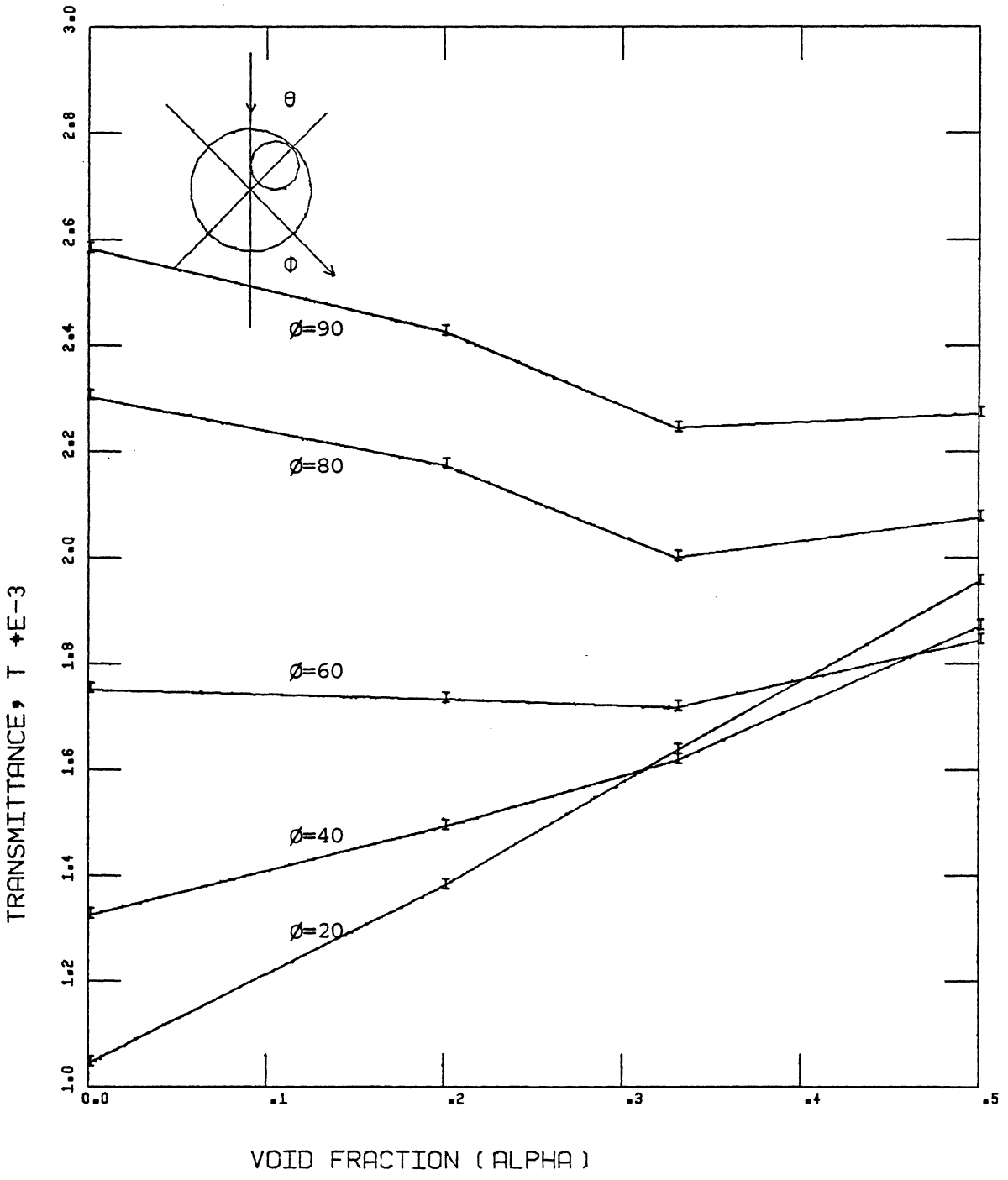

FIGURE 41: Transmittance versus
For Sample #1,11,12,13; $\theta = 180^{\circ}$

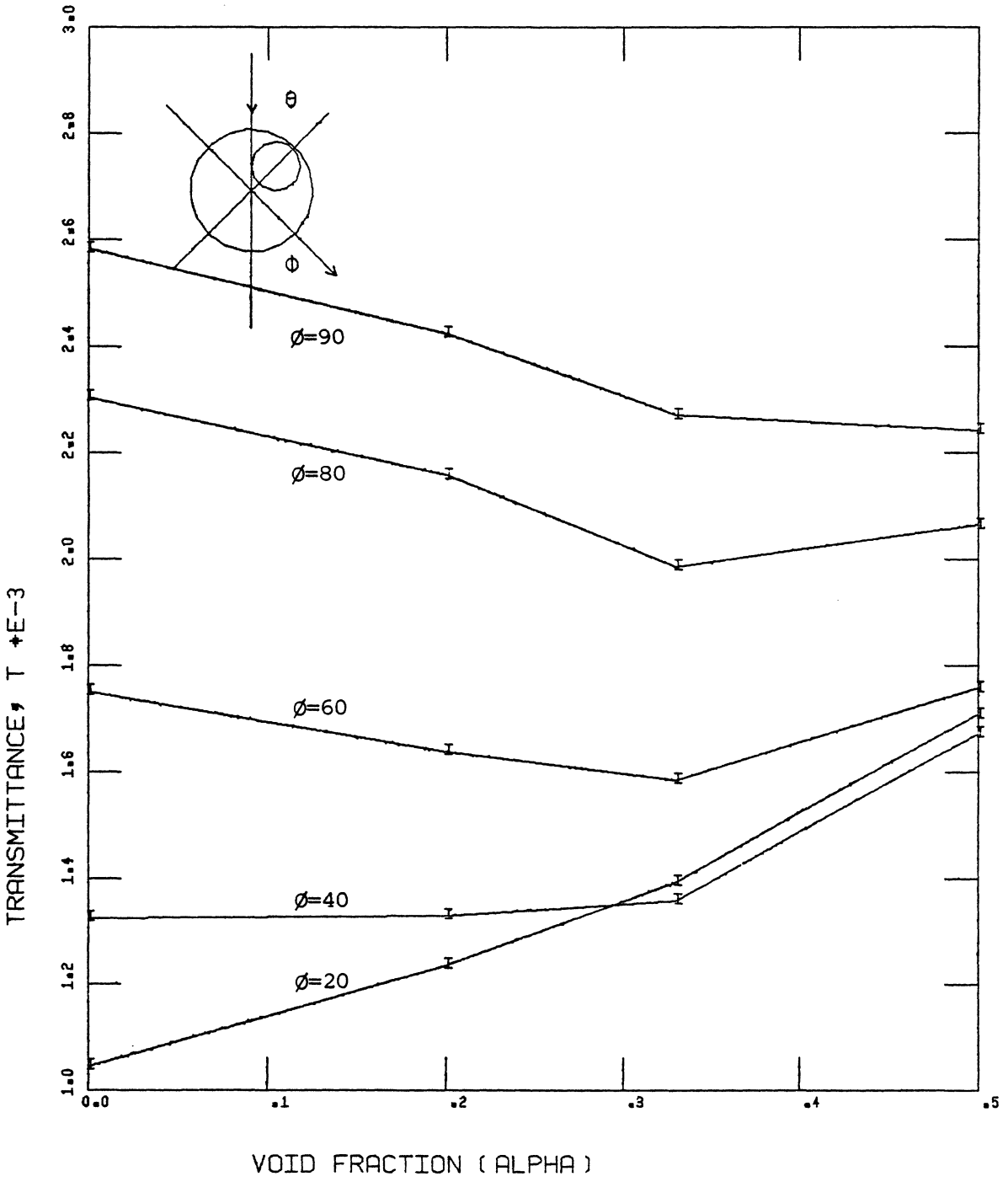

FIGURE 42: Transmittance versus
For Sample #1,11,12,13; $\theta = 225^{\circ}$

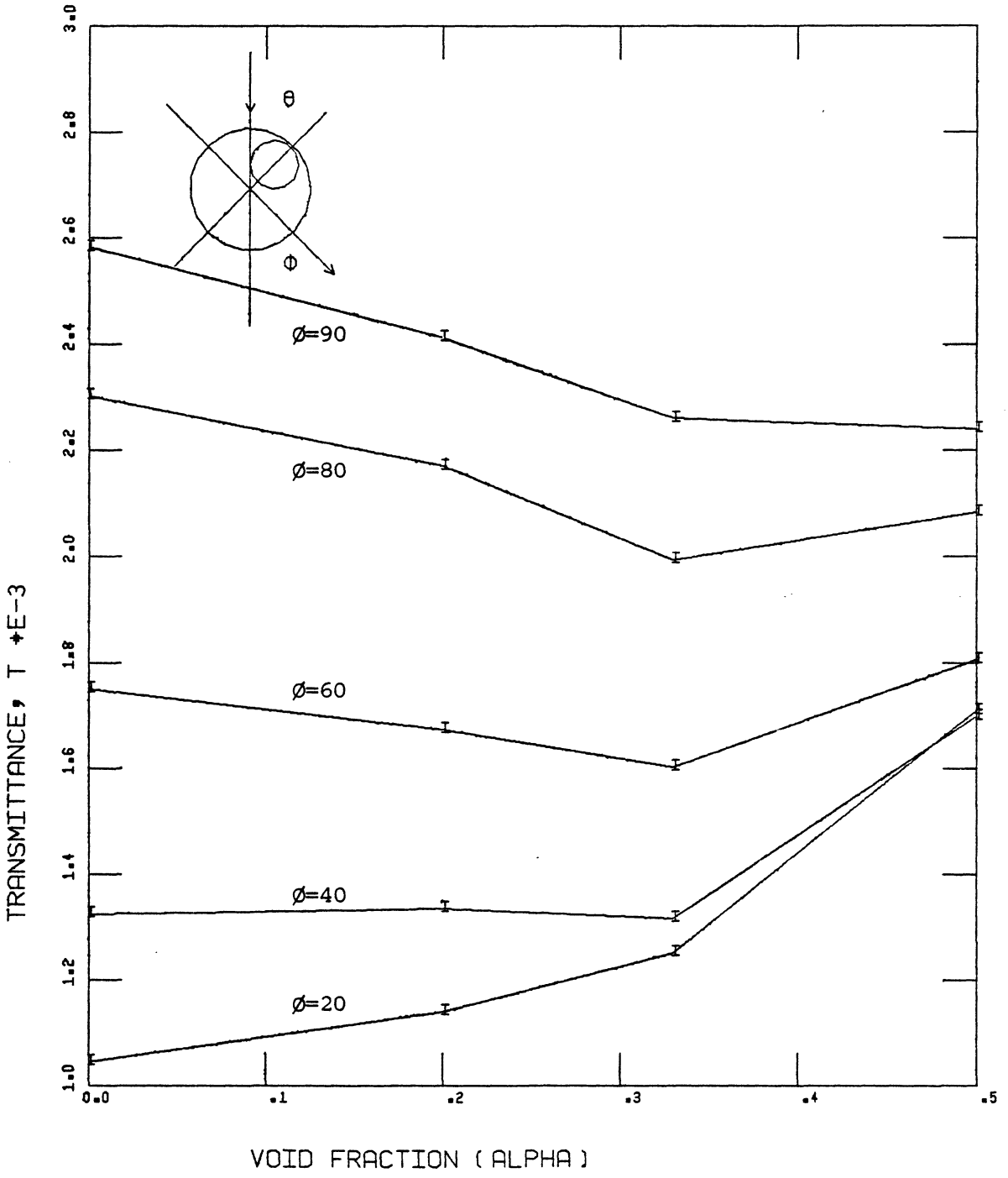

FIGURE 43: Transmittance versus
For Sample #1,11,12,13; $\theta = 270^{\circ}$

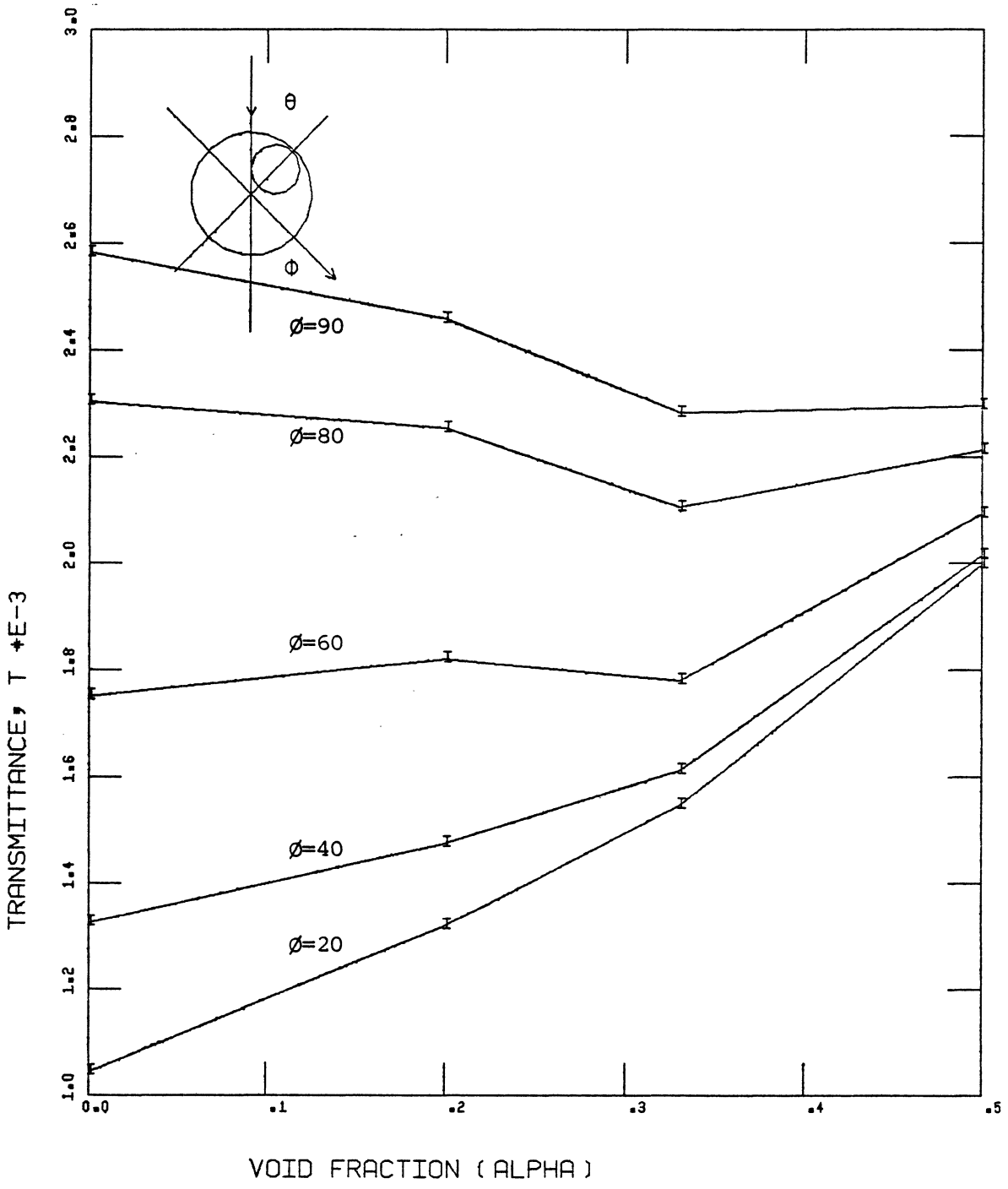

FIGURE 44: Transmittance versus
For Sample #1,11,12,13; $\theta = 315^{\circ}$

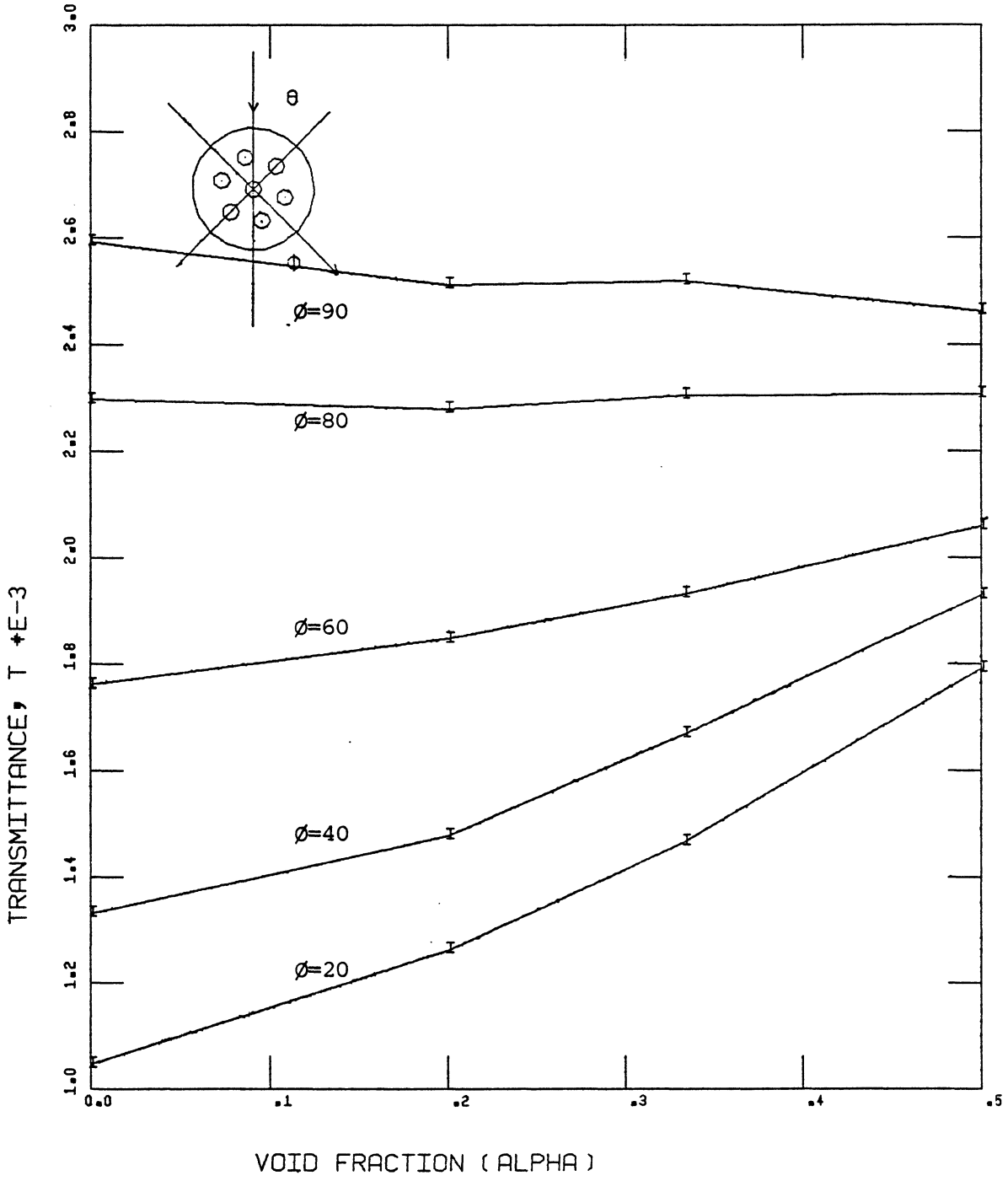

FIGURE 45: Transmittance versus
For Sample #1,14,15,16; $\theta = 0^{o}$

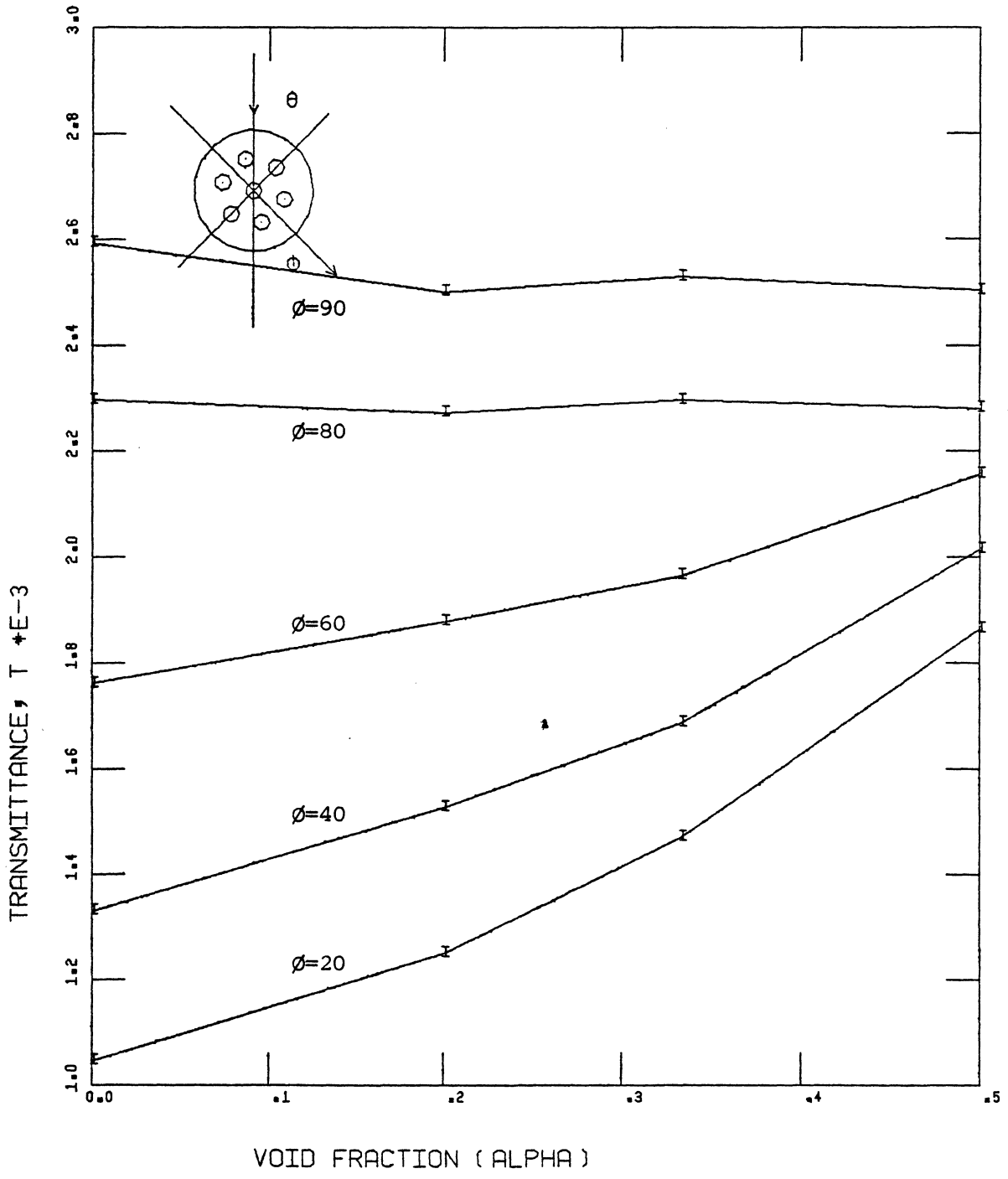

FIGURE 46: Transmittance versus
For Sample #1,14,15,16; $\theta = 45^{\circ}$

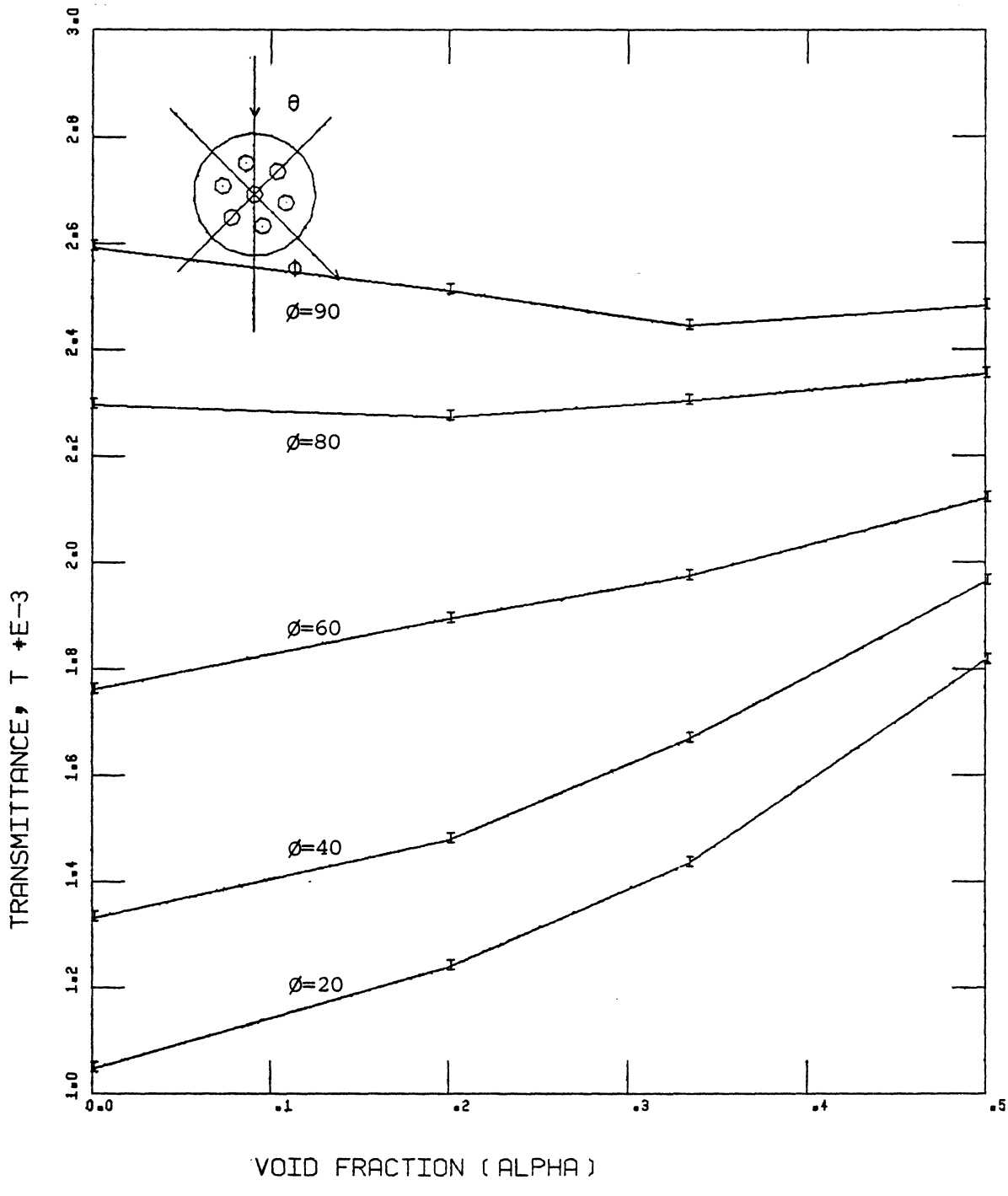

FIGURE 47: Transmittance versus
For Sample #1,14,15,16; $\theta = 90^{o}$

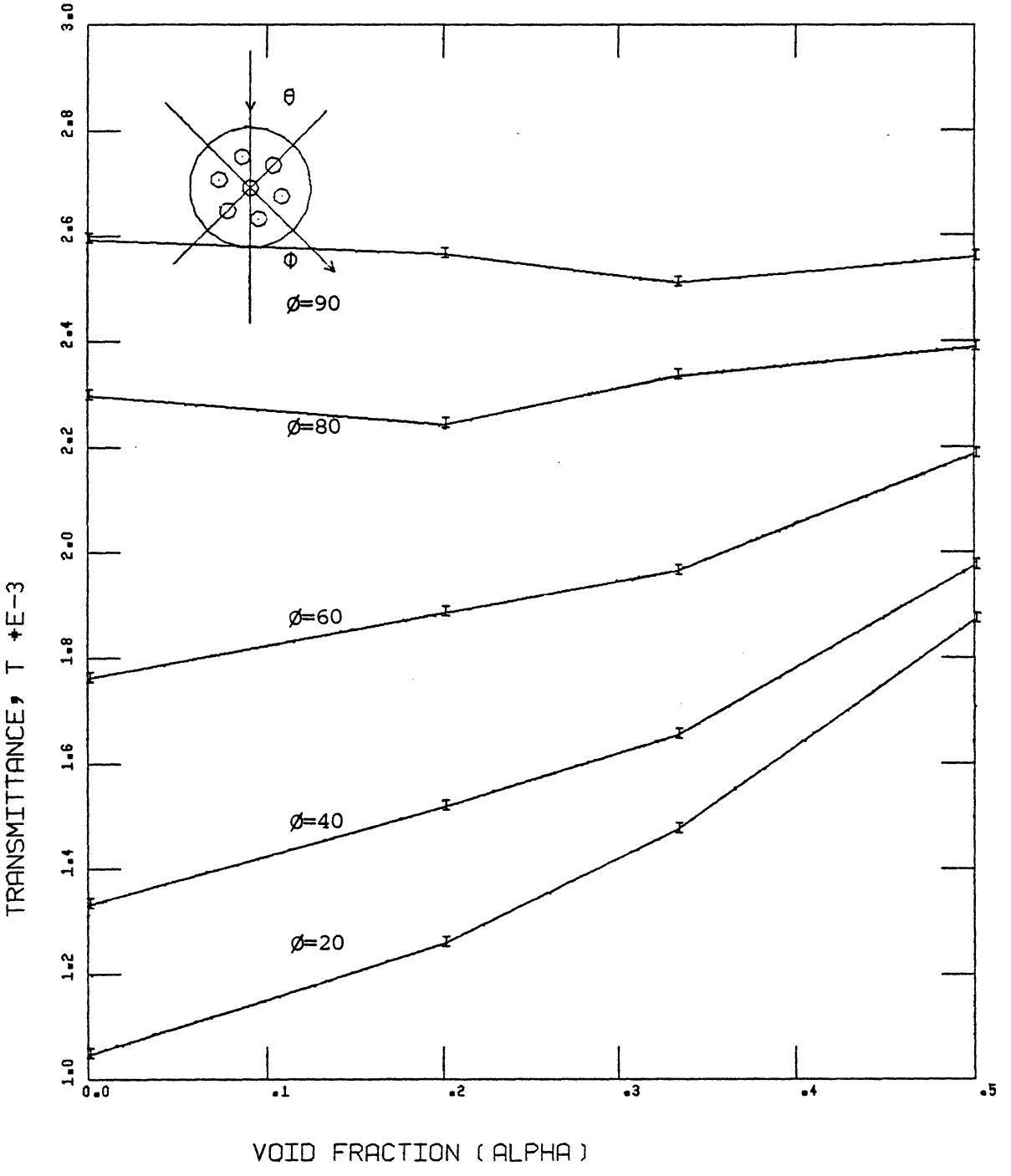

FIGURE 48: Transmittance versus
For Sample #1,14,15,16; $\Theta = 135^{o}$

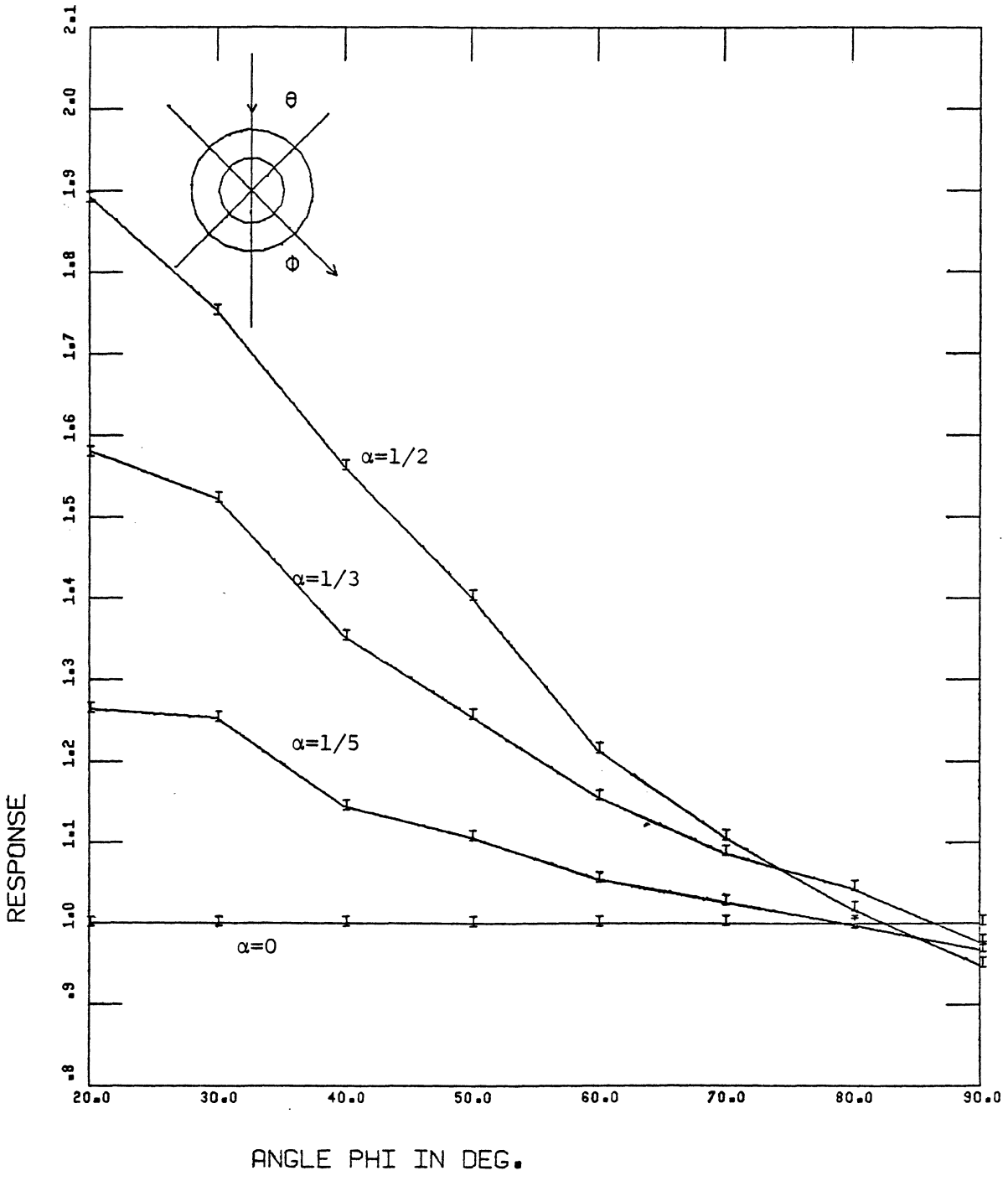

FIGURE 49: Response versus Ø
For Sample #1,2,3,4

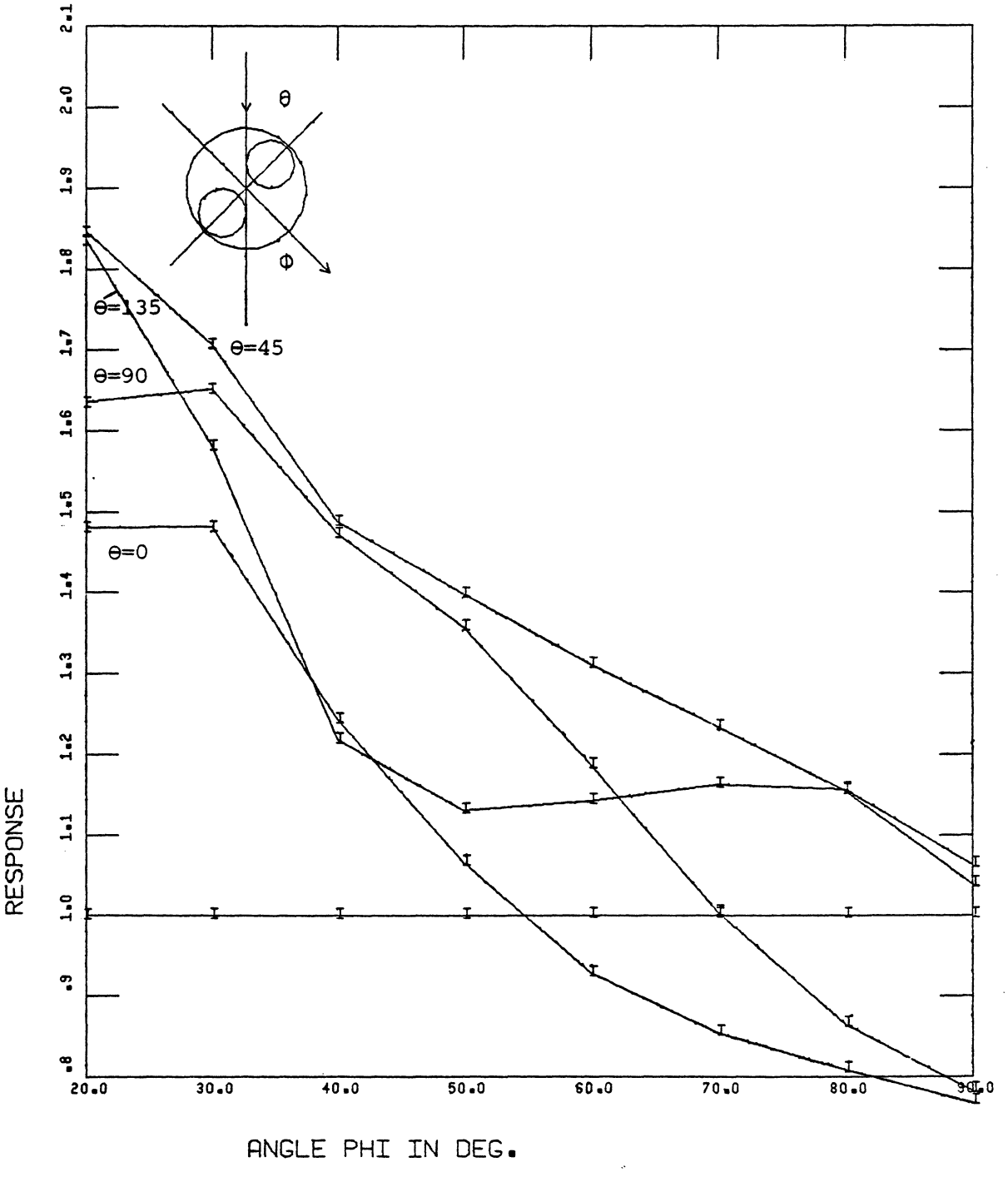

FIGURE 50: Response versus Ø
For Sample #5; θ = 0,45,90,135°

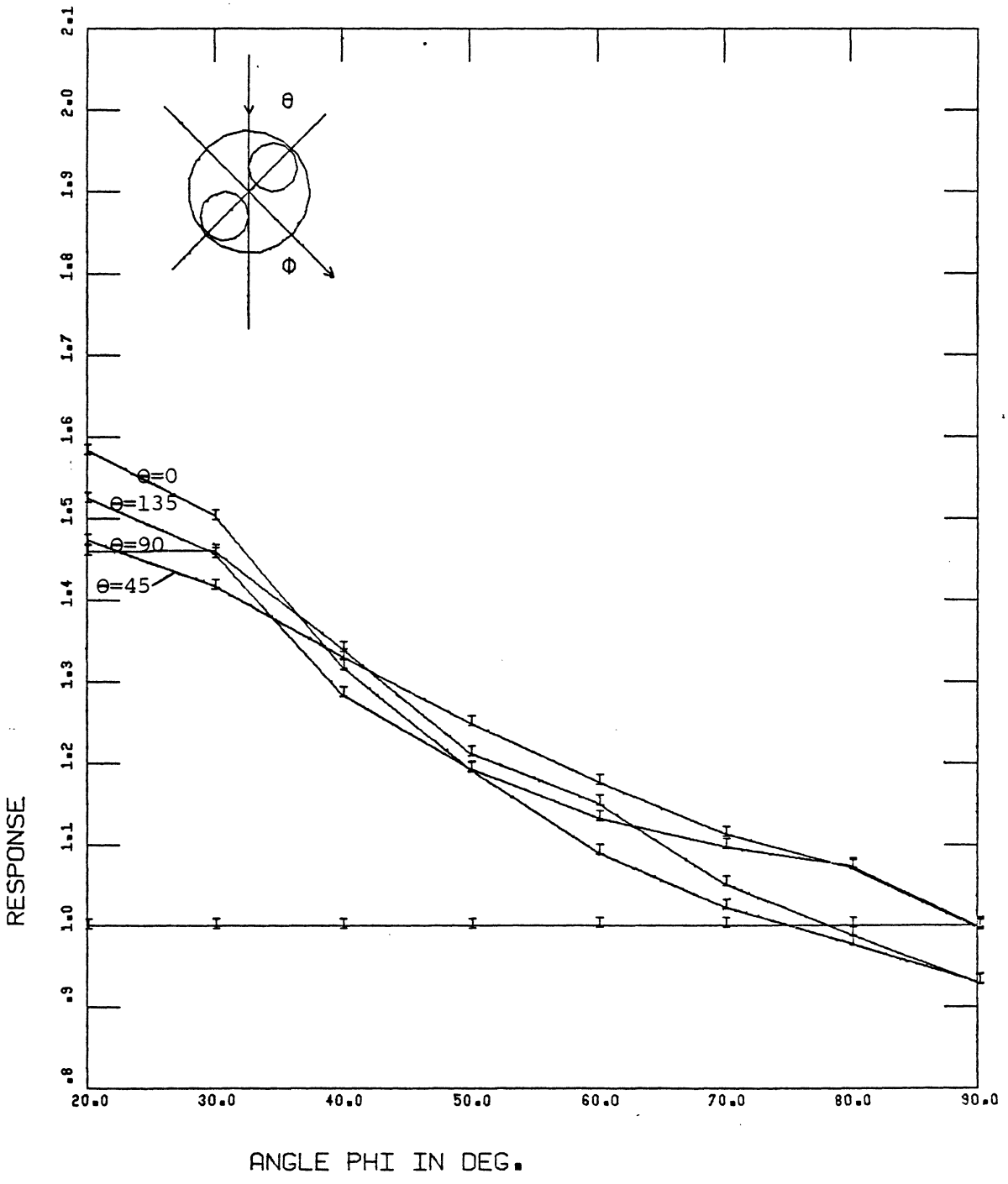

FIGURE 51: Response versus Ø
For Sample #6; Θ = 0,45,90,135°

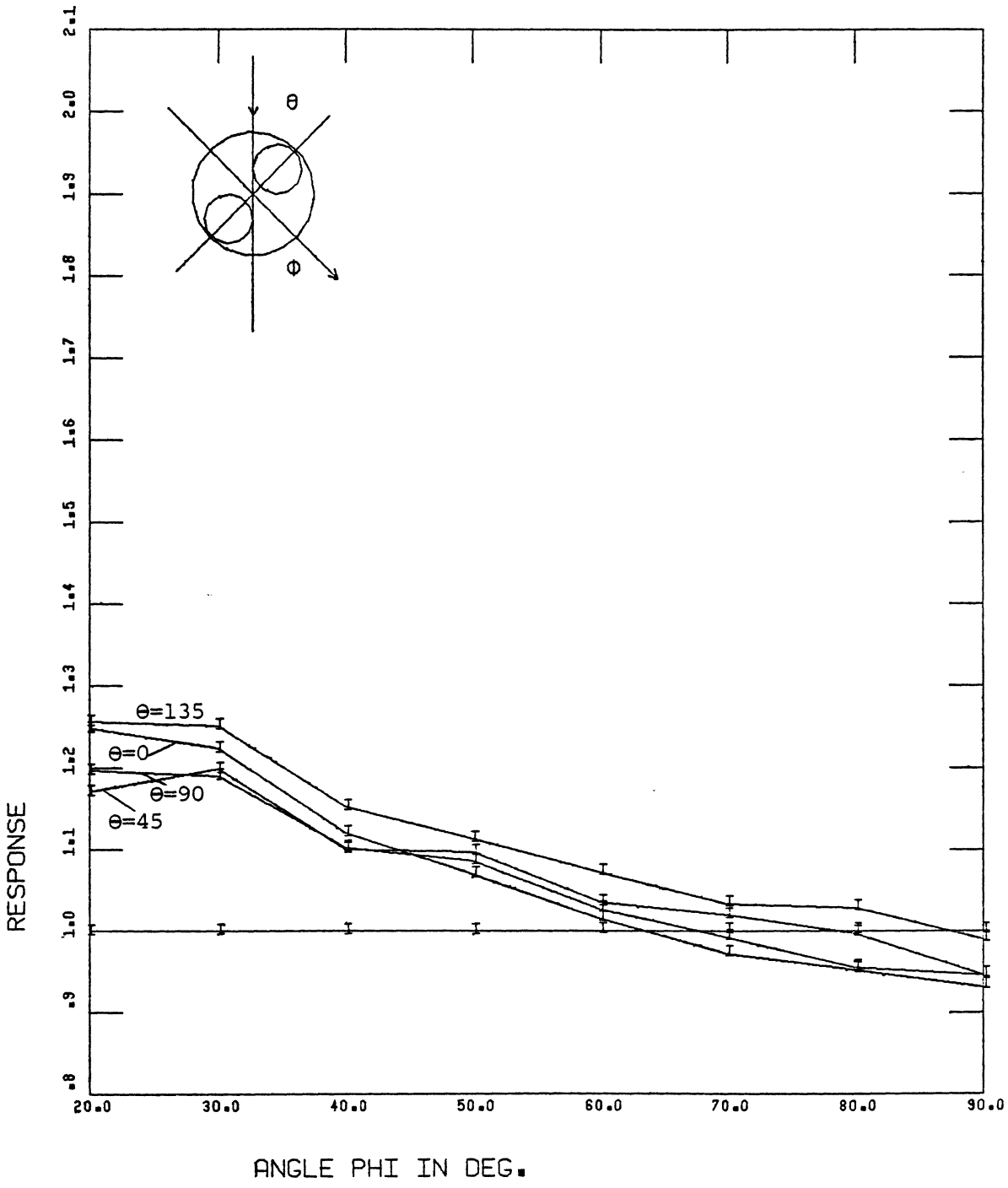

FIGURE 52: Response versus Ø
For Sample #7; Θ = 0,45,90,135°

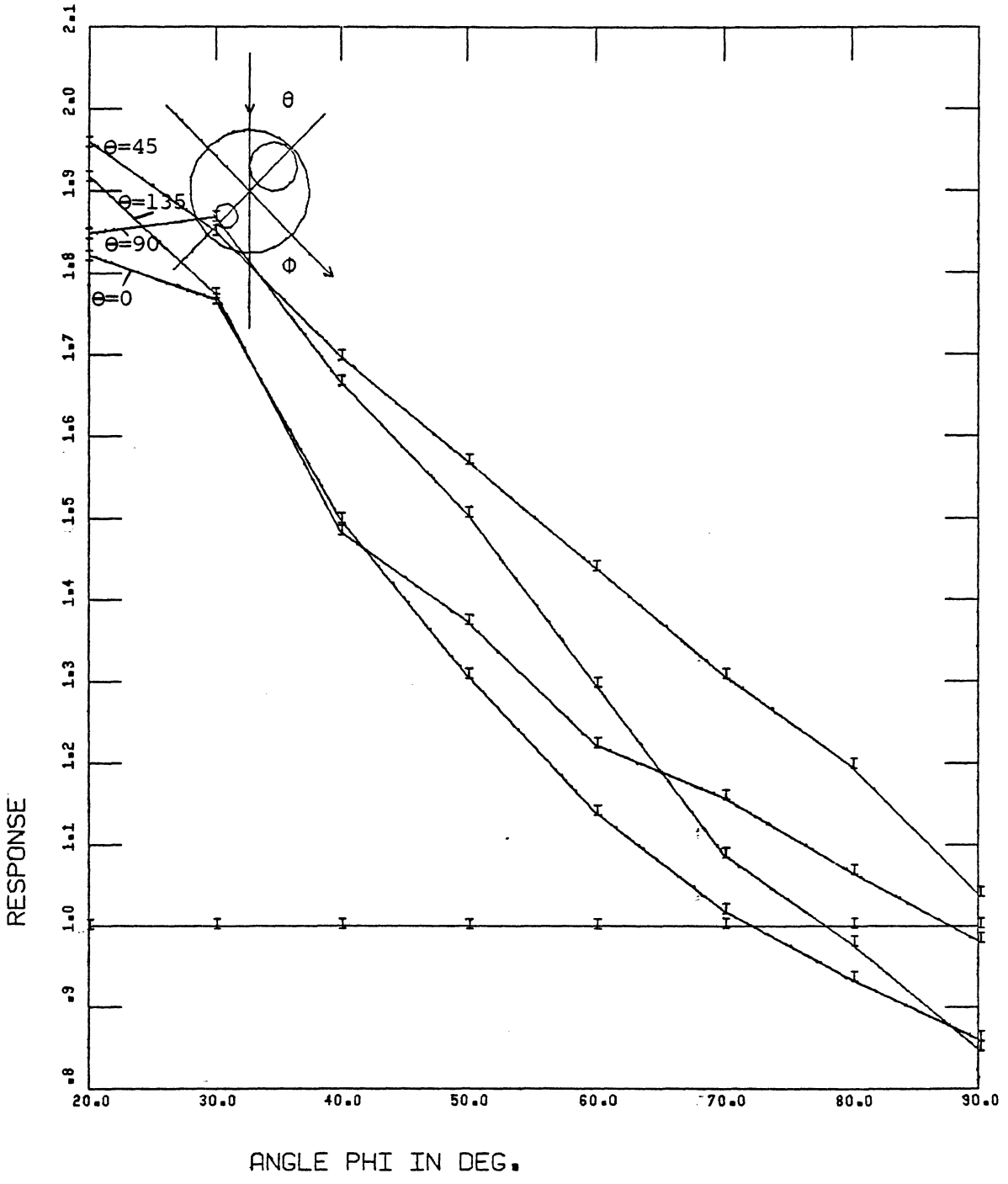

FIGURE 53: Response versus Ø
For Sample #8; θ = 0,45,90,135°

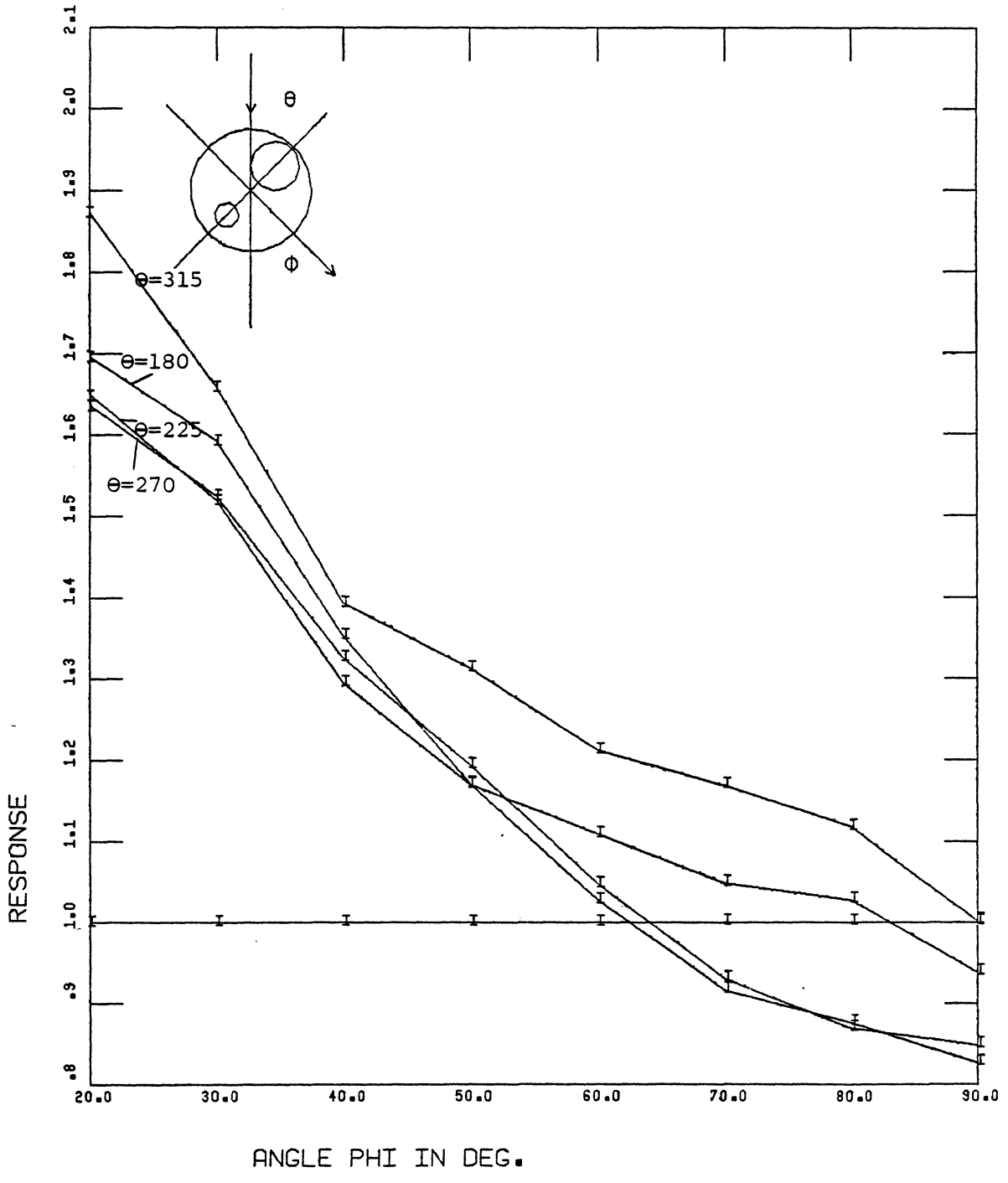

FIGURE 54: Response versus Ø
For Sample #8; θ = 180,225,270,315°

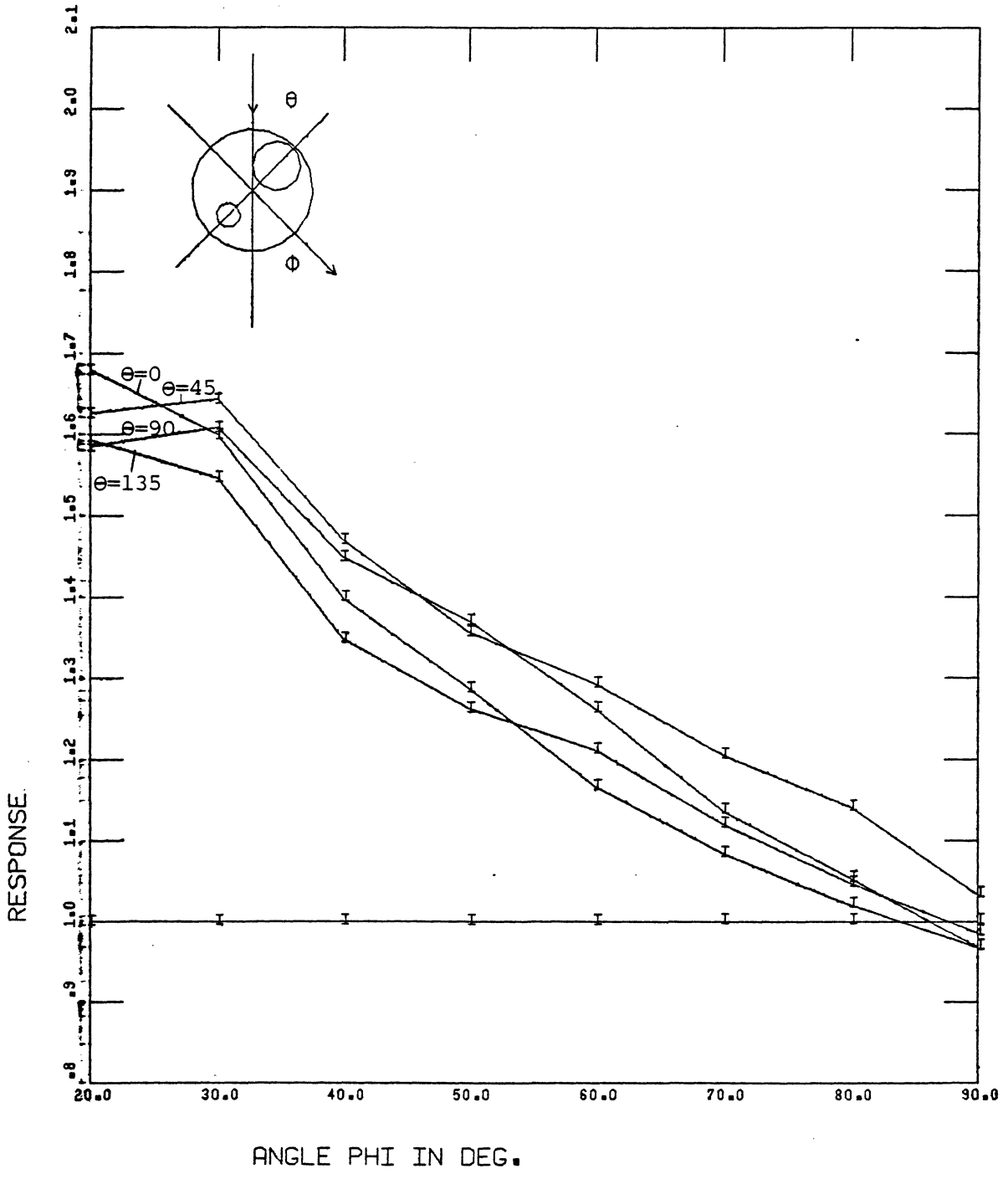

FIGURE 55: Response versus Ø
For Sample #9; θ = 0,45,90,135°

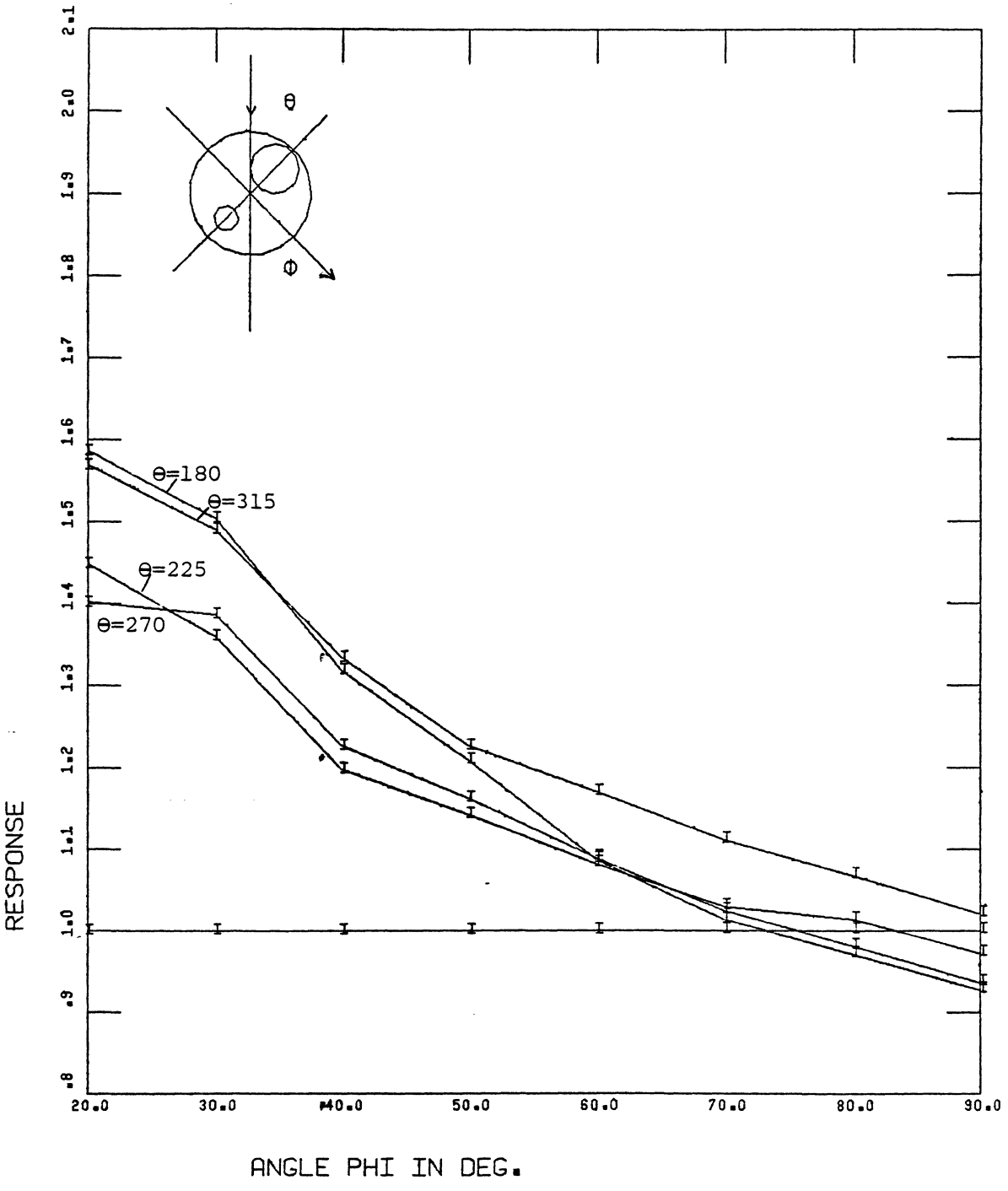

FIGURE 56: Response versus ø
For Sample #9; Θ = 180,225,270,315°

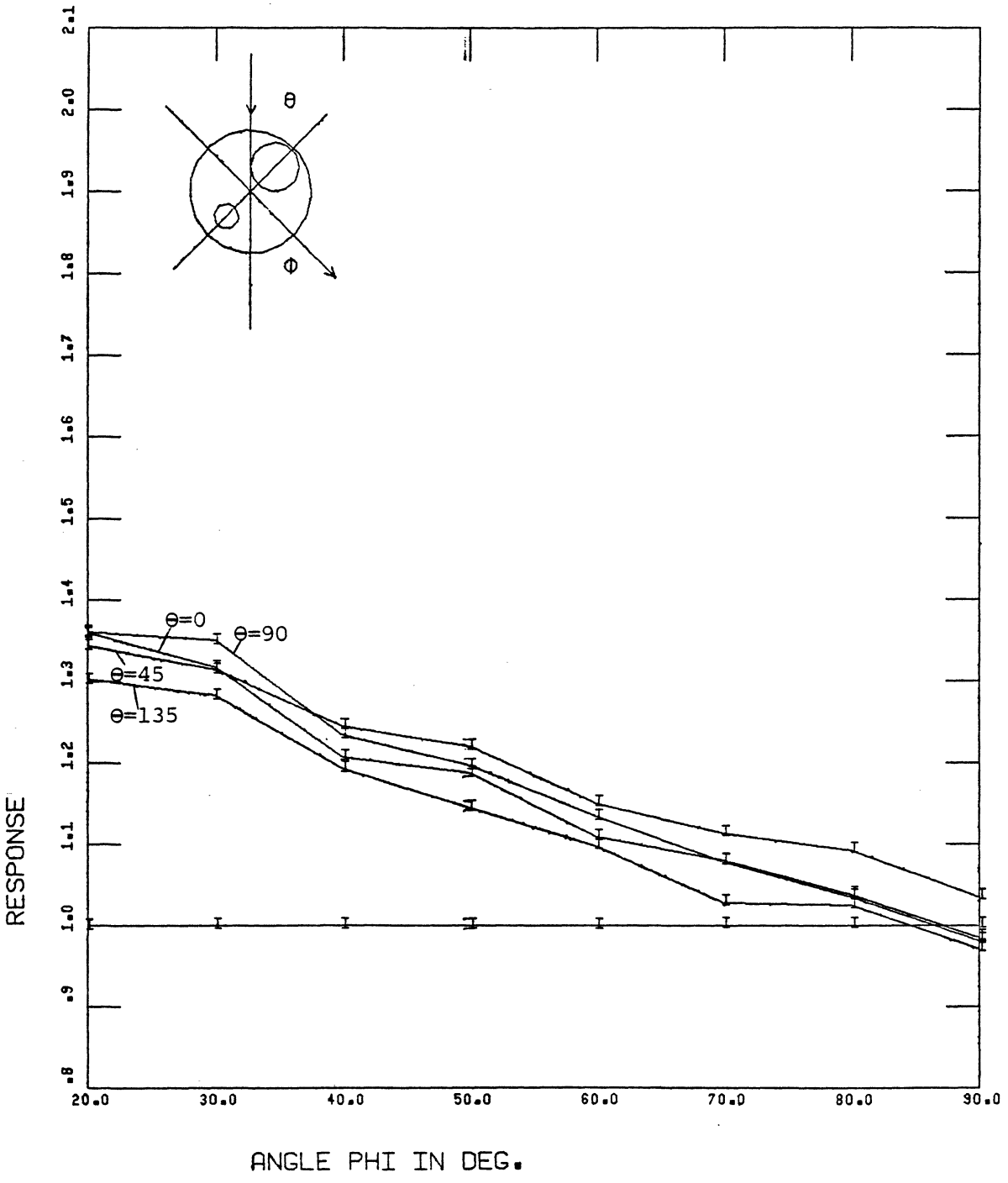

FIGURE 57: Response versus Ø
For Sample #10; θ = 0,45,90,135°

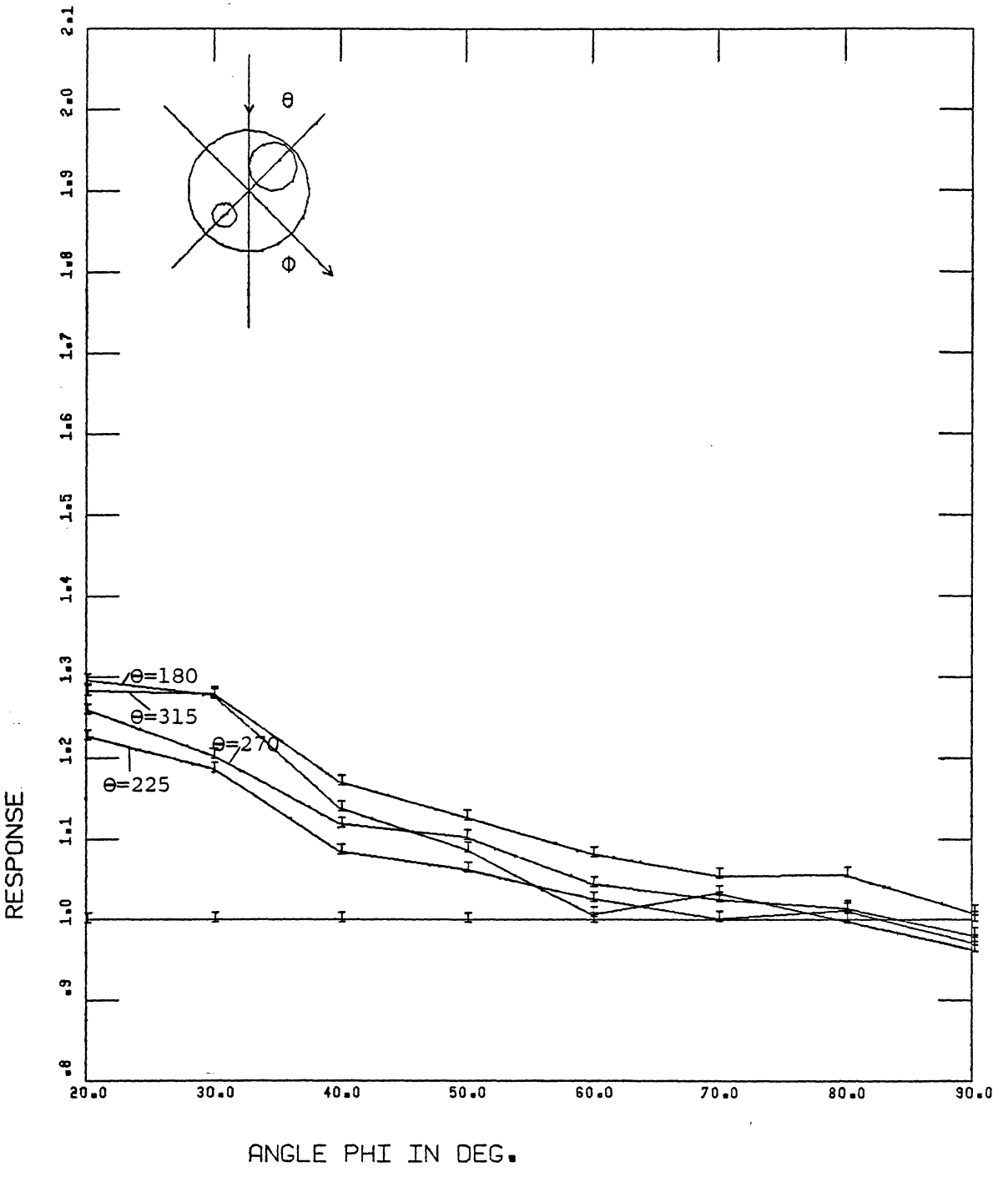

FIGURE 58: Response versus Ø
For Sample #10; θ = 180,225,270,315°

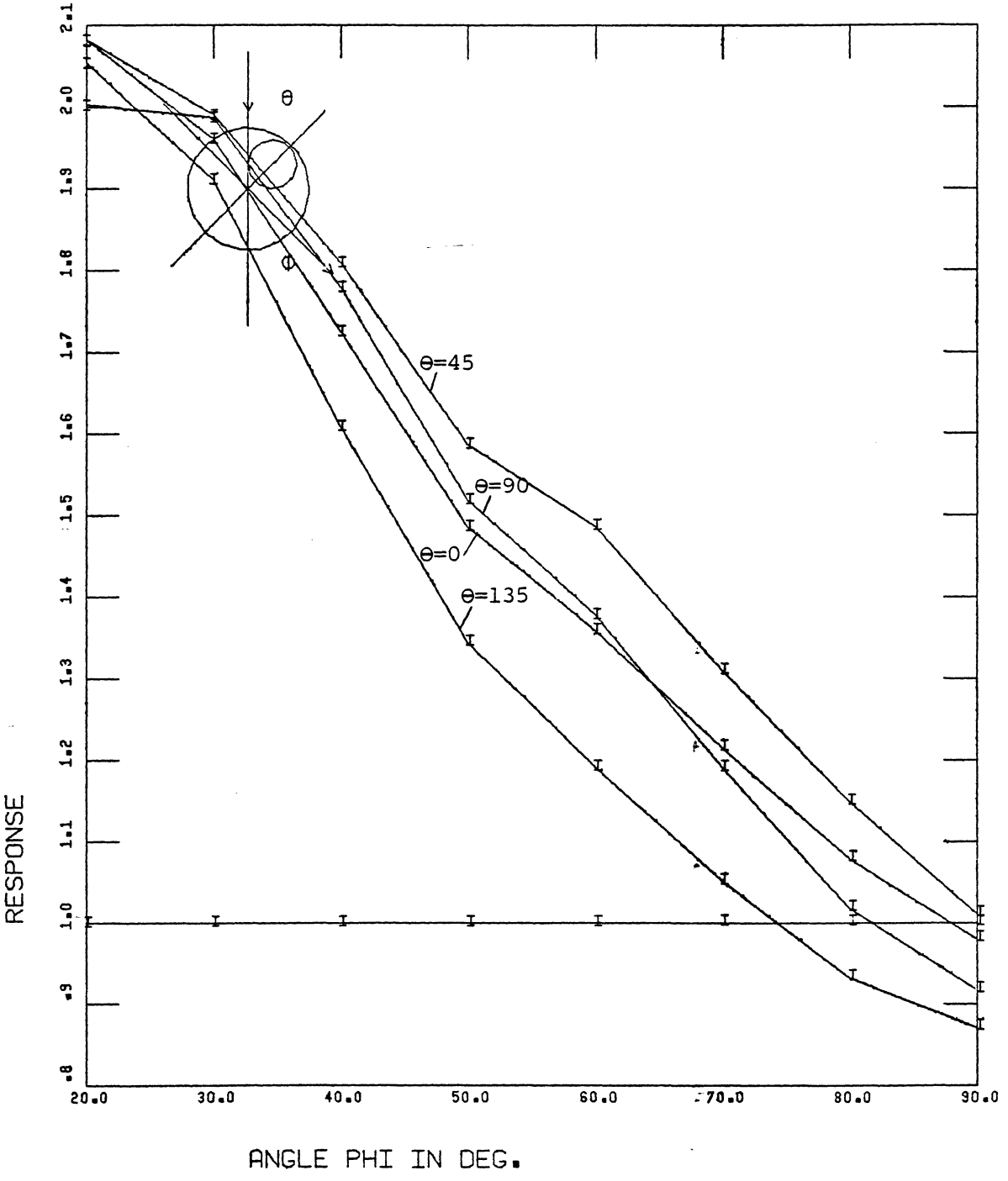

FIGURE 59: Response versus Ø
For Sample #11; θ = 0,45,90,135°

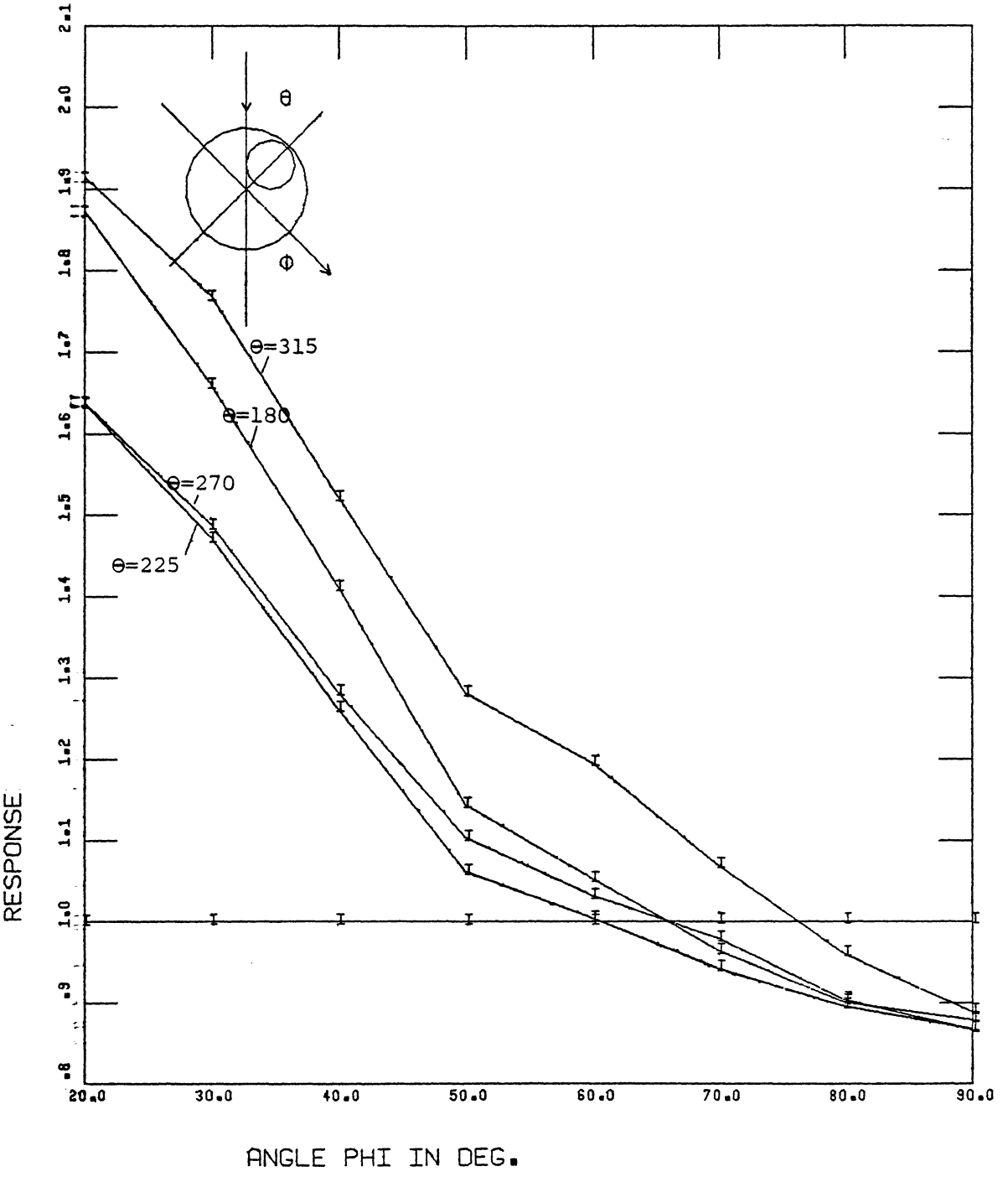

FIGURE 60: Response versus Ø
For Sample #11; Θ = 180,225,270,315°

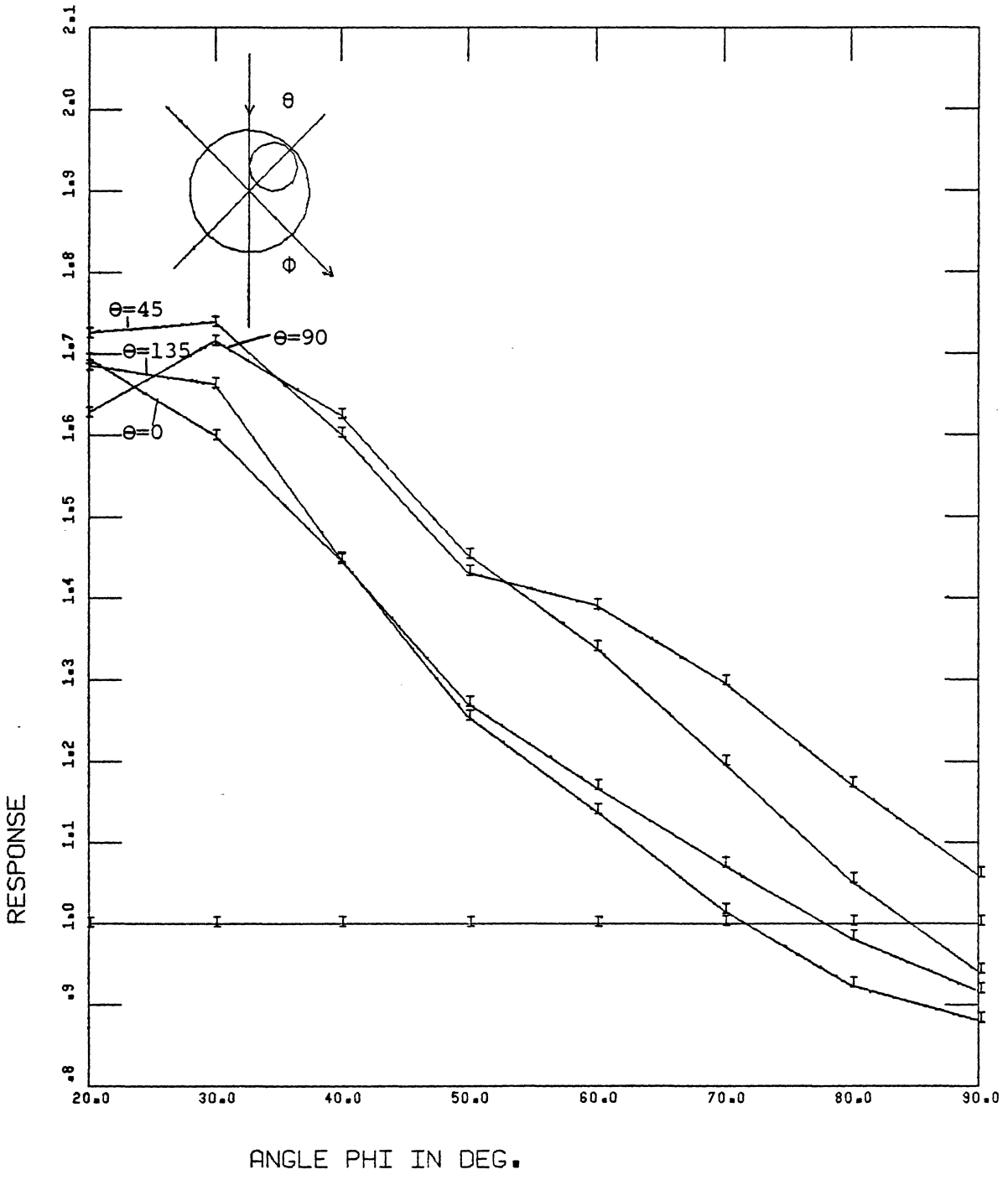

FIGURE 61: Response versus Ø
For Sample #12; θ = 0,45,90,135°

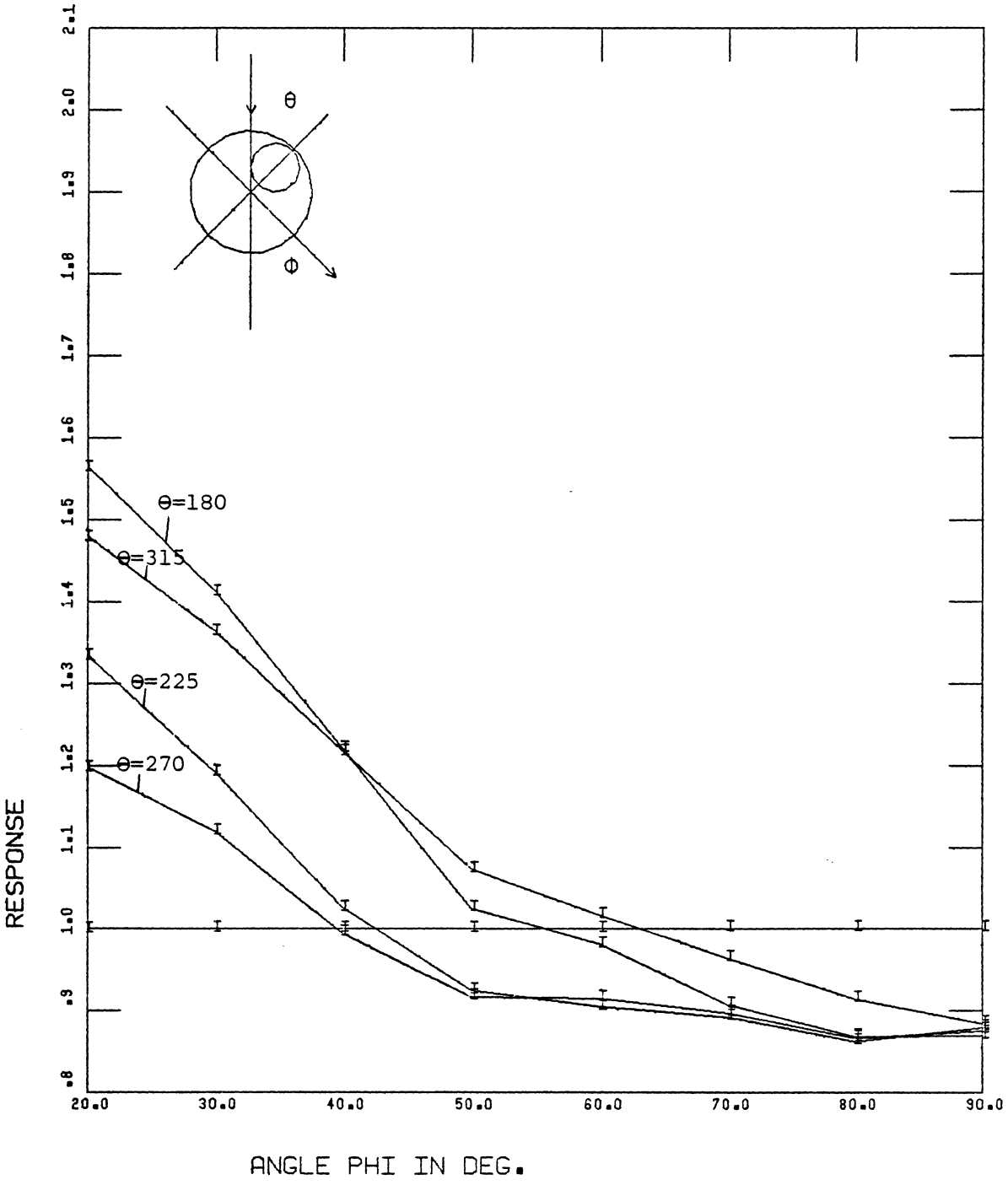

FIGURE 62: Response versus Ø
For Sample #12; θ = 180,225,270,315°

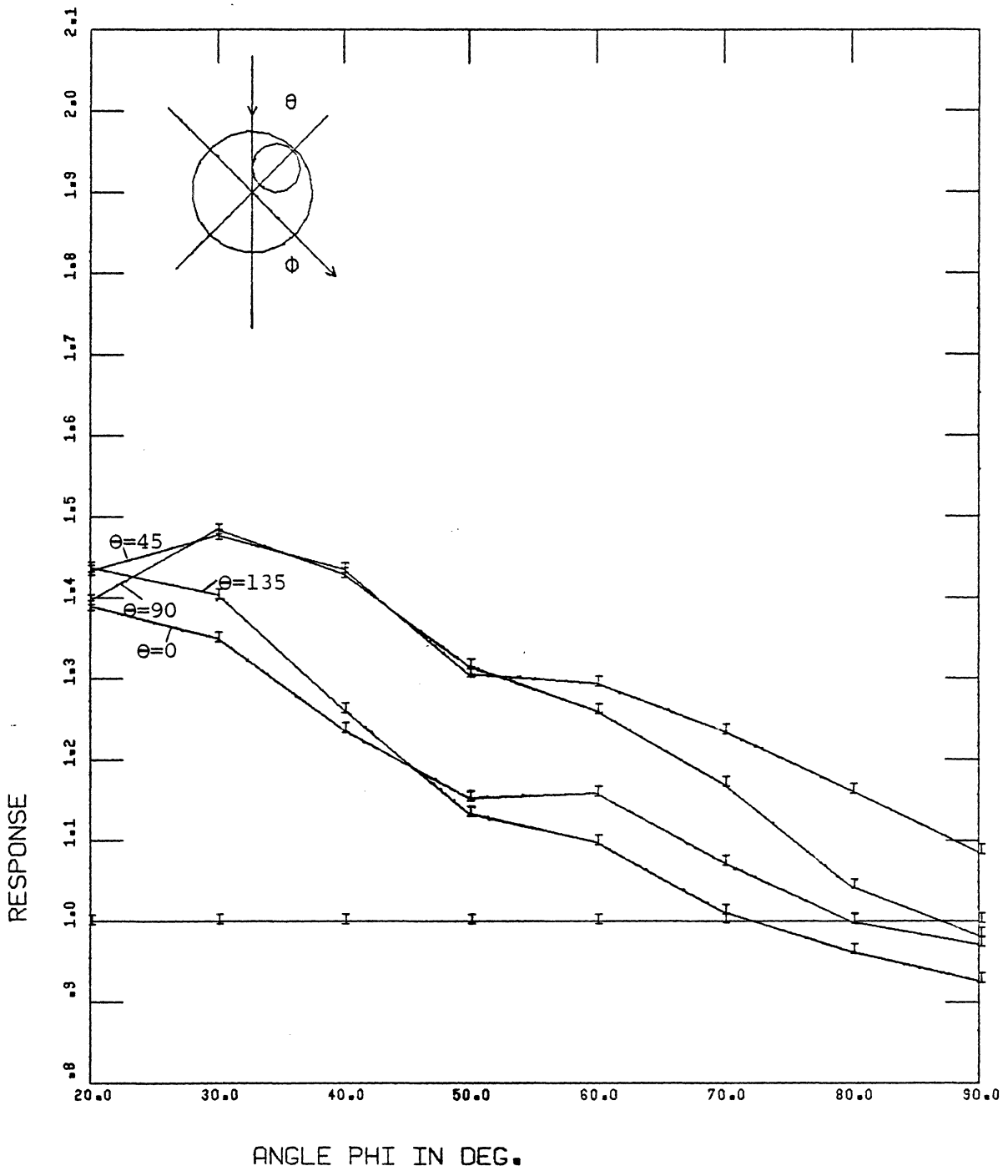

FIGURE 63: Response versus Ø
For Sample #13; θ = 0,45,90,135°

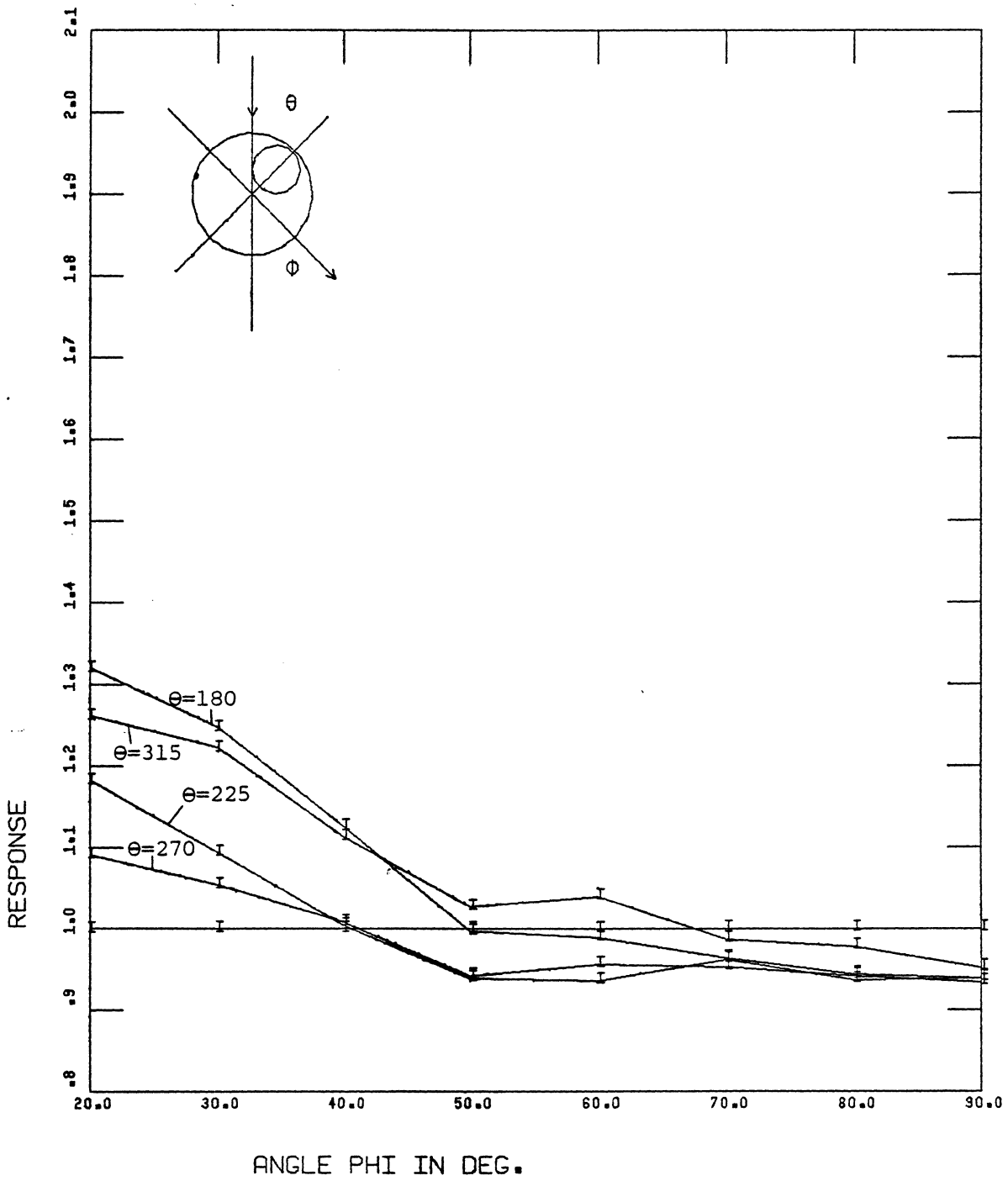

FIGURE 64: Response versus Ø
For Sample #13; θ = 180,225,270,315°

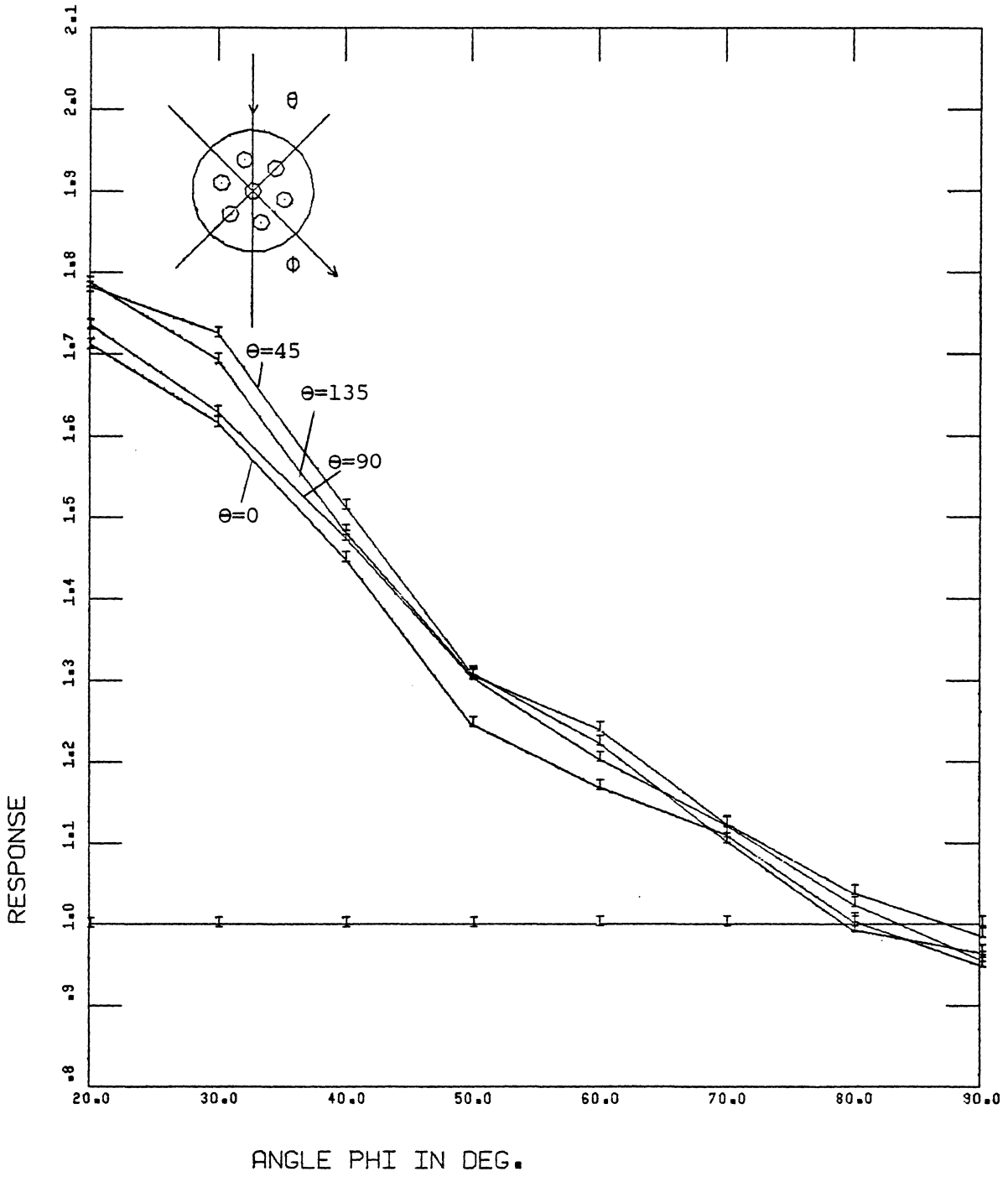

FIGURE 65: Response versus Ø
For Sample #14; Θ = 0,45,90,135°

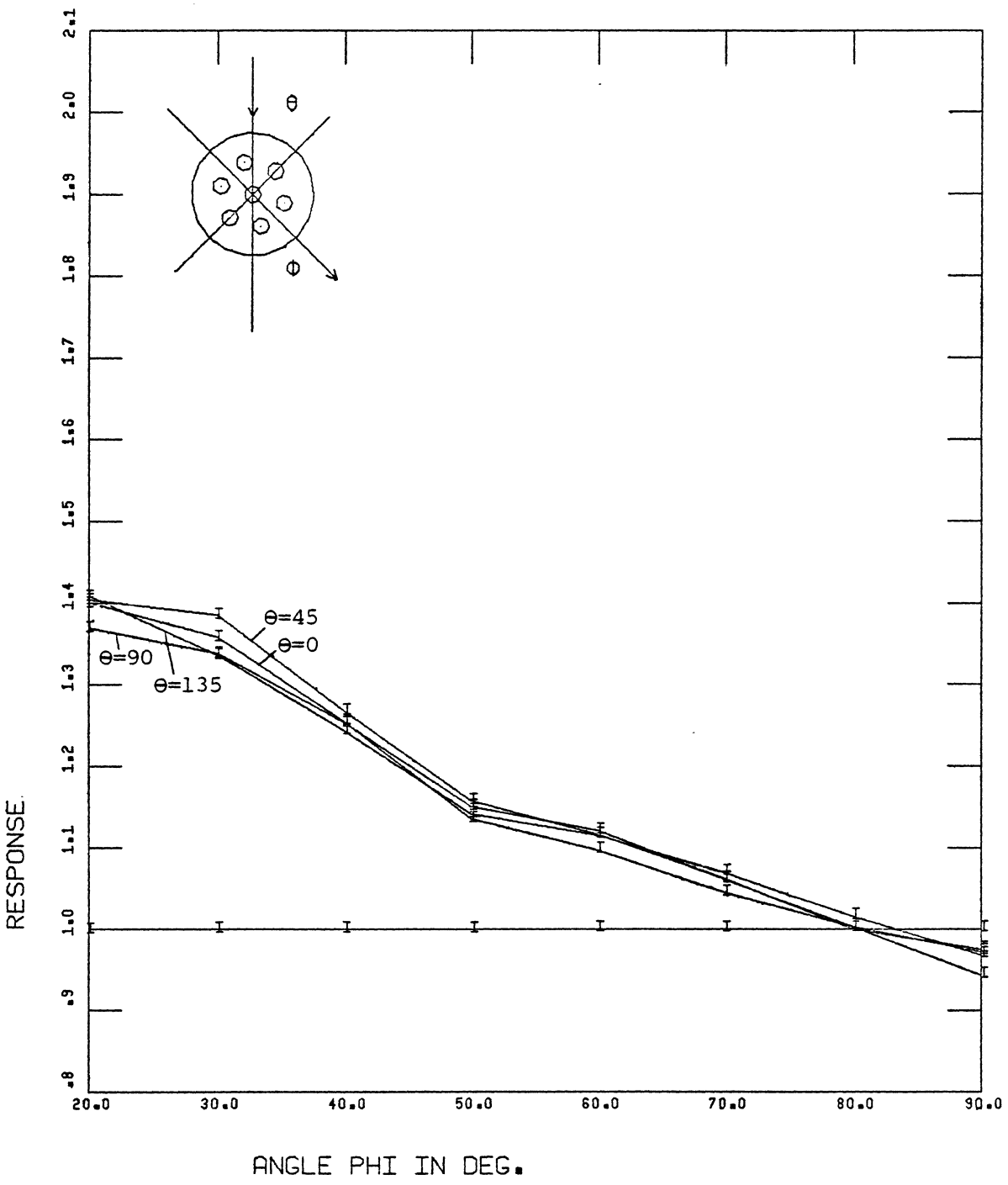

FIGURE 66: Response versus Ø
For Sample #15; θ = 0,45,90,135°

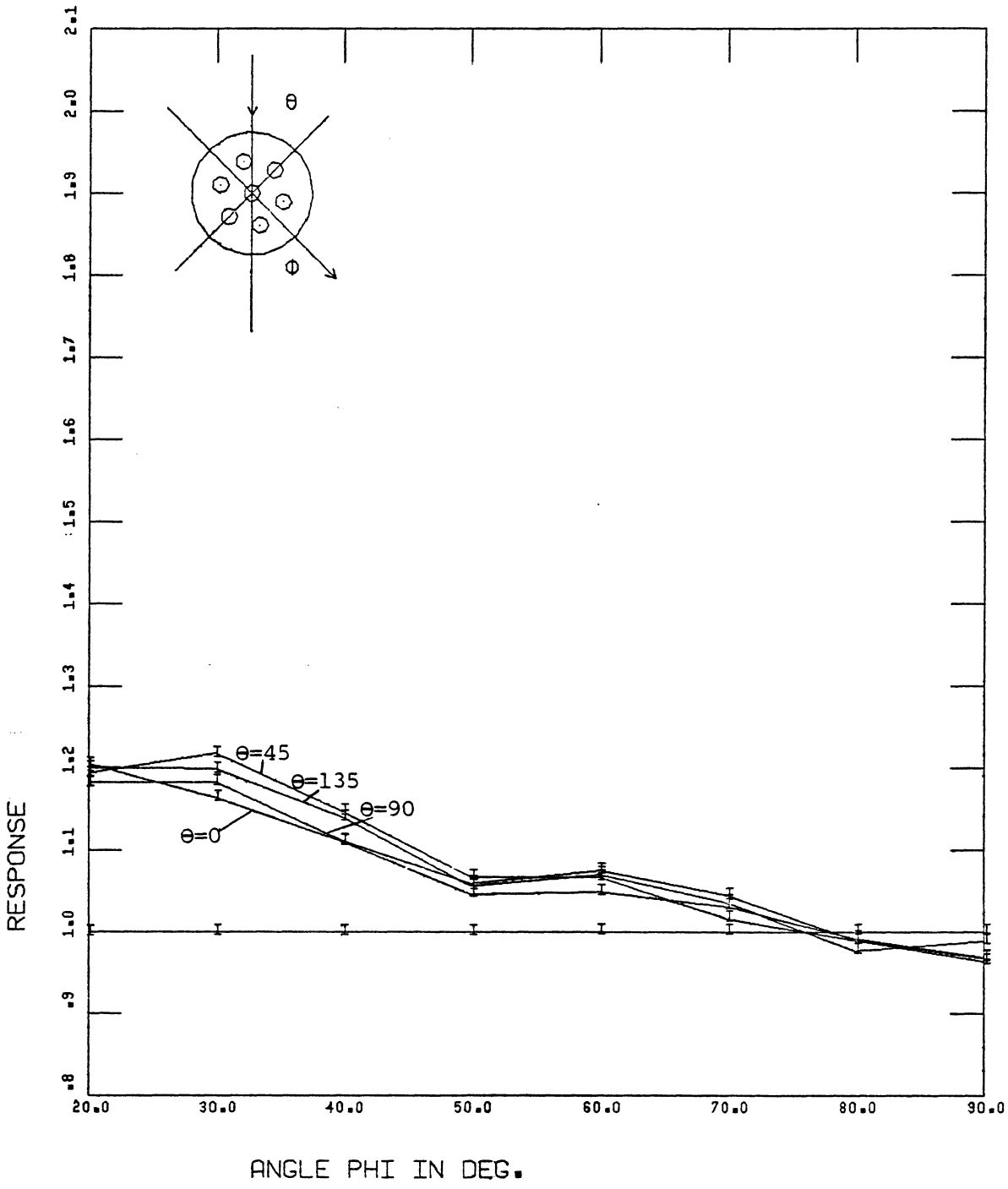

FIGURE 67: Response versus Ø
For Sample #16; θ = 0,45,90,135°

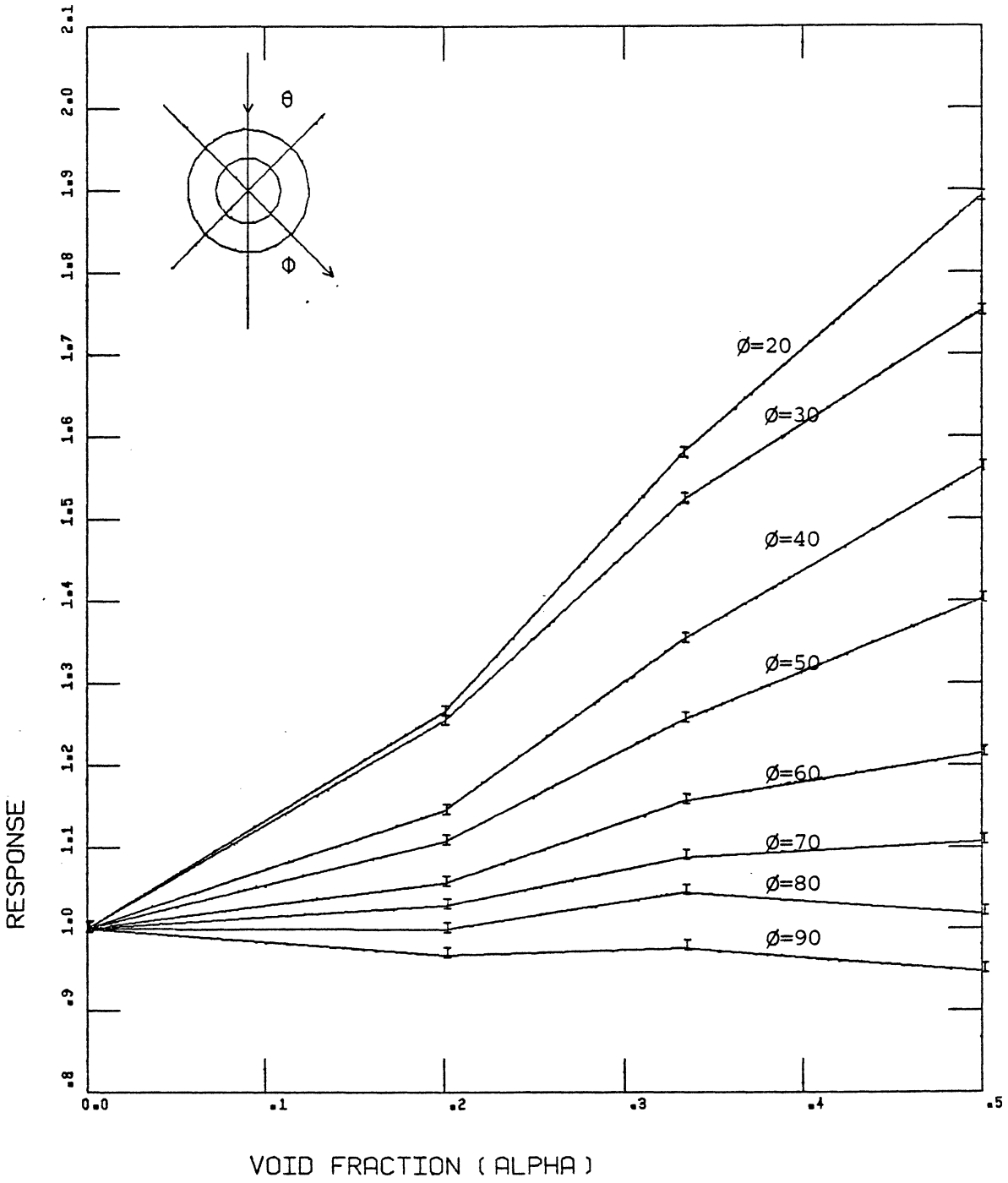

FIGURE 68: Response versus
For Sample #1,2,3,4; $\theta = 0^{\circ}$

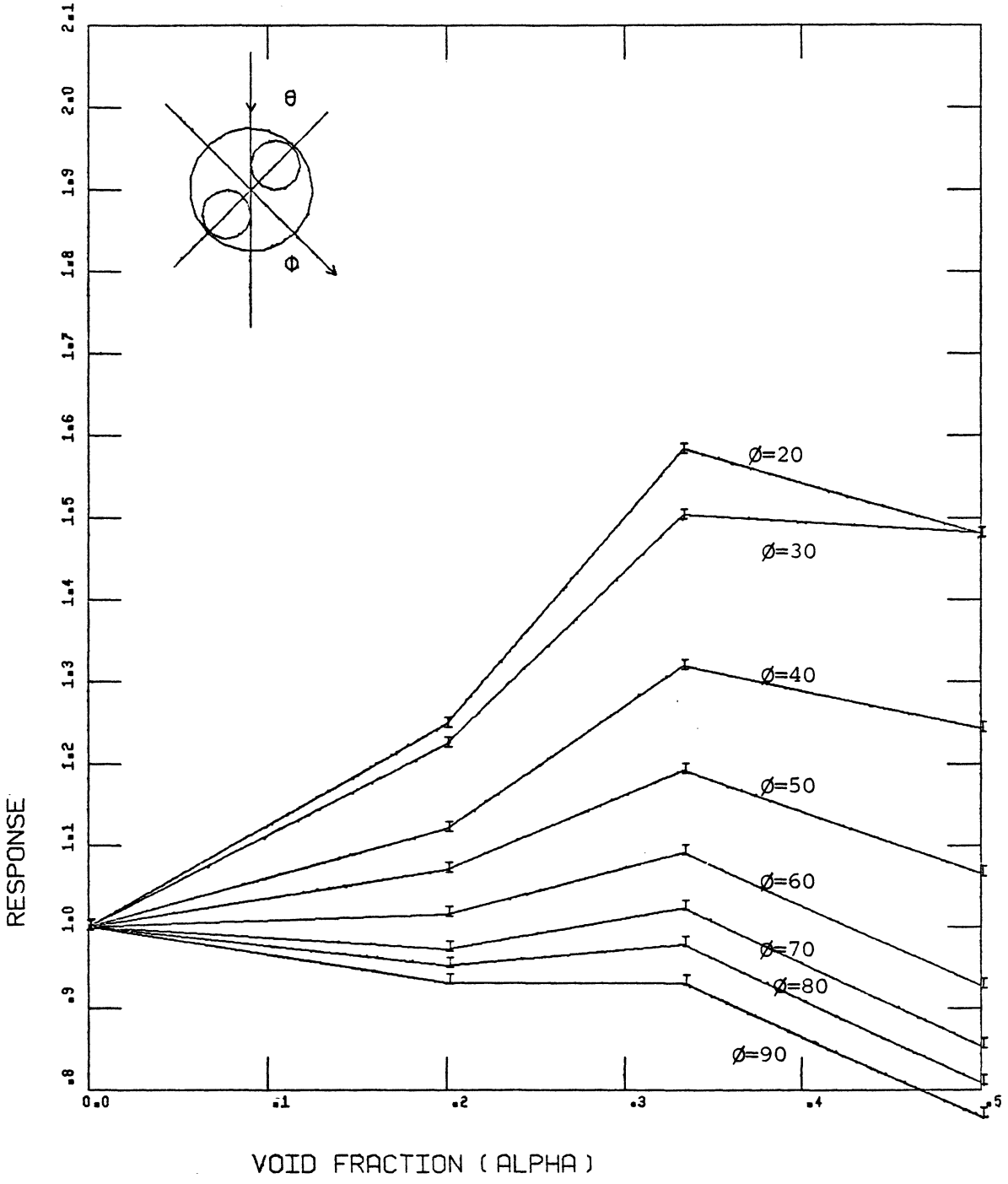

FIGURE 69: Response versus
For Sample #1,5,6,7; Θ = 0

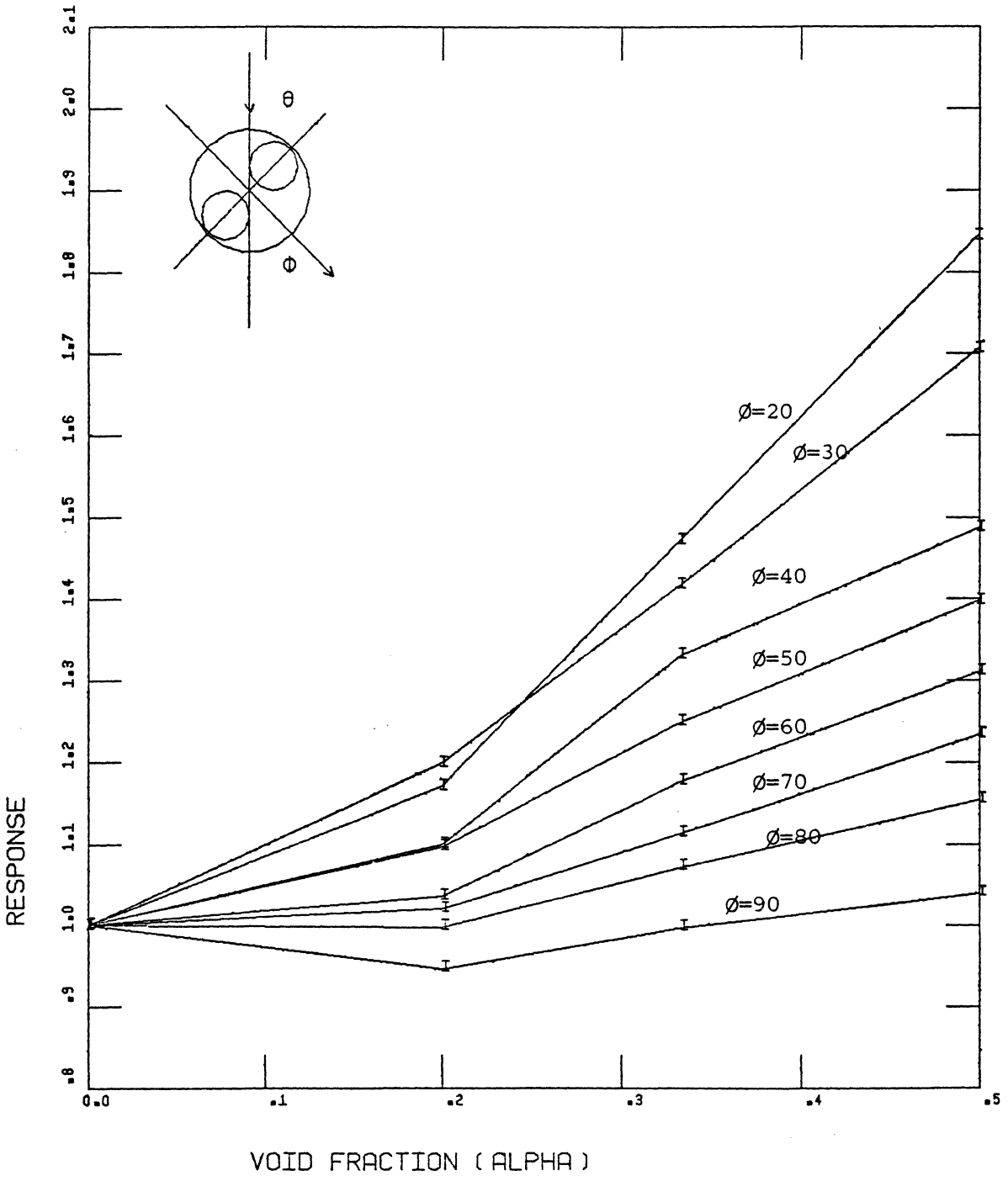

FIGURE 70: Response versus
For Sample #1,5,6,7; $\Theta = 45^{\circ}$

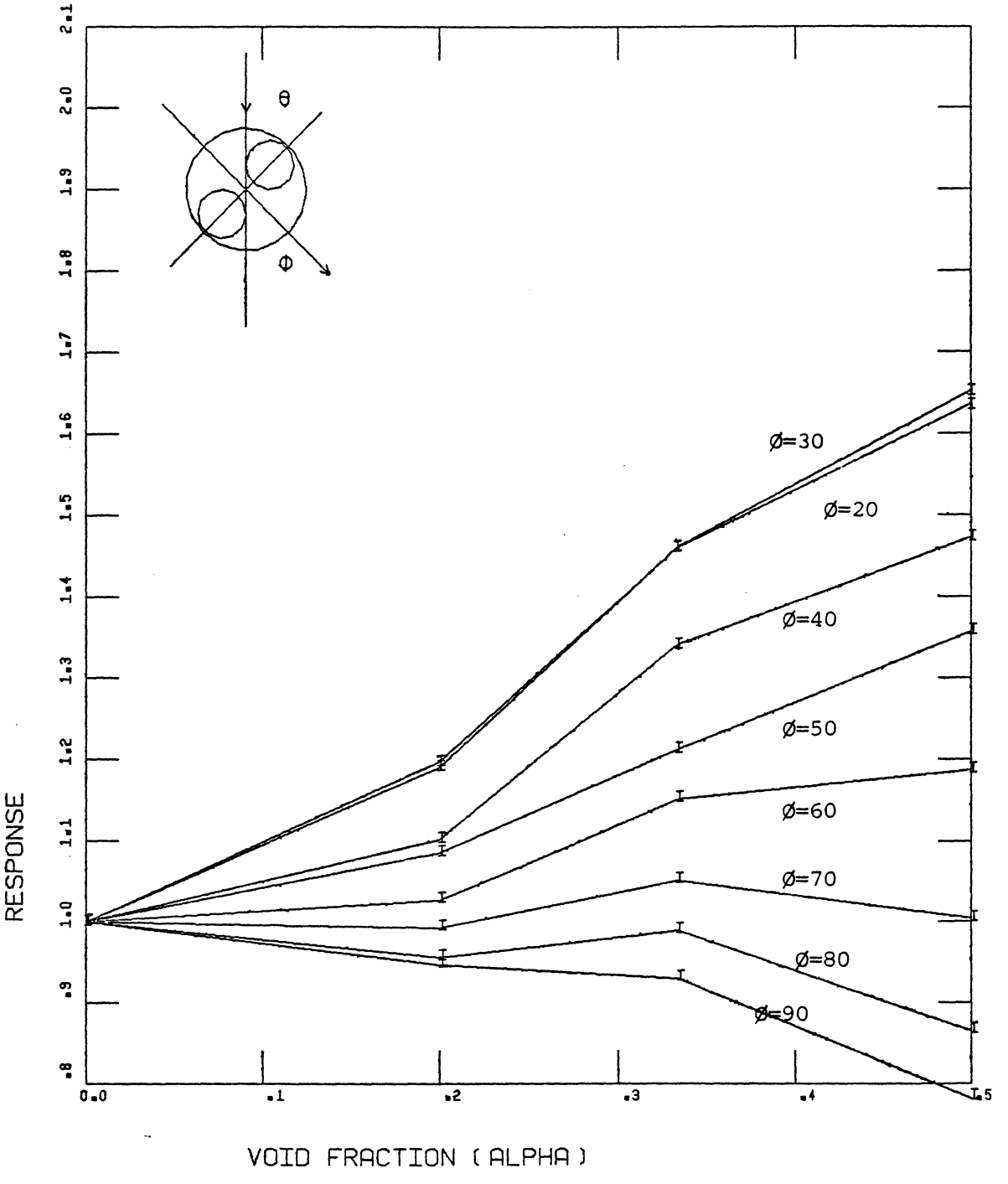

FIGURE 71: Response versus
For Sample #1,5,6,7; $\Theta = 90^{\circ}$

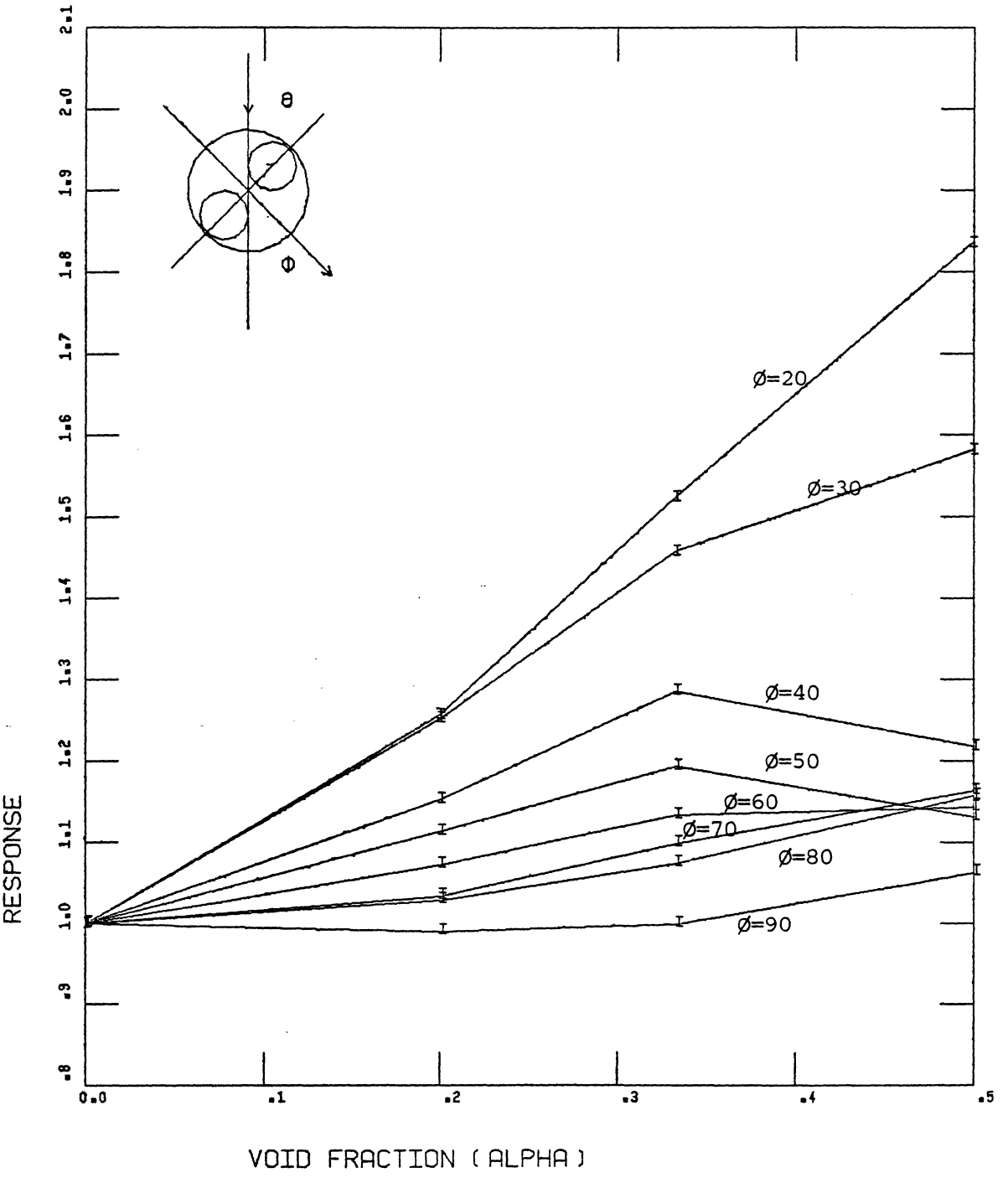

FIGURE 72: Response versus
For Sample # 1,5,6,7 $\theta = 135^{\circ}$

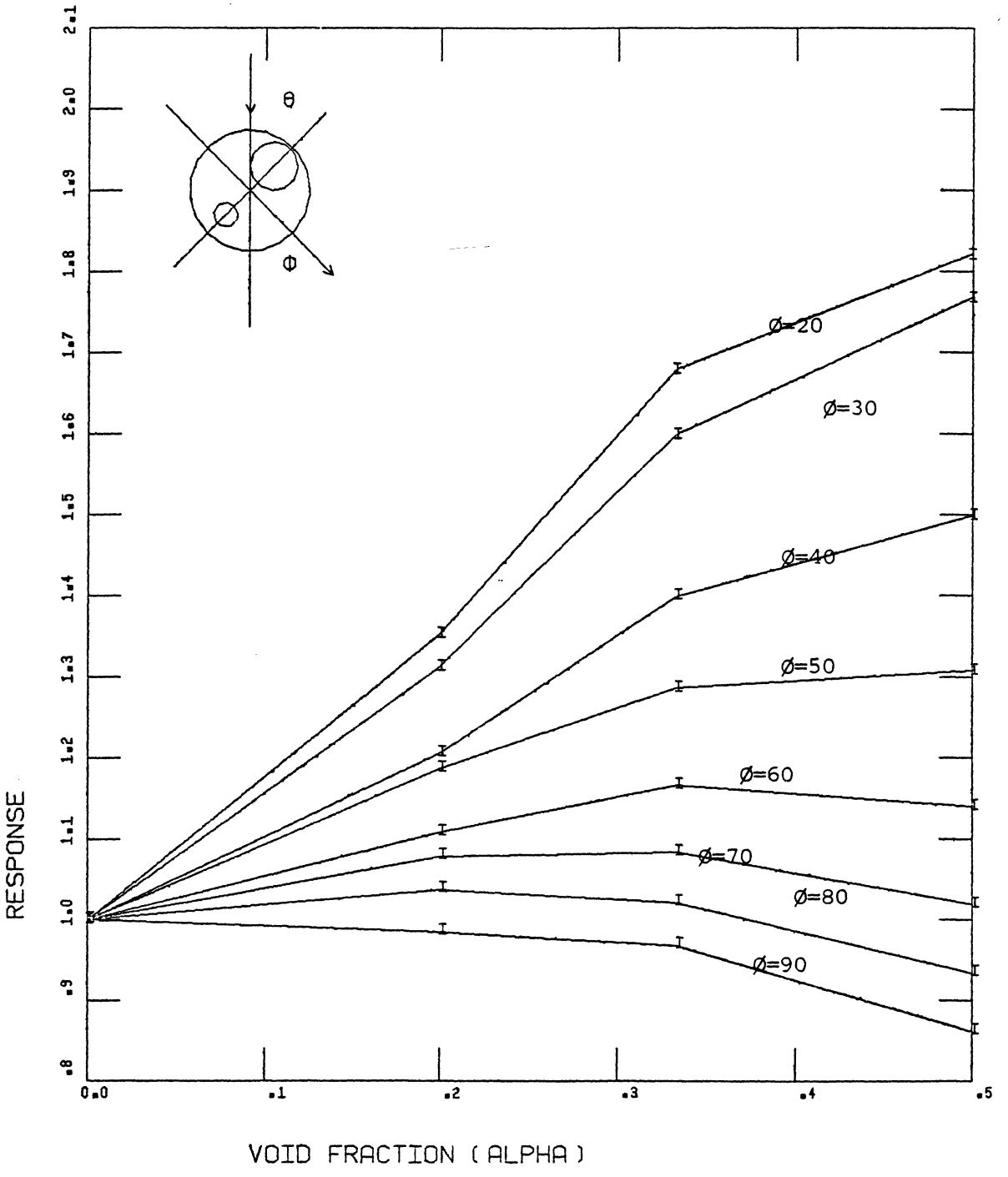

FIGURE 73: Response versus
For Sample #1,8,9,10; $\Theta = 0^{\circ}$

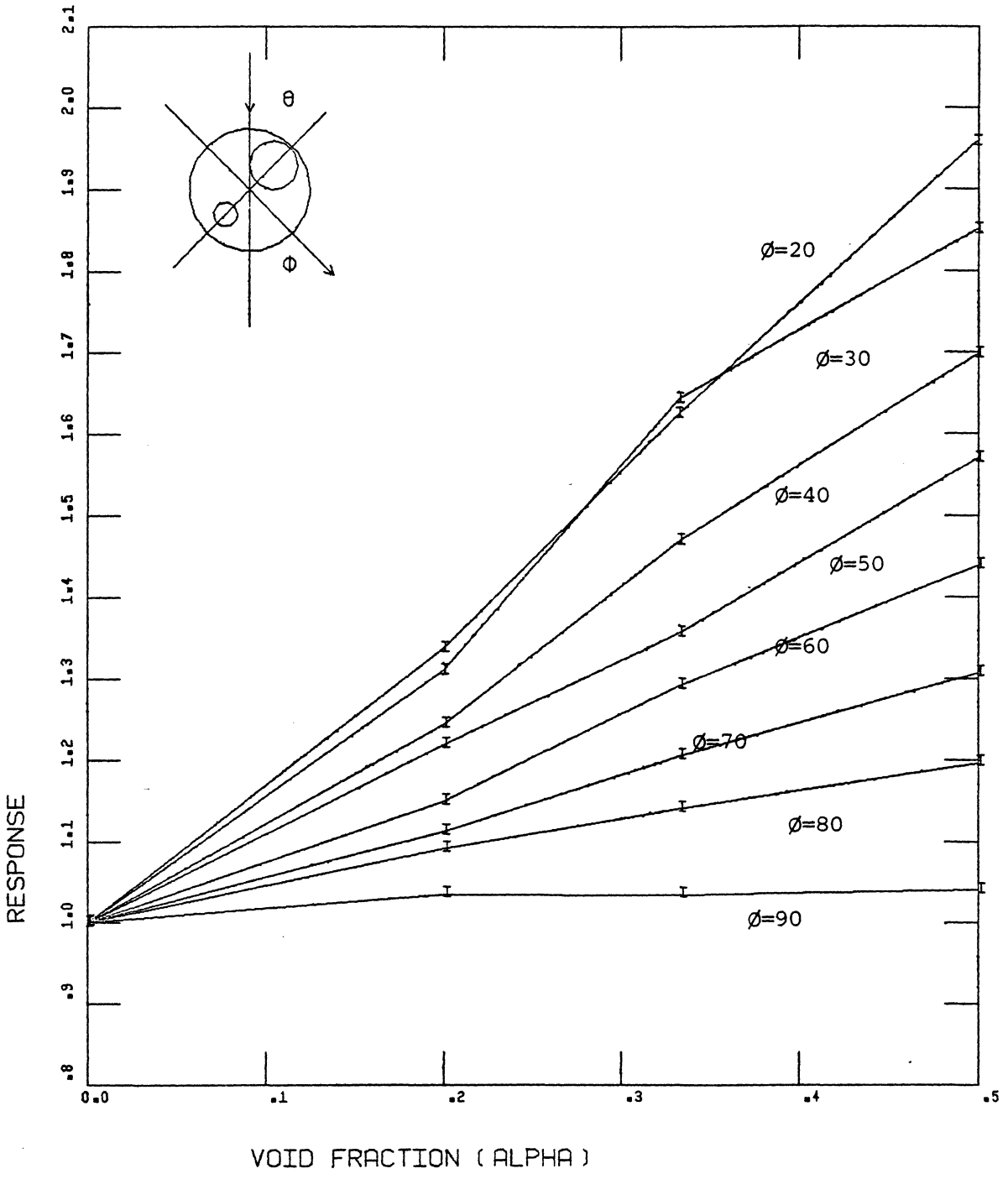

FIGURE 74: Response versus
For Sample #1,8,9,10; $\theta = 45^{\circ}$

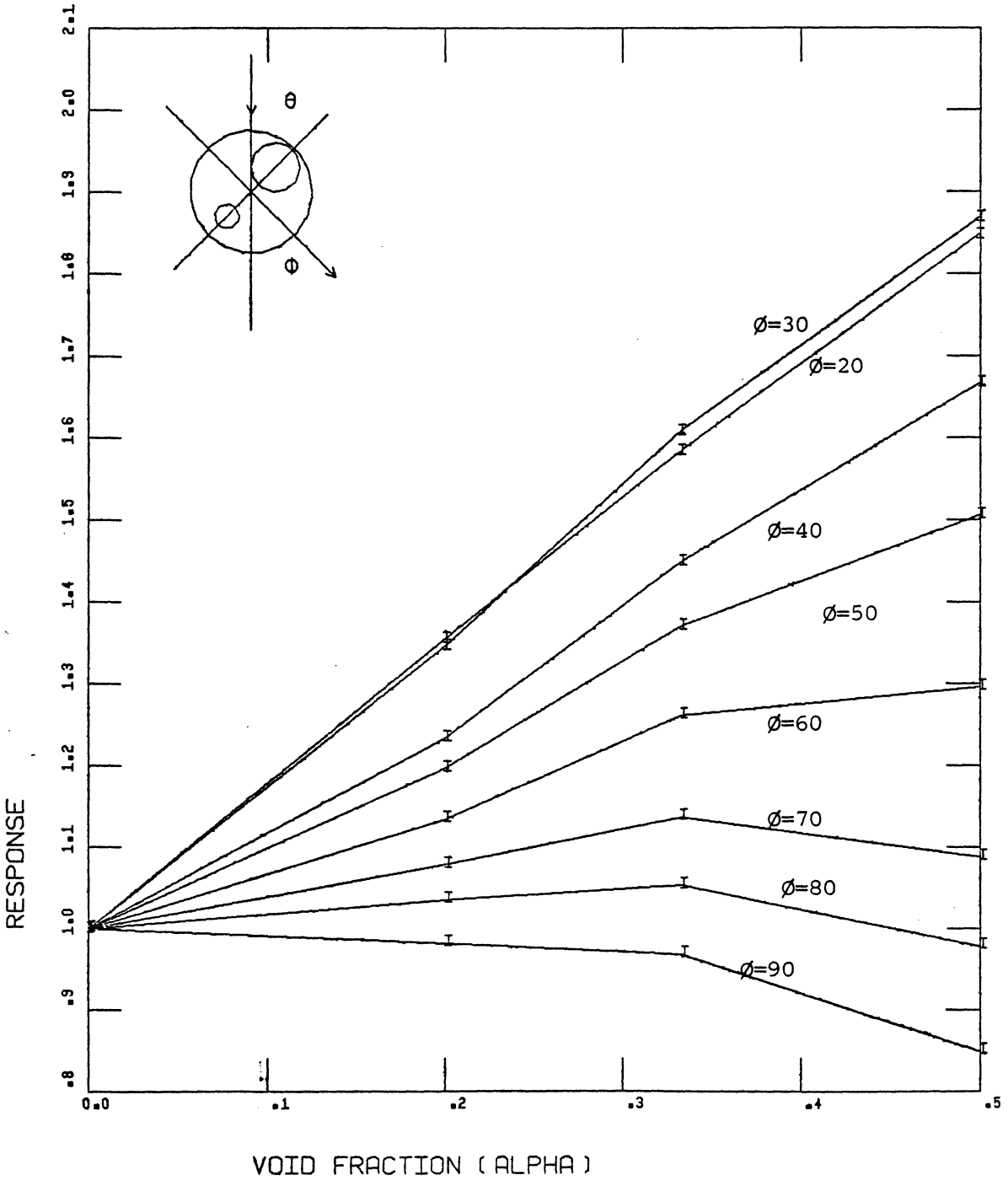

FIGURE 75: Response versus
For Sample #1,8,9,10; $\Theta = 90^{\circ}$

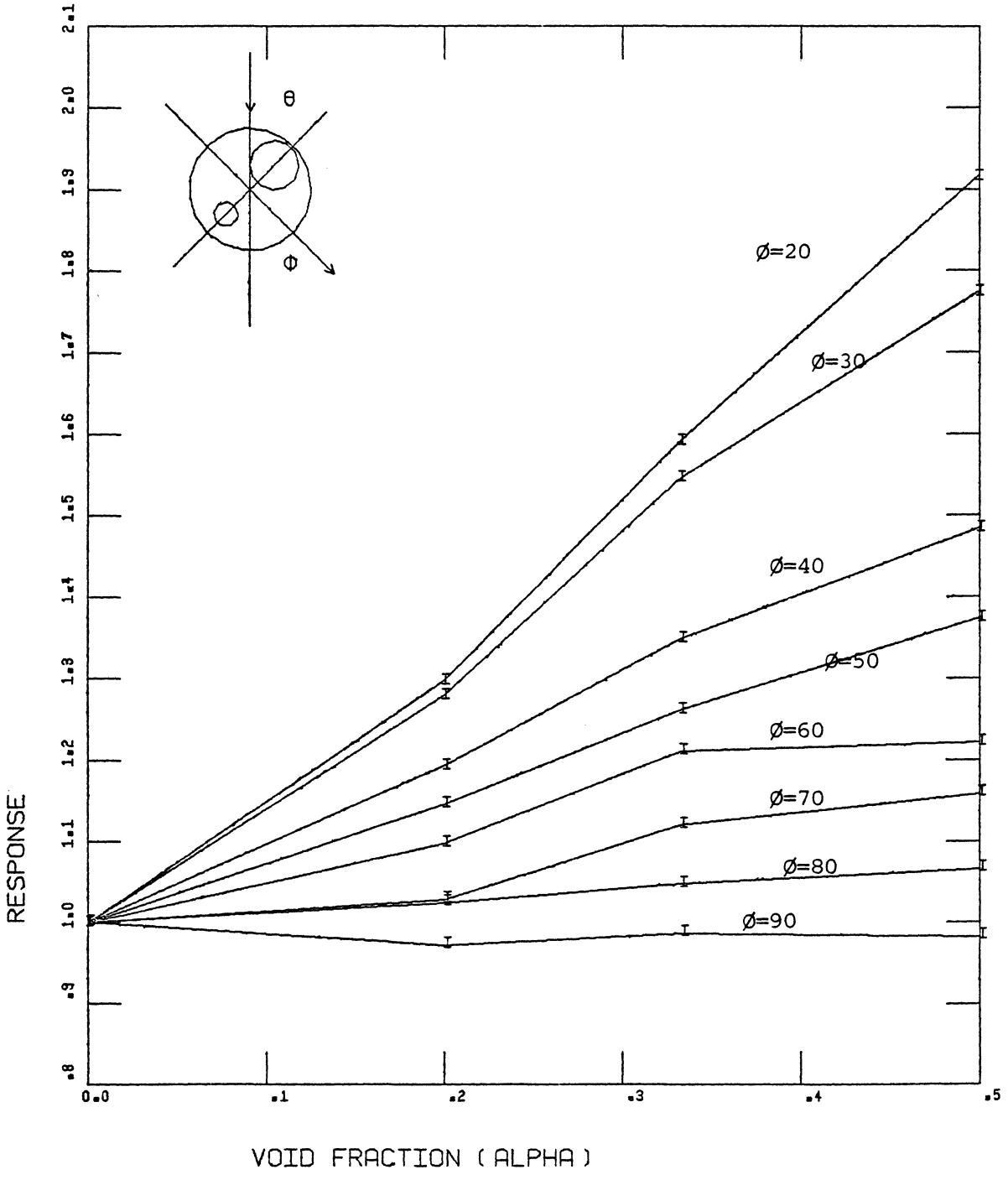

FIGURE 76: Response versus
For Sample #1,8,9,10; $\theta = 135^{o}$

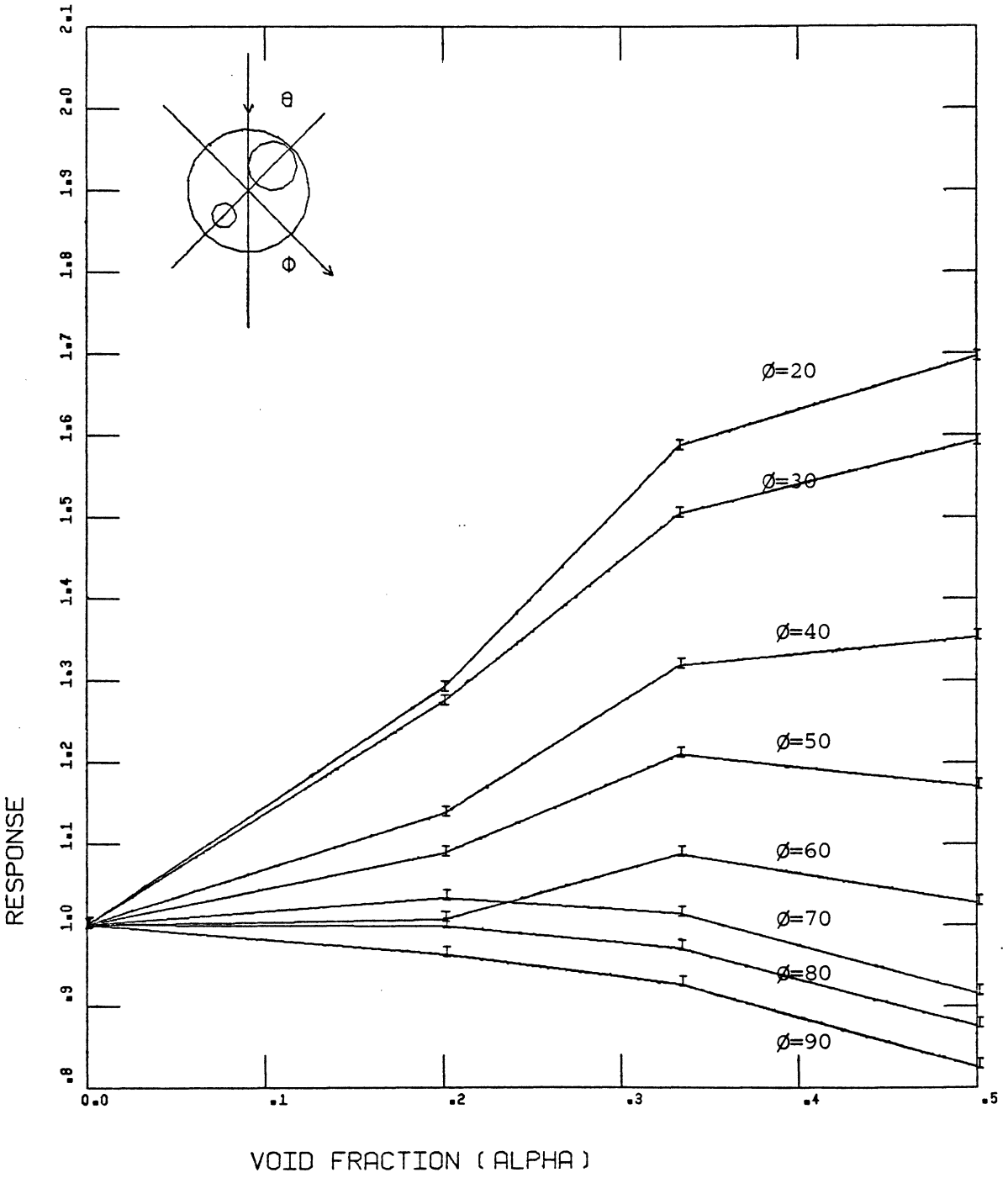

FIGURE 77: Response versus
For Sample #1,8,9,10; $\Theta = 180^{\circ}$

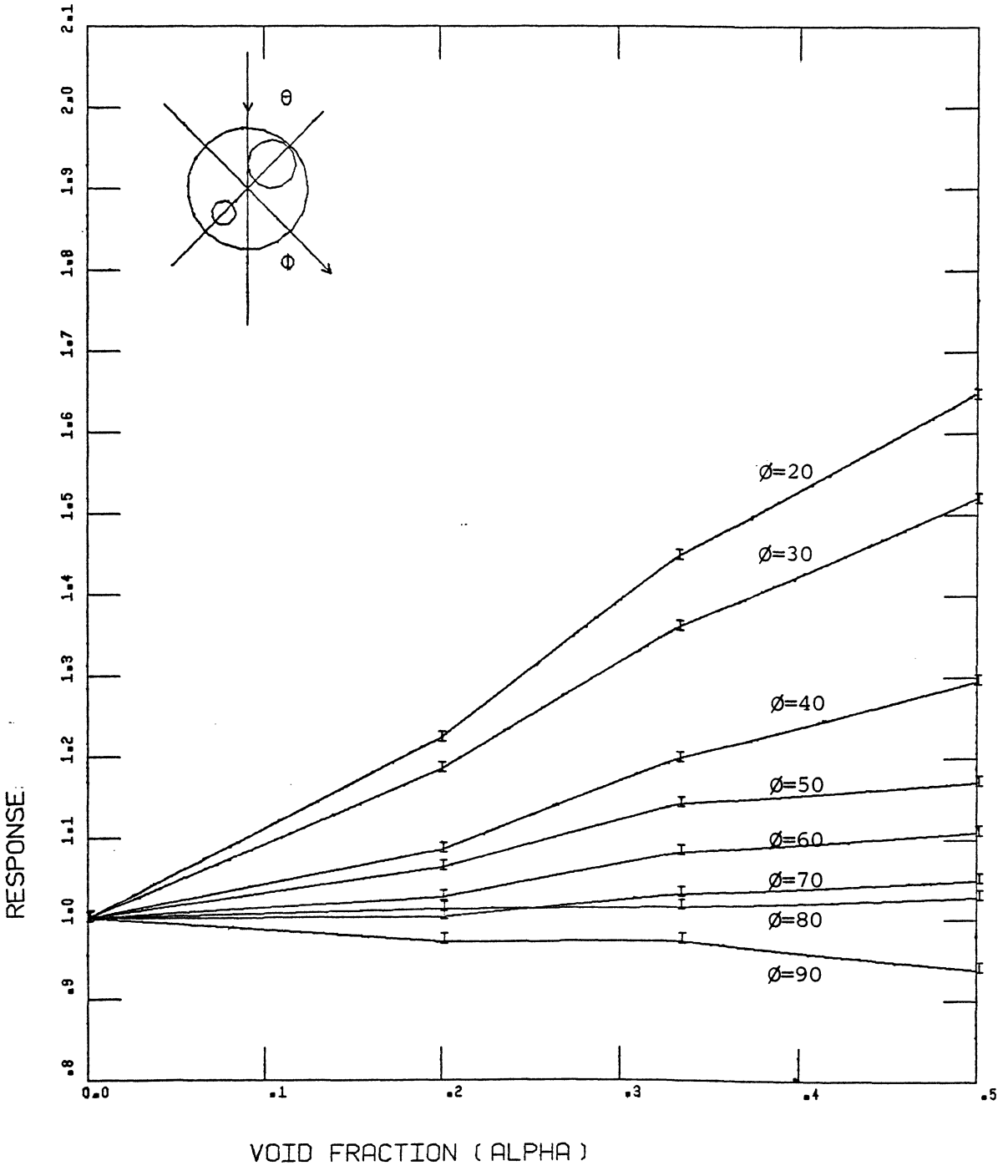

FIGURE 78: Response versus
For Sample #1,8,9,10; $\theta = 225^{\circ}$

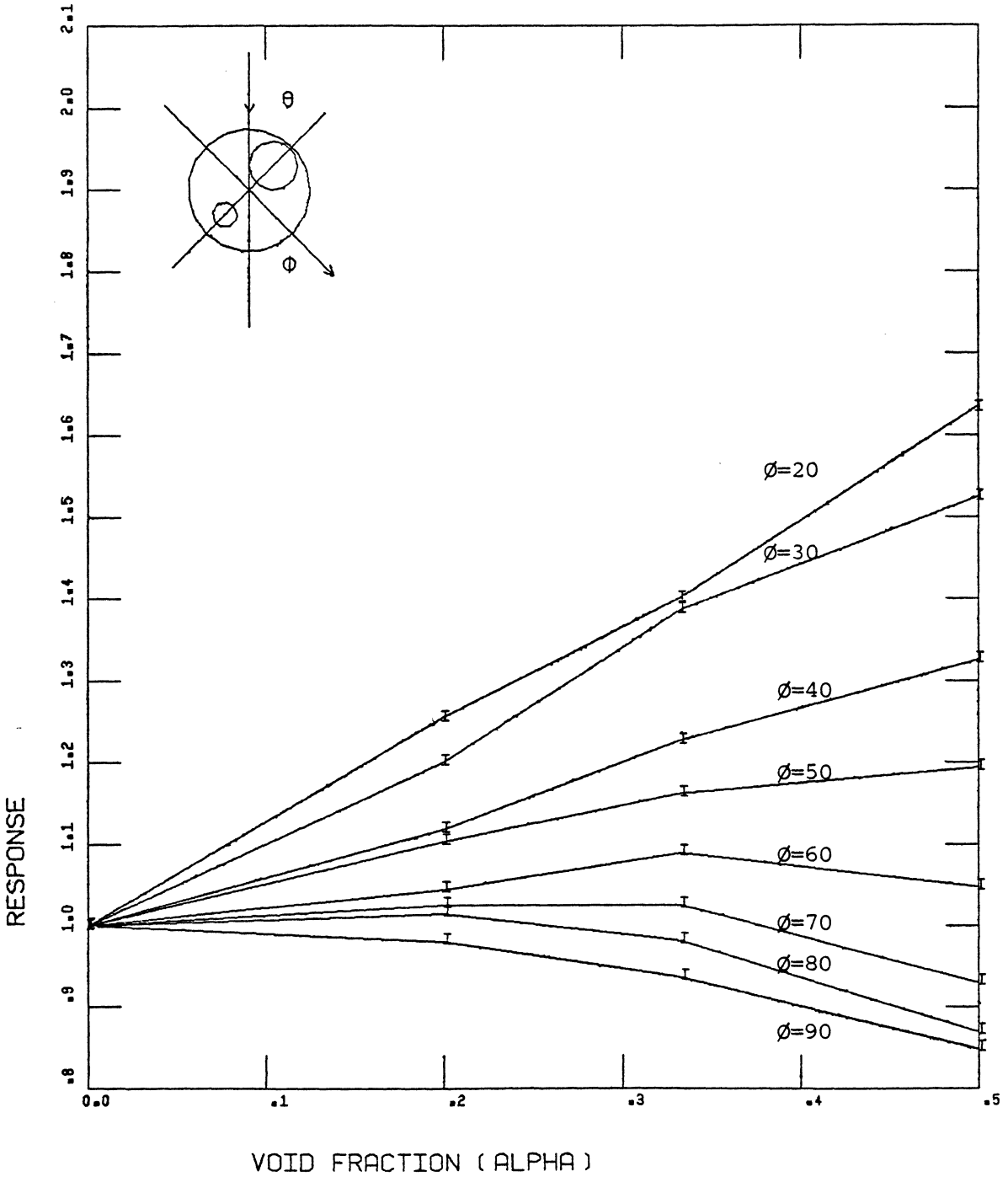

FIGURE 79: Response versus
For Sample #1,8,9,10; $\theta = 270^{\circ}$

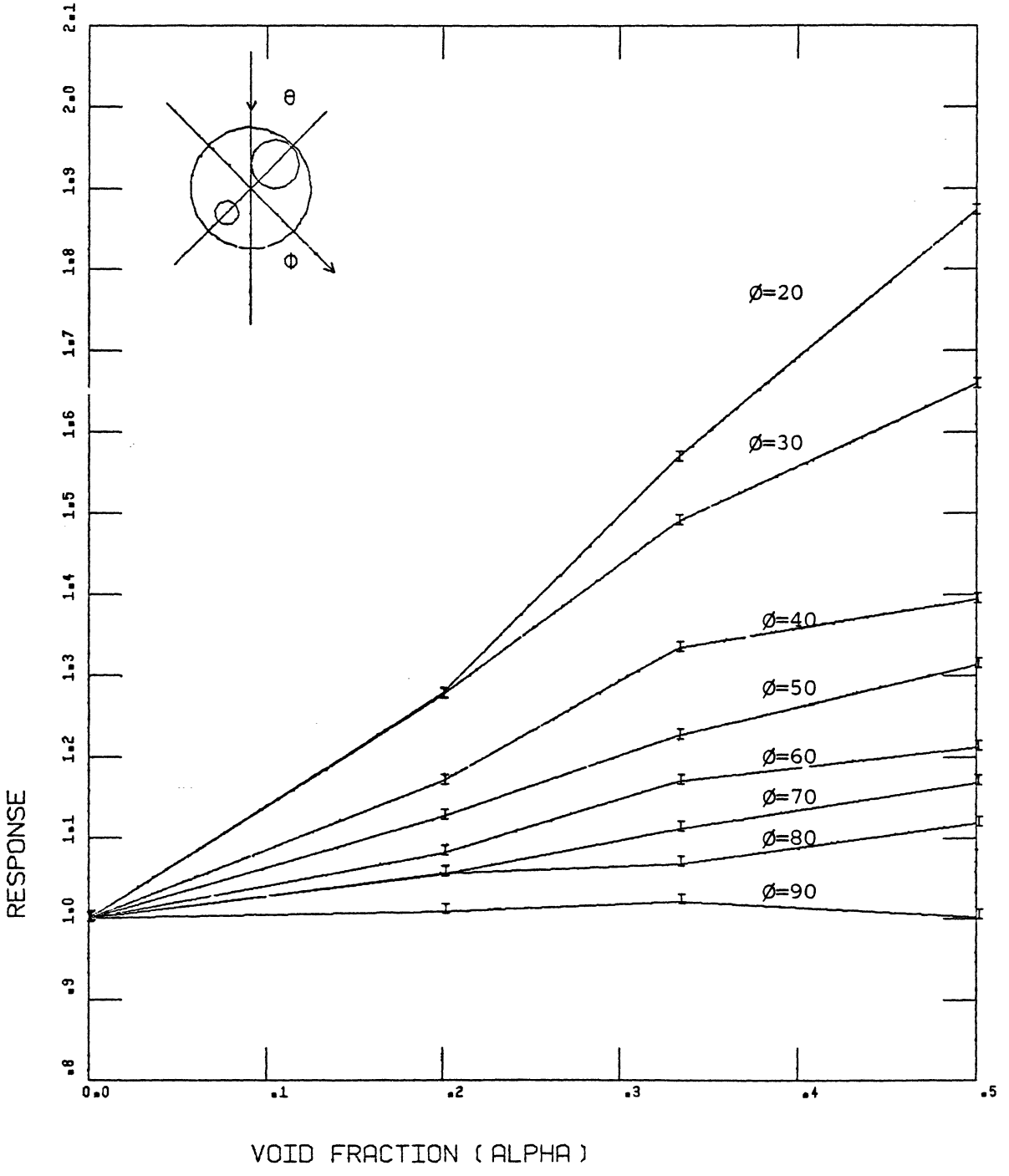

FIGURE 80: Response versus
For Sample #1,8,9,10 ; $\theta = 315^{\circ}$

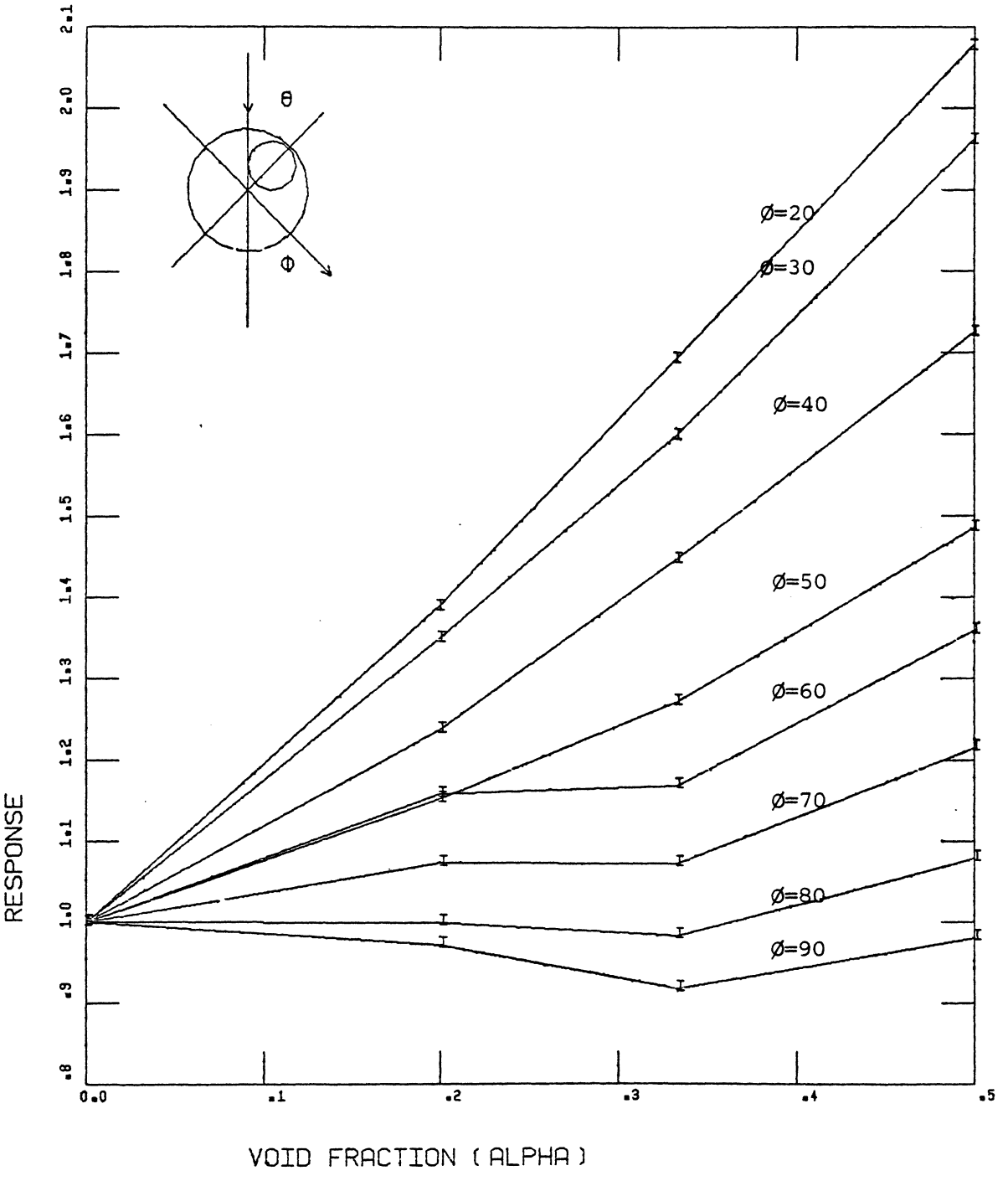

FIGURE 81: Response versus
For Sample #1,11,12,13; $\Theta = 0^{\circ}$

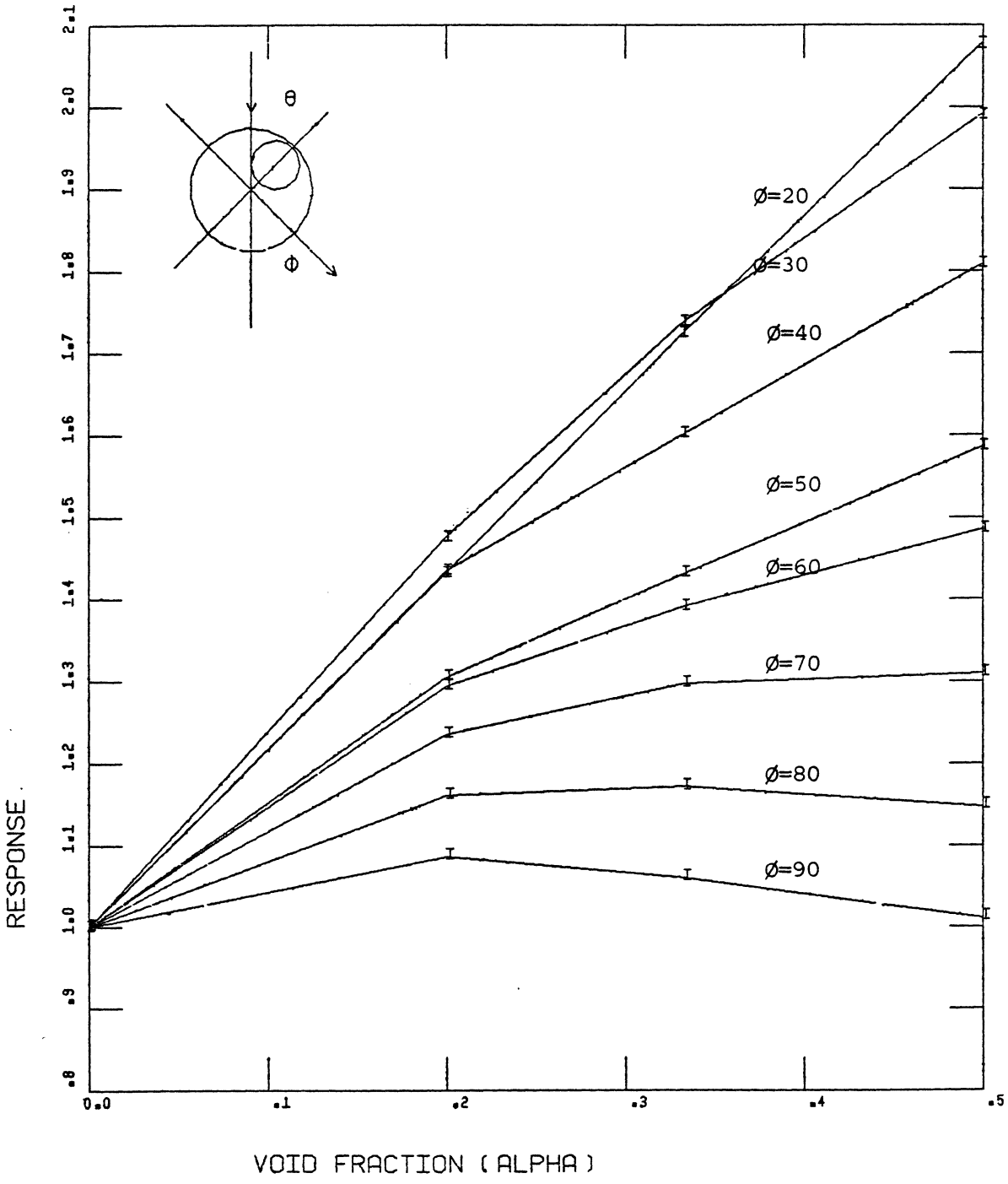

FIGURE 82: Response versus
For Sample #1,11,12,13; $\Theta = 45^{\circ}$

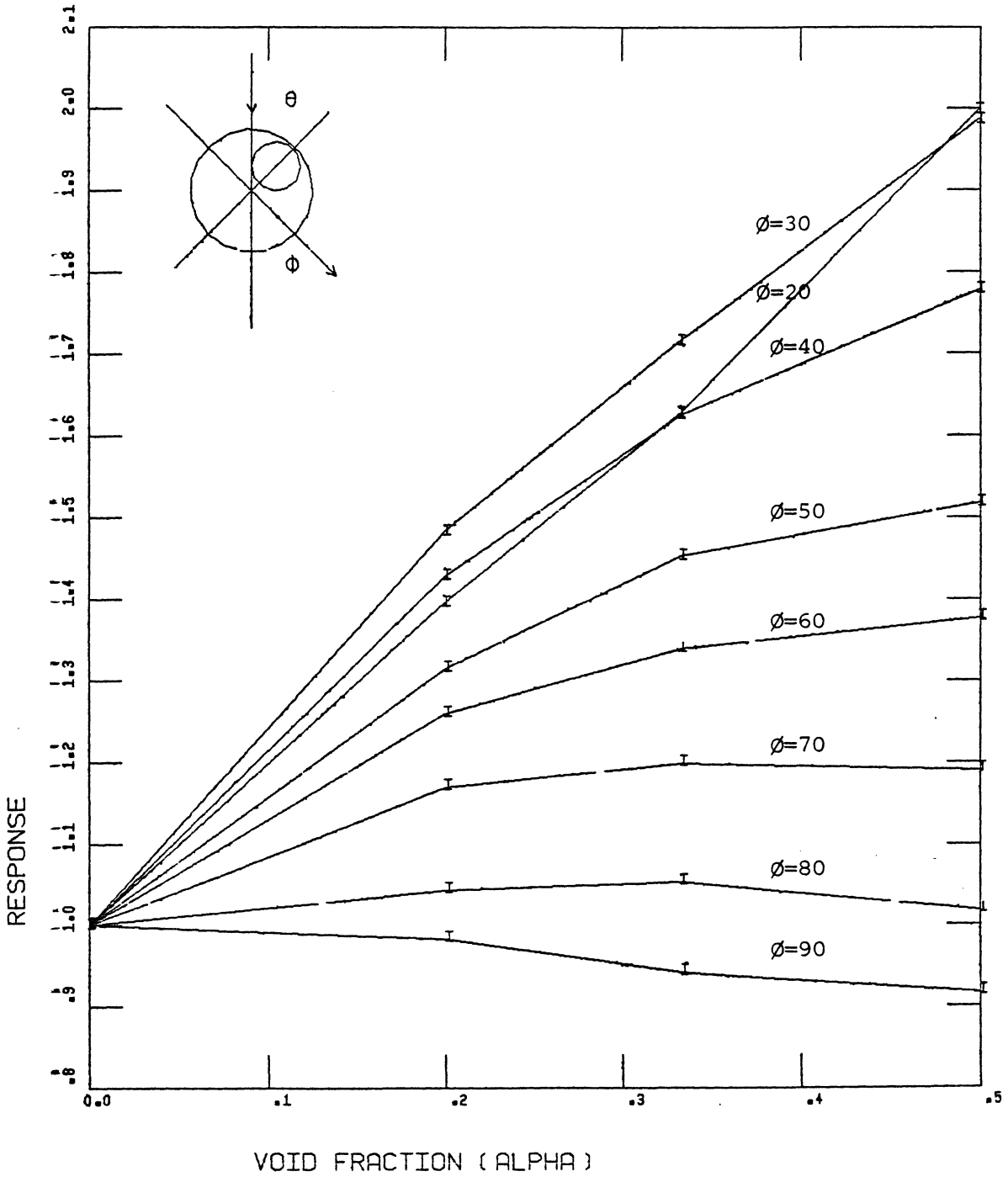

FIGURE 83: Response versus
For Sample #1,11,12,13; $\theta = 90^{\circ}$

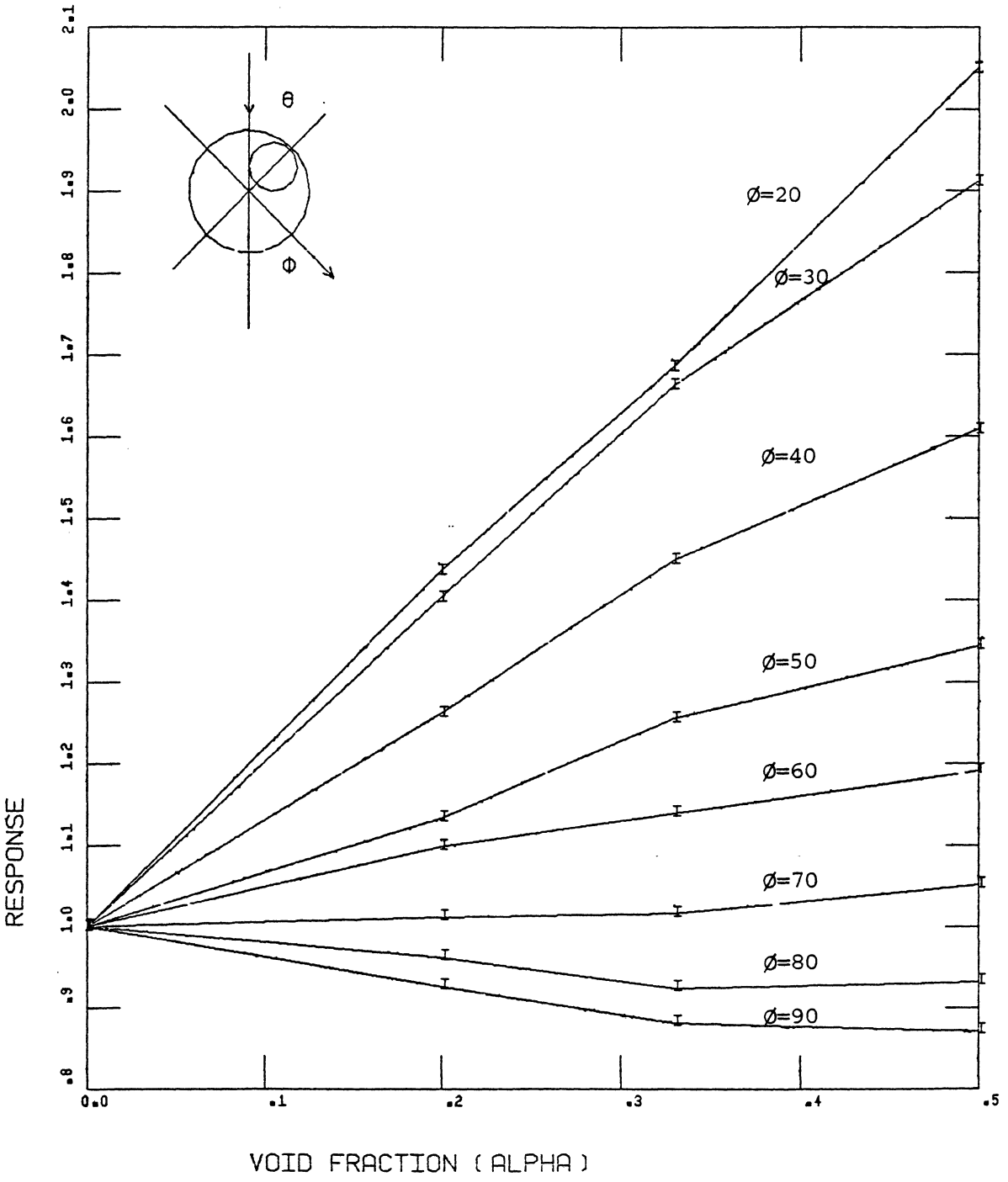

FIGURE 84: Response versus
For Sample #1,11,12,13; $\theta = 135^{\circ}$

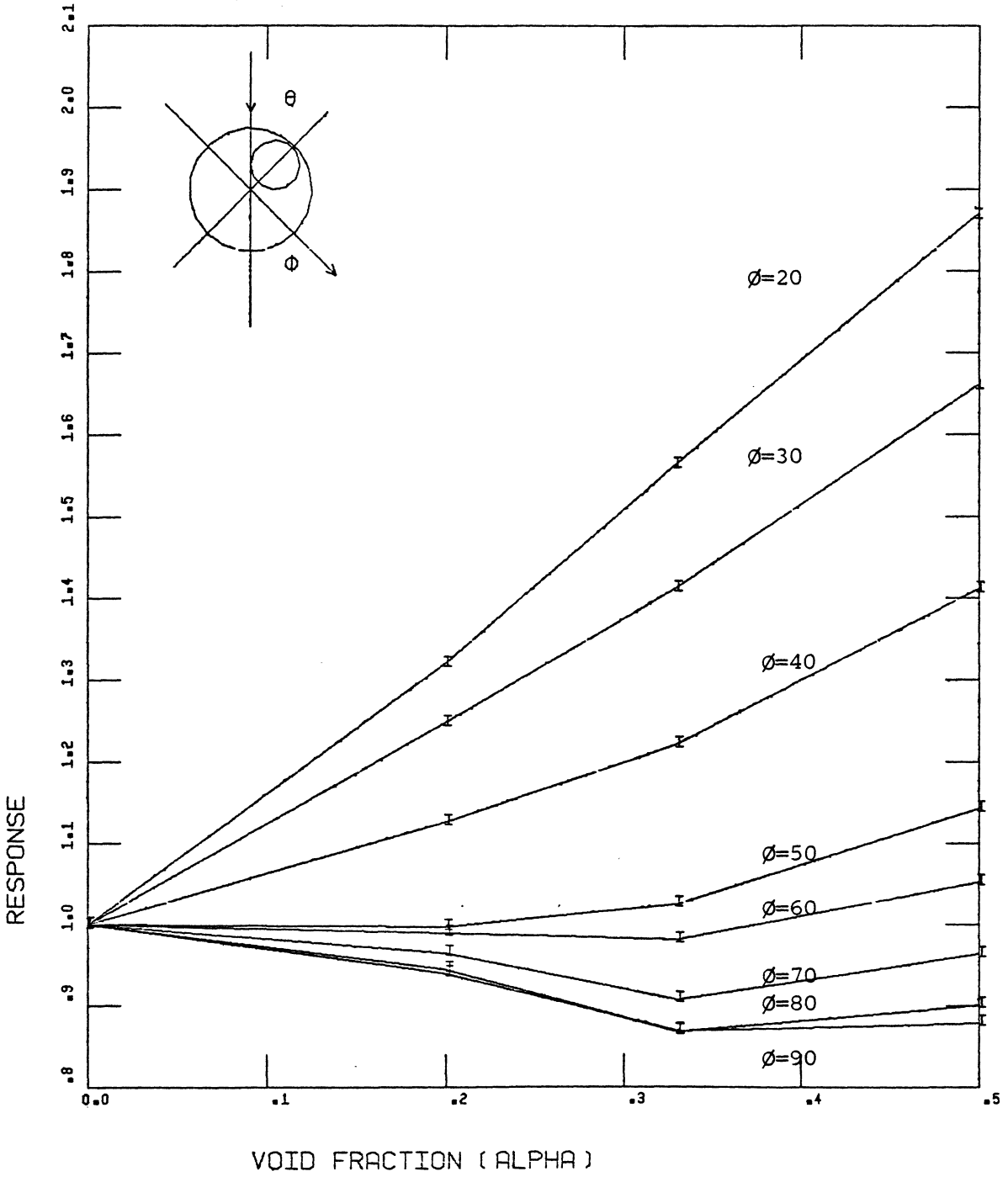

FIGURE 85: Response versus
For Sample #1,11,12,13; θ =180 °

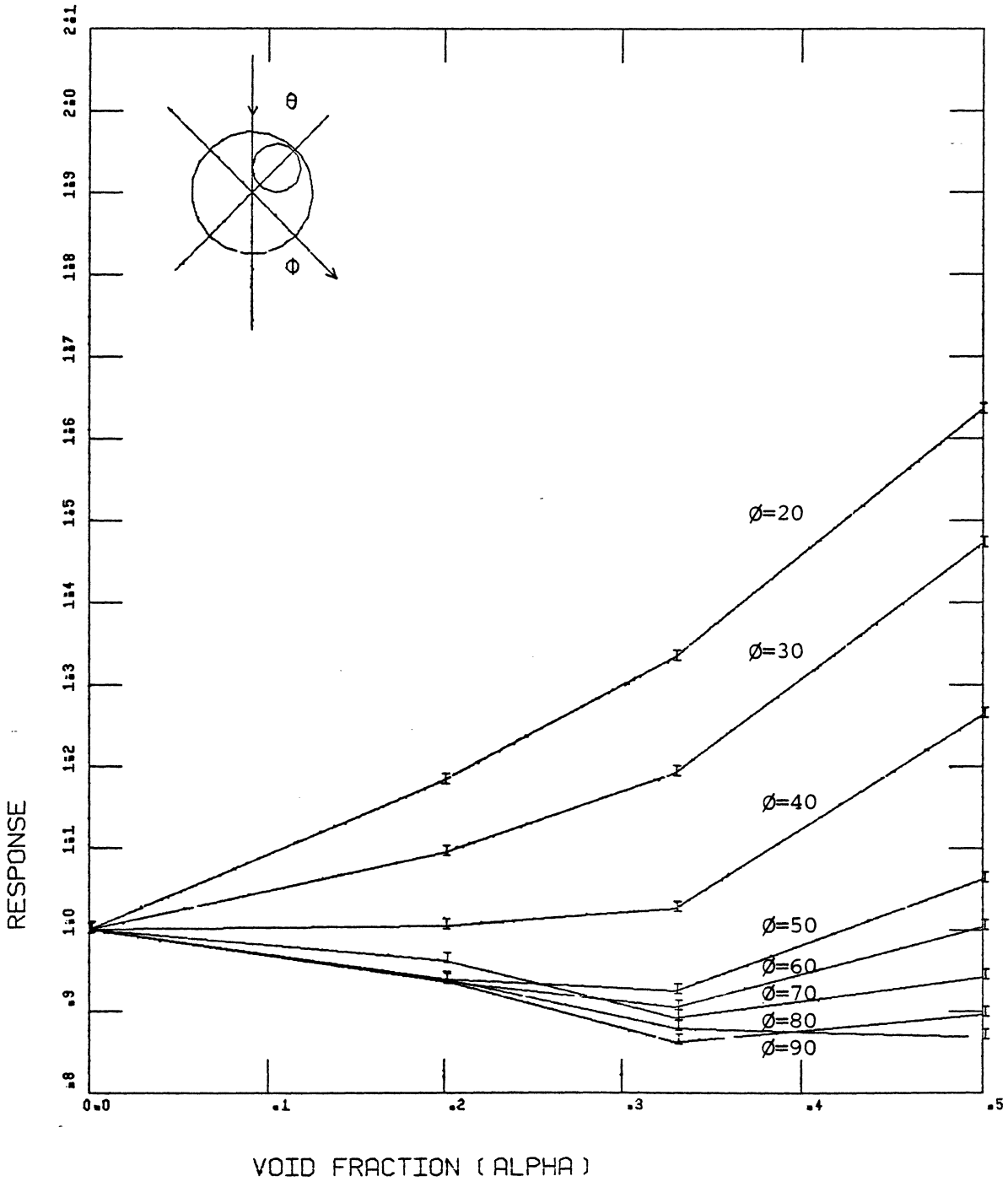

FIGURE 86: Response versus
For Sample #1,11,12,13; $\theta = 225^{\circ}$

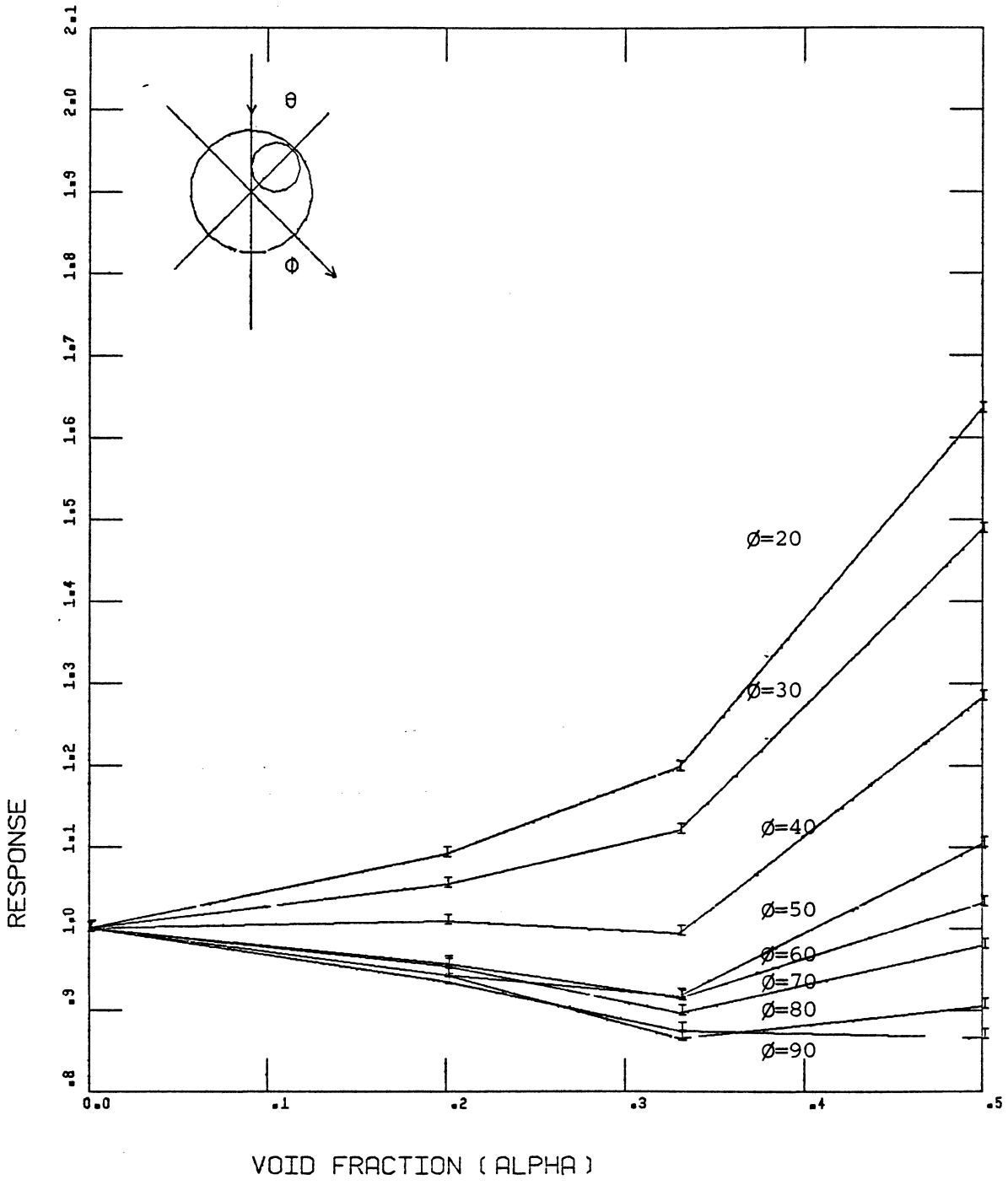

FIGURE 87: Response versus
For Sample #1,11,12,13; $\theta = 270^{\circ}$

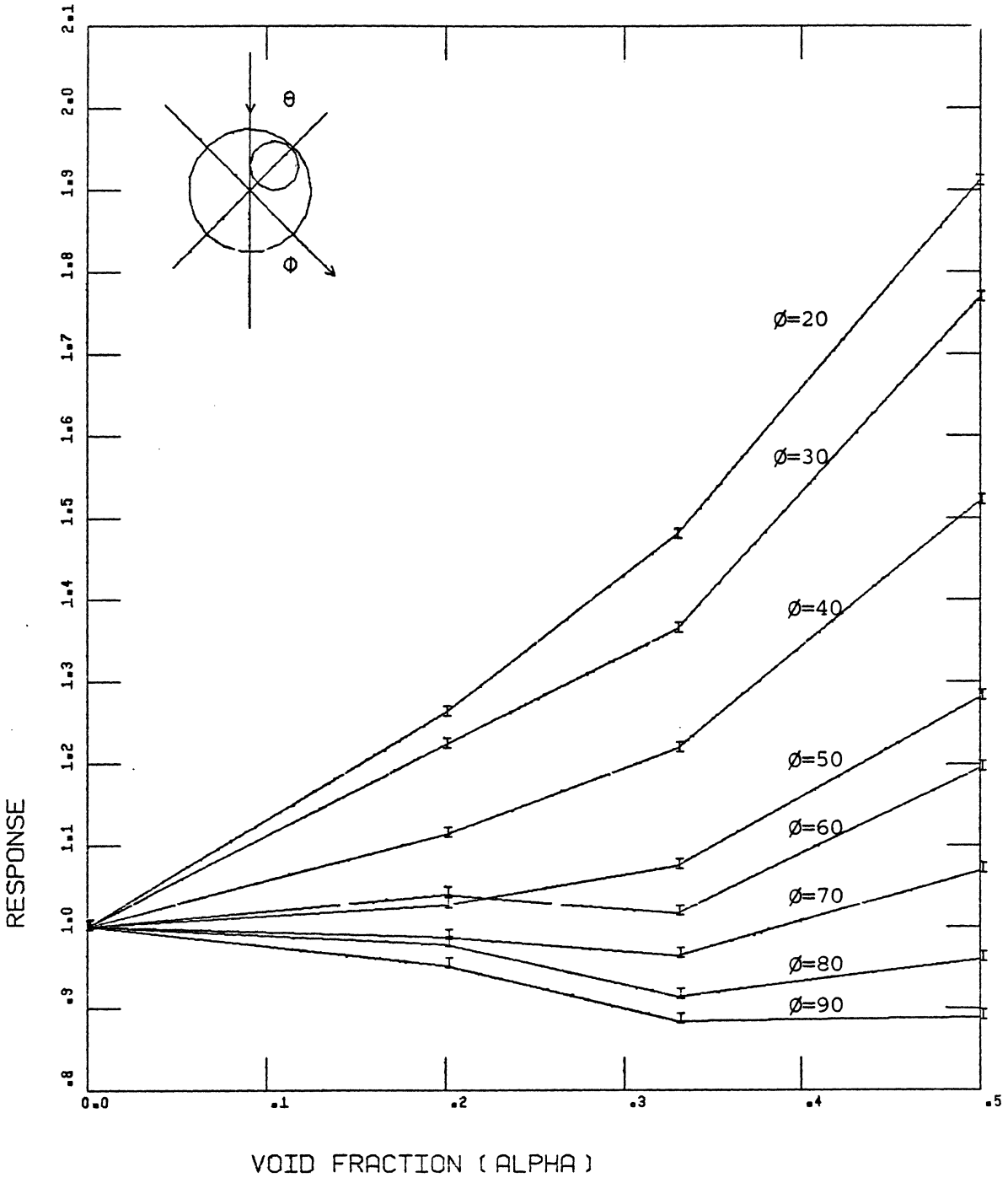

FIGURE 88: Response versus
For Sample #1,11,12,13 $\theta = 315^{\circ}$

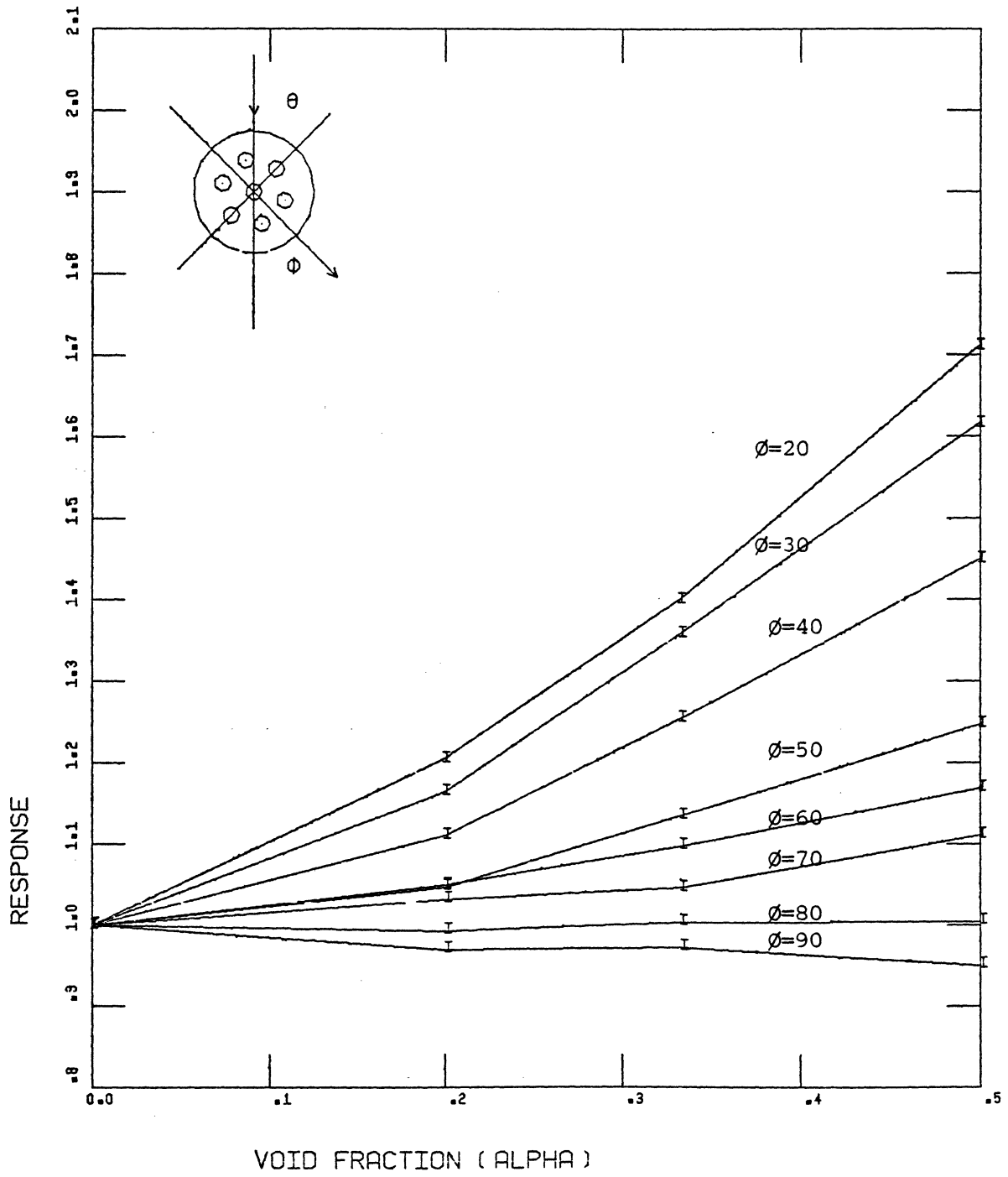

FIGURE 89: Response versus
For Sample #1,14,15,16; $\theta = 0^{o}$

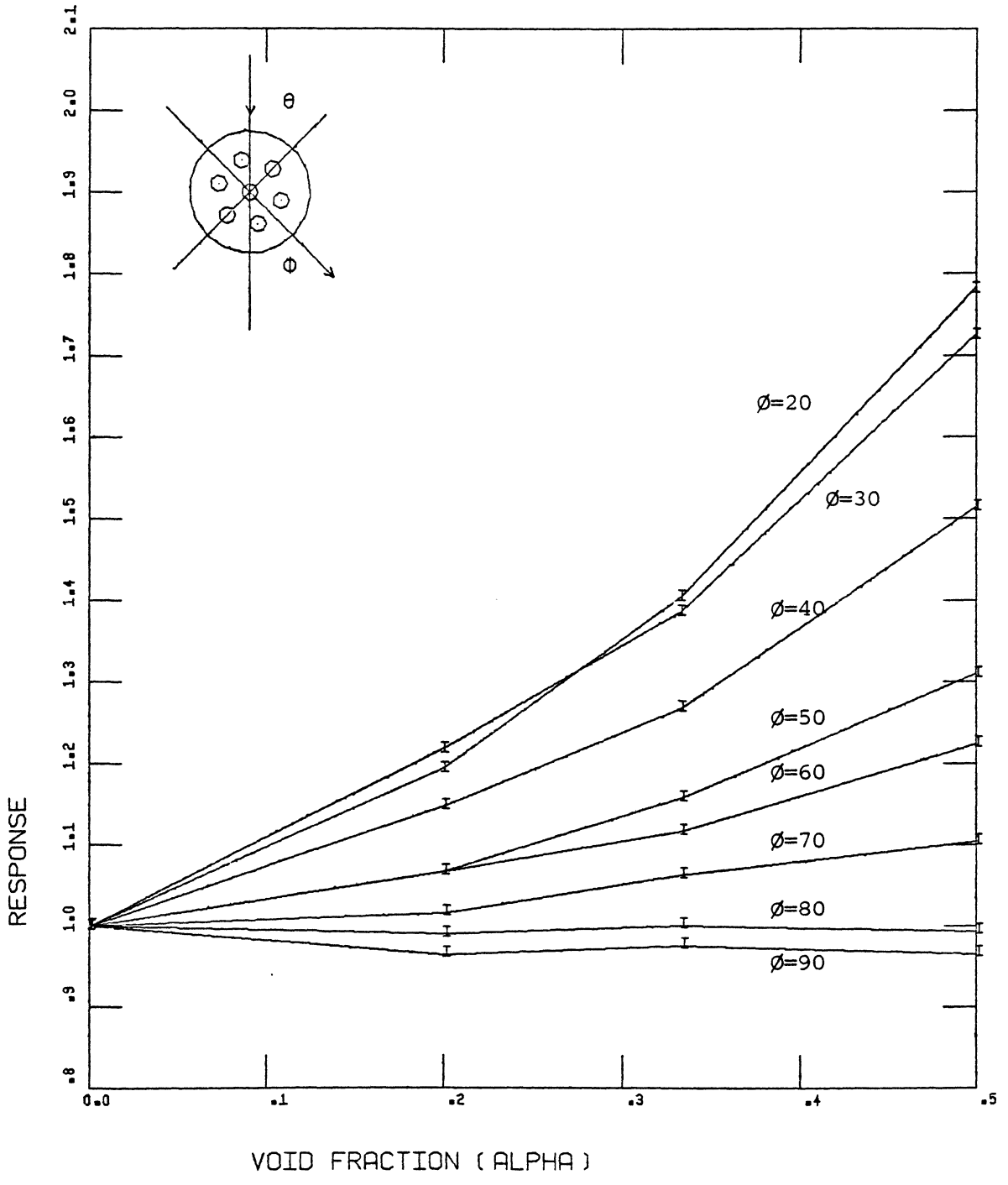

FIGURE 90: Response versus
For Sample #1,14,15,16; $\theta = 45^{\circ}$

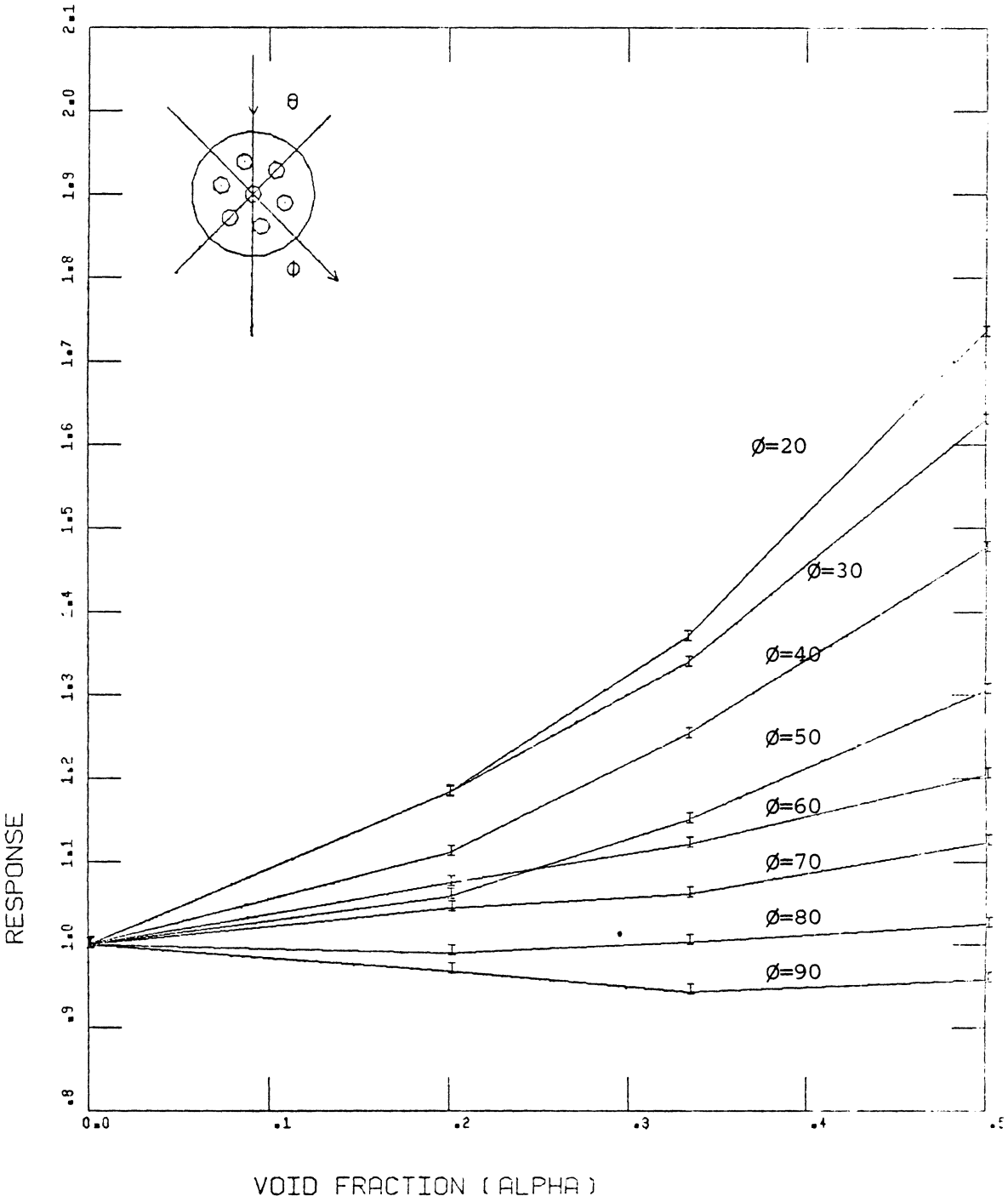

FIGURE 91: Response versus void fraction (α)
For Sample #1,14,15,16; $\Theta = 90^{o}$

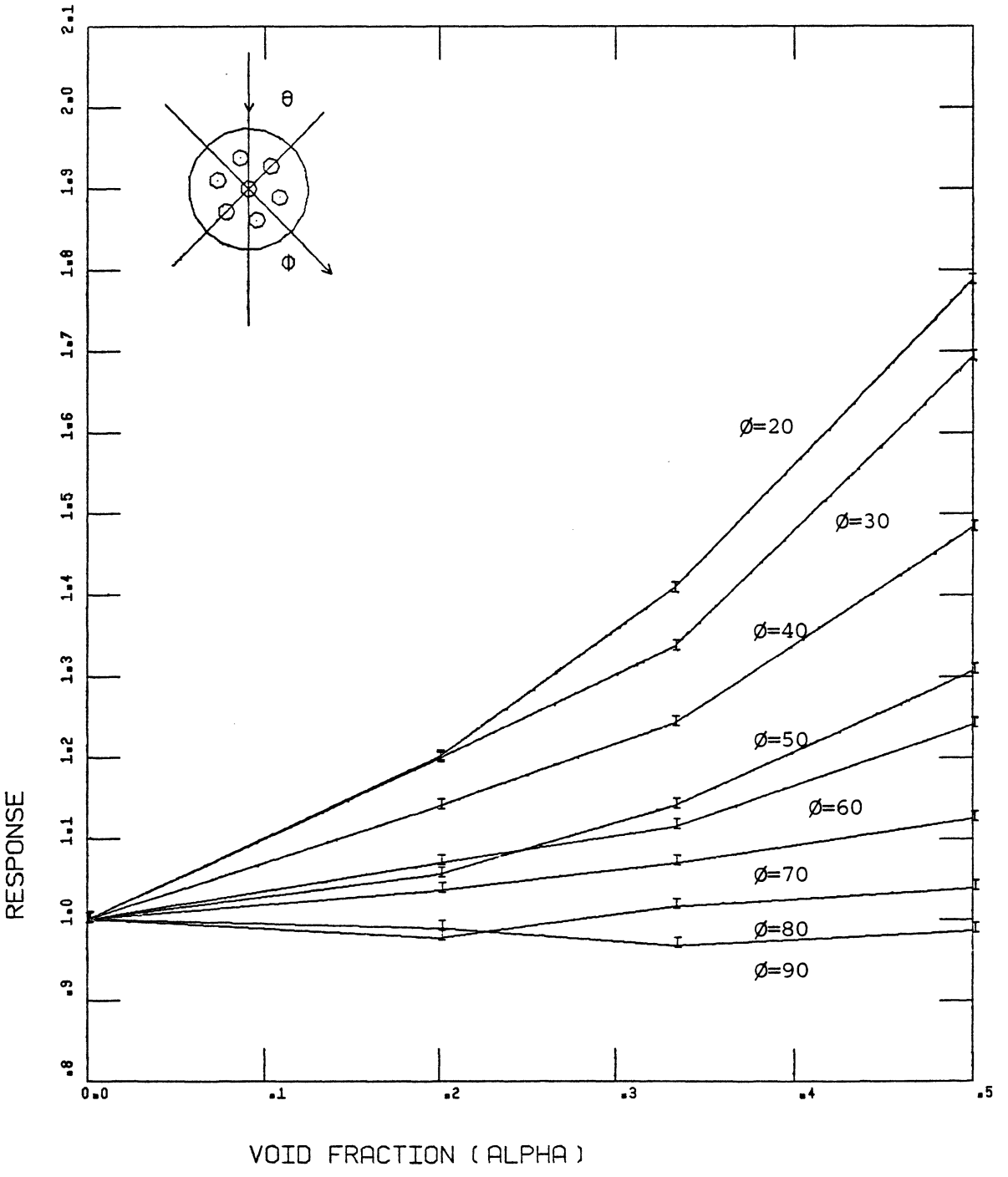

FIGURE 9 2: Response versus
For Sample #1,14,15,16; $\Theta = 135^{\circ}$

REFERENCES

(1) Hancox, W.T., Forrest, C.F., Harms, A.A., 'Void Determination in Two Phase Systems Employing Neutron Transmission', ASME72-HT-2, Heat Transfer Conference, Denver, Colorado, 1972 August.

(2) Hahn, O.J., 'Void Fraction Determination with Fast and Thermal Neutrons from a Californium Source', CONF-720902, American Nuclear Society National Topical Meeting, Austin, Texas (1972).

(3) Harms, A.A., Lo, S., Hancox, W.T., 'Measurements of Time Averaged Voids by Neutron Diagnosis', Journal of Applied Physic, Vol. 42,10, Pp. 4080-4332, 1971 September.

(4) Harms, A.A., Laratta, F.A.R., 'The Dynamic-bias in Radiation Interrogation of Two Phase Flow', Journal of Heat and Mass Transfer, Vol. 16, Pp. 1459-1465.

(5) Younis, M.H., Harms, A.A., Hoffman, T.W., 'Source Fluctuations Effects in Radiation Diagnosis of Voided Fluidic Systems', Nuclear Eng. and Design 24 (1973), Pp. 145-151.

(6) Harms, A.A., Forrest, C.F., 'Dynamic Effects in Radiation Diagnosis of Fluctuating Voids', Nuclear Science and Eng. 46, Pp. 408-413, 1971.

(7) Rousseau, J.C., Czerny, J., Riegel, B., 'Void Fraction Measurements During Blowdown by Neutron Absorption or Scattering Methods', CECO/NEA Specialist meeting of Transient Two Phase Flow, Toronto, Ont., 1976 August.

(8) Sha, W.T., Bonilla, C.F., 'Out of File Steam Fraction Determination by Neutron Beam Attenuation', Nuclear Application 1, Pp. 69-75, 1965 February.

(9) Banerjee, S., Chan, A.M.C., Ramanathan, N., Yuen, P.S.L., 'Fast Neutron Scattering and Attenuation Techniques for Measurement of Void Fractions and Phase Distribution in Transient Flow Boiling'. International Heat Transfer Conference, Toronto, Ont. 1978 August.

(10) Rousseau, J.C., 'Blowdown Experiments and Interpretation', Annual meeting of Two Phase Flow Group, Haifa, Israel, 1-5 June 1975, CEA-CONF-3546.

(11) Jackson, C.N., Allemann, R.T., Spear, W.G., 'Neutron Densitometer for Measuring Void Fraction in Steam-Water Flow'.

(12) Moss, F.A., Kelly, A.J., 'Neutron Radiographic Study of Limiting Planar Heat Pipe Performance', Journal of Heat and Mass Transfer, Vol. 13, Pp. 491-502.

(13) Banerjee, S., Heidrick, J.R., Saltvold, J.R., 'Measurement of Void Fraction and Mass Velocity in Transient Two Phase Flow', CECO/NEA specialist meeting in Transient Two Phase Flow, August, Toronto, Ont. 1976.

(14) Ashfaf-Atta, Mott, J.E., Fry, C., 'Determination of Void Fraction in BWR Using Neutron Noise Analysis', Institute of Nuclear Science and Technology - Pakistan.

(15) Semel, S., Helf, S., 'Measurement of Low Concentrations of Moisture by Fast Neutron Moderation'. Journal of Applied Radiation and Isotopes, 1969, Vol. 20, Pp. 229-239.

(16) Boisvert, J., 'Void Fraction Measurement Using an AM-BE Source', Washington, 1976, Transaction of the American Nuclear Society International Meeting.